



---

# **Design and fabrication of microstructured and mechanically-controlled electrospun corneal membranes**

---

By:

Danilo S. Villanueva Navarrete

A thesis submitted in partial fulfilment of the requirements for  
the degree of Doctor of Philosophy

School of Clinical Dentistry

The University of Sheffield

September 2020

## Abstract

Corneal blindness is the third leading cause of blindness worldwide. Current treatments require the use of donor corneas or amniotic membrane as a cell carrier. While these treatments are successful to a degree, they present downsides including accessibility of tissue and the risk of disease transmission. The use of synthetic scaffolds is a potential solution; current research has exhibited the importance of controlling mechanical properties when designing new approaches to corneal regeneration. The aim of this project is to create synthetic electrospun scaffolds with mechanically tailored stiffness to explore corneal cell behaviour *in vitro*, as well as to explore the inclusion of topographical cues in these membranes. Mechanically tailored membranes were fabricated using electrospinning and blending PLGA (poly(lactic-co-glycolic acid)) and PCL (Polycaprolactone) in different concentrations. Membranes were characterised in dry (storage) and wet conditions (submerged in PBS at 37°C). Characterisation of the membranes was done using Scanning Electron Microscopy (SEM) to analyse microstructure and fibre diameter. Uniaxial tensile testing was used to obtain stiffness, Ultimate Tensile Strength (UTS), and strain at UTS from the membranes. Gas chromatography was performed to measure the remnant solvents in them. Differential Scanning Calorimetry (DSC) was executed to analyse the thermal properties in the membranes. Biological testing was accomplished using rabbit and porcine limbal explants on the membranes and growing them for 2 and 3 weeks. Cell outgrowth in the membranes was analysed using different microscopy techniques (SEM, Light Sheet microscopy, and epifluorescence microscopy). Topographical cues were introduced in electrospun membranes by casting metal collectors with particular designs after the input of specialist of L. V. Prasad Eye Institute. Fibre alignment and fibre orientation were examined in the membranes by analysing SEM images and processing them with the ImageJ software with a protocol developed by us introduced in this thesis.

Electrospun scaffolds with different mechanical properties were successfully manufactured blending PLGA and PCL. DCM and DMF as solvents produced a lower amount of remnant solvents in the electrospun scaffolds made of PLGA and PCL than the maximum permissible by EMA and FDA. Adding PCL showed statistical differences in the stiffness of the

membrane for blends with 10% or more PCL on it, an effect that is increased when the membranes are analysed in dry and wet conditions. From all the conditions analysed, 30%PCL - 70%PLGA is able to maintain its mechanical properties in wet/warm and dry conditions which we envisage is a very important point for the material to be used in theatre. PLGA and PLGA-PCL membranes showed outgrowth from rabbit and porcine limbal explants at 2 and 3 weeks no differences were observed in the amount of cell outgrowth between them. All mechanically tailored membranes developed in this research showed good capacity as cell carriers of limbal corneal cells. 30%PCL – 70%PLGA displayed cell outgrowth in both sides of the membrane, suggesting that the cells penetrated through the membrane and populated the other side. As well, Topographical cues in the membranes were successfully introduced and characterised analysing fibre orientation and fibre alignment in different zones on them. With all this in mind, 30%PCL – 70%PLGA showed the best results in its mechanical properties and its cell outgrowth when seeded with porcine limbal explants for two weeks and we suggest moving forward the research using this electrospun membrane with longer culture times.

All the research protocols and findings highlighted above as well as the state-of-the-art relevant to the proposed topic have been described in this thesis. The work has been divided into 5 Chapters; additionally, a COVID-19 related appendix has been also incorporated to explain in details how the experiments planned to be included in this thesis were affected by the pandemic.

## Acknowledgments

I would like to thank my main supervisor, Dr. Ilida Ortega, for her continuous support, encouragement and trust during these 4 years. Dr. Ilida Ortega supported me not only in my research, giving me the tools needed to successfully move forward this work; but as well professionally encouraging me to take growing opportunities like doing a secondment in L. V. Prasad Eye Institute (Hyderabad, India), guiding students in their research, and letting me participate in Biotech: YES. I would like to thank as well to my other supervisors, Dr. Frederik Claeysens and Prof. Sheila MacNeil, for their constant advises and trust they gave me to lead this research.

Additionally, I like to thank to all the people that helped me during my research without being directly involved in it. Dr. Thomas Paterson and Dr. Sabiniano Roman for being my co-supervisors and friend during a big part of my research; Dr. David Patrick for teaching me and always assisting me in the collector making process with an infinite patience; Dr. Robert Moorehead for teaching me and guide me in all the 3D printing process; and Robert Hanson for his help doing Gas Chromatography and Differential Scanning Calorimetry.

I would like to thank as well to all my friends I have made in this research; Beatriz Monteiro, Alex Bolger, Maha Omran, Katharina Clitherow, , and the rest of the dsrs. As well, extend my thanks to all my friends that have supported me outside the university; my best friend Diego Poblete, Juan Mujica, Sven Niklander, Bernabe Alvarez, Esther Alvarez, Samanta Elgueta, Hector Jorquera, Natalia Campos, and the rest of the Chilean community!

Finally, and incredibly importantly, I want to thank my loved ones; my dad, my mom, and my brother; for always encouraging me to achieve more in my life and always loving me regardless of anything. As well as my girlfriend Grace Barnes and her family, for making my life so incredibly beautiful. I love you more Grace!.

## Outputs

### Prizes/awards or external funding

**MeDe innovation PhD secondment scheme 2018:** Secondment of three weeks in L. V. Prasad Eye Institute (Hyderabad, India). **Funded:** 1298.2 pounds.

**TA:SURE Scheme 2019:** "Tailoring substrate stiffness on electrospun scaffolds to investigate human limbal epithelial cell behaviour". **Funded:** 978.72 pounds.

**Biotech YES 2019:** Group name: CONTUCURA with the product name: "BruiGO". Participating in Biomedical Workshop. **Funded:** Participation and accommodation.

### Oral Presentation

"The effects of mechanically tailored 3D nanofibrous scaffolds for corneal regeneration" D. Villanueva, T. Paterson, S. MacNeil, F. Claeysens, I. Ortega. **Talk**, UKSB 2020, United Kingdom.

### Poster Presentations

"Tailoring substrate stiffness to investigate corneal epithelial cell behaviour" D. Villanueva, T. Paterson, S. MacNeil, F. Claeysens, I. Ortega. **Poster**. ESB 2018, Netherlands.

"Development of Synthetic corneal microfabricated membranes with controlled stiffness" D. Villanueva, T. Paterson, S. MacNeil, F. Claeysens, I. Ortega. **Poster**, TCES 2018, United Kingdom.

"Manufacturing Mechanically Tailored Electrospun Scaffolds for Corneal Regeneration" D. Villanueva, S. Roman, T. Paterson, S. MacNeil, I. Ortega. **Poster**, MeDe 2017, United Kingdom.

“Tailoring substrate stiffness to improve rabbit limbal explant outgrowth” D. Villanueva, S. Roman, T. Paterson, S. MacNeil, I. Ortega. **Poster**, BiTeg 2017, United Kingdom

“Developing biodegradable scaffolds containing stem cell niche features for cornea regeneration” D. Villanueva, S. Roman, T. Paterson, S. Mittar, I. Ortega, S. MacNeil. **Poster**, BiTeg 2016, United Kingdom

## Table of Contents

Abstract.....	1
Acknowledgments.....	3
Outputs .....	4
Prizes/awards or external funding.....	4
Oral Presentation .....	4
Poster Presentations.....	4
List of abbreviation .....	11
Chapter 1: Literature Review.....	13
1.1. Corneal blindness overview.....	13
1.2. Characteristics of the human cornea.....	14
1.3. Stem cells in the human eye .....	17
1.3.1. Stem cells in the cornea .....	17
1.3.2. Stem cells in the conjunctival epithelium .....	20
1.4. Human corneal versus other animal species .....	21
1.5. Corneal Disease.....	23
1.6. Corneal replacement surgical techniques.....	24
1.6.1. Penetrating keratoplasty .....	25
1.6.2. Selective lamellar keratoplasty .....	25
1.6.3. Endothelial keratoplasty .....	26
1.6.4. Ocular surface transplantation and new surgical approaches .....	27
1.7. Corneal scaffolds.....	30
1.7.1. Amniotic membrane .....	31
1.7.2. Biological scaffolds aside of amniotic membrane .....	32
1.7.3. Synthetic Polymeric scaffolds .....	33
1.8. Electrospinning .....	34
1.9. Effects of stiffness of scaffolds in cell culture .....	38
1.10. Findings from literature review and motivation for the project. ....	40
1.11. Aim and objectives.....	42
Chapter 2: Modifying mechanical properties of electrospun PLGA membranes via the addition of Polycaprolactone .....	44
2.1.- Introduction .....	44
2.2.- Aim .....	46
2.3.- Materials and Methods.....	47
2.3.1.- Materials .....	47

2.3.2.-	Electrospinning.....	48
2.3.3.-	Rheology .....	49
2.3.4.-	Tensile Testing.....	50
2.3.5.-	Fibrin Glue coating .....	50
2.3.6.-	Extraction-Capillary Gas Chromatography.....	51
2.3.7.-	Differential Scanning Calorimetry.....	51
2.3.8.-	Scanning Electron Microscopy .....	52
2.3.9.-	Studying differences between dry and wet scaffolds.....	52
2.3.10.-	Statistical analysis .....	53
2.4.-	Results.....	53
2.4.1.-	Optimising electrospinning conditions .....	53
2.4.2.-	Studying possible plasticising effects of PCL.....	56
2.4.3.-	Rheology properties of different electrospun solutions.....	58
2.4.4.-	Mechanical properties of scaffolds.....	60
2.4.5.-	Remnant solvent in scaffolds after electrospinning .....	69
2.4.6.-	Thermal properties in scaffolds .....	70
2.4.7.-	Scaffolds morphology and degradation.....	71
2.5.-	Discussion.....	74
2.6.-	Conclusion.....	79
<b>Chapter 3: Studying limbal explant behaviour on electrospun scaffolds with controlled mechanical properties .....</b>		<b>80</b>
3.1.-	Introduction .....	80
3.2.-	Aim .....	82
3.3.-	Materials and Methods.....	82
3.3.1.-	Materials and cells used.....	82
3.3.2.-	Animal limbal explant isolation.....	84
3.3.3.-	Animal limbal epithelial cell culture.....	86
3.3.4.-	Animal limbal explants seeding into membranes.....	86
3.3.5.-	Cell outgrowth on electrospun scaffolds and staining techniques.....	87
3.3.6.-	Analysing and quantifying cell outgrowth on electrospun scaffolds.....	88
3.3.7.-	Statistical analysis .....	90
3.4.-	Results.....	90
3.4.1.-	Rabbit limbal explants v/s porcine limbal explants .....	90
3.4.2.-	Studying cell outgrowth at 2 and 3 weeks of culture on scaffolds .....	92
3.4.3.-	Porcine explants in mechanically tailored scaffolds (2 weeks of culture) .....	96

3.4.4.-	Quantification of cellular outgrowth on the membranes.....	97
3.4.5.-	COVID-19 Considerations.....	100
3.5.-	Discussion.....	101
3.6.-	Conclusion.....	104
Chapter 4: Introducing complexity within electrospun membranes via the incorporation of defined 3D-microfeatures.....		105
4.1.-	Introduction .....	105
4.2.-	Aim .....	108
4.3.-	Materials and Methods.....	108
4.3.1.-	Materials .....	108
4.3.2.-	Manufacturing collectors for electrospinning templating.....	110
4.3.3.-	Electrospinning on collectors.....	114
4.3.4.-	Human limbal cell culture .....	114
4.3.5.-	Shrinkage of electrospun PLGA membranes.....	115
4.3.6.-	Analysis of alignment in complex scaffolds .....	116
4.3.7.-	Statistical analysis .....	117
4.4.-	Results.....	118
4.4.1.-	Design of collectors to create complex topography in electrospun membranes.....	118
4.4.2.-	Exploring a reliable methodology of collector manufacturing for electrospun membranes.....	121
4.4.3.-	Human limbal explant culture on electrospun PLGA membranes with topographical cues	123
4.4.4.-	Analysis of electrospun membrane shrinkage.....	126
4.4.5.-	Analysing topographical cues included in electrospun membranes made with special shaped collectors. ....	128
4.4.6.-	COVID-19 Considerations.....	142
4.5.-	Discussion.....	143
4.6.-	Conclusion.....	147
Chapter 5: Final conclusions and future work.....		148
5.1	Final Conclusions.....	148
5.2	Future work.....	149
References .....		150
Appendix A – Effects of COVID-19 on this research.....		167
Introduction .....		167
Research Planning affected .....		167

Discussion .....	169
Appendix B – Fibre Alignment methodology explained .....	171
Appendix C – Ethical approval .....	180
University of Sheffield Answer.....	180
Ethics Committee Approval Letter.....	180



## List of abbreviation

3D =	3 dimensions
DCD=	Different collector designs
DCM=	Dichloromethane
DMF=	Dimethylformamide
DMP=	Different mechanical properties
DSC =	Differential Scanning Calorimetry
EMA=	European Medicines Agency
FDA=	Food and drug administration
HAM=	Human Amniotic Membrane
HD=	Hemispherical design
HR=	Hemispherical ring
ND=	No Design
PBS=	Phosphate buffered solution
PCL=	Polycaprolactone
PD=	Plain design
PLGA =	Poly(lactic-co-glycolic acid)
PLLA=	Poly(lactic acid)
PPM=	Parts per million
PR=	Plain ring
SEM =	Scanning Electron Microscopy

UTS= Ultimate Tensile Strength

UV= Ultraviolet

WHO= World Health Organisation

## Chapter 1: Literature Review

### 1.1. Corneal blindness overview

Corneal blindness is the third leading cause of blindness in the world (after cataract and glaucoma) with approximately 10 million people suffering from bilateral corneal disease (Pascolini and Mariotti, 2012). In a study that collected the information of 148 countries (out of a 157 total, representing 95% of world population) it was stated that, globally, 12.7 million people are waiting for a corneal transplantation of which only 1 in 70 will eventually receive one (Gain *et al.*, 2016). It has been also reported that approximately only 35.7% of the world's population has satisfactory access to corneal transplantation (Gain *et al.*, 2016).

The epidemiology of corneal blindness is complex and can be a result of a wide variety of inflammatory or infectious eye diseases that give rise to corneal scarring (John and Madan, 2001). Some diseases that can cause corneal blindness are corneal ulcers, ophtalmia neonatorum, trachoma, xerophthalmia, onchocerciasis, viral infections, leprosy, ocular trauma and traditional eye medicines (Pascolini and Mariotti, 2012; Wong *et al.*, 2016). Additionally, the prevalence of corneal disease fluctuates from country to country. If only the less developed countries are considered, corneal disease scales to the second most prevalent cause of blindness (Oliva, Gulati and Schottman, 2012). The amount of patients needing corneal transplantation is greater than the number of available donor corneas and, although corneal transplantation is well-established and relatively successful (Mccolgan, 2009), donor corneas present associated risks that are important to highlight, including storage issues and expensive quality control procedures; these procedures include serology of donor blood for the number and quality of corneal endothelial cells, hepatitis B and C, and human immunodeficiency virus (HIV) (Gain *et al.*, 2016; Griffith, Alarcon and Brunette, 2016). According to this, we can assume that cornea donation needs to be encouraged (Lawlor and Kerridge, 2011), but, also and alternative solution is needed, and the answer for this is likely to come from a Bioengineering approach (Patel, 2012; Wong *et al.*, 2016).

Bioengineering has developed through the years interesting approaches to aid in solving corneal problems. The first approach is the use of corneal grafts, in which an initial graft

includes transplantation of a piece of corneal limbal tissue from a donor eye (Griffith and Harkin, 2014; Wong *et al.*, 2016). In this approach we can include techniques like Conjunctival limbal autograft (CLAU) or the simple limbal epithelial transplantation (SLET) that are reviewed later on in this review (Sangwan *et al.*, 2012). In addition, it is important to highlight as well the techniques in which corneal stem cells are expanded *in vitro* to later be transplanted to the patient (Singh *et al.*, 2019). There are other approaches based on the use of other stem cell sources including cultured oral mucosa epithelium transplantation (COMET) or the use of mesenchymal stromal cells which has been also reported (Dobrowolski *et al.*, 2011). Finally, other approaches consider the use of biomaterials for corneal regeneration, in which materials like chitosan, silk, fibrin or self-assembling peptides have been utilised with different results (Griffith *et al.* 2016).

The above cited treatments are effective to a certain extent, but, it becomes clear that new approaches must be pursued in order to fully address the challenges that corneal transplantation is currently facing.

## 1.2. Characteristics of the human cornea

The human eye is a highly specialized photoreceptive organ that provides the ability to process visual details and consists of internal structures that can be separated into conjunctiva, iris, pupil, cornea, lens, retina, vitreous humour, sclera, choroid and the optic nerve as can be seen in the figure 1.1. (Di Girolamo, 2011; Kivela, Messmer and Rymgayllo-Jankowska, 2015; Ramos, Scott and Ahmad, 2015). The eyes present considerable variations when compared to each other in size and corneal curvature. The axial length of the eye can range from 17 to 33 mm, but normally is 23 mm. The size of the cornea is approximately 9-11 mm vertically and 11-12 mm horizontally, with 0.5 mm thick in the centre and 0.75 mm thick peripherally (Smerdon, 2000). The increase of thickness from central to periphery in the cornea is due to the amount of collagen in the peripheral stroma. The cornea has an anterior curvature of 7.8 mm and a posterior curvature of 6.5 mm, making it convex and aspheric (Sridhar, 2018). In figure 1.1 we can see the structure of the eye.

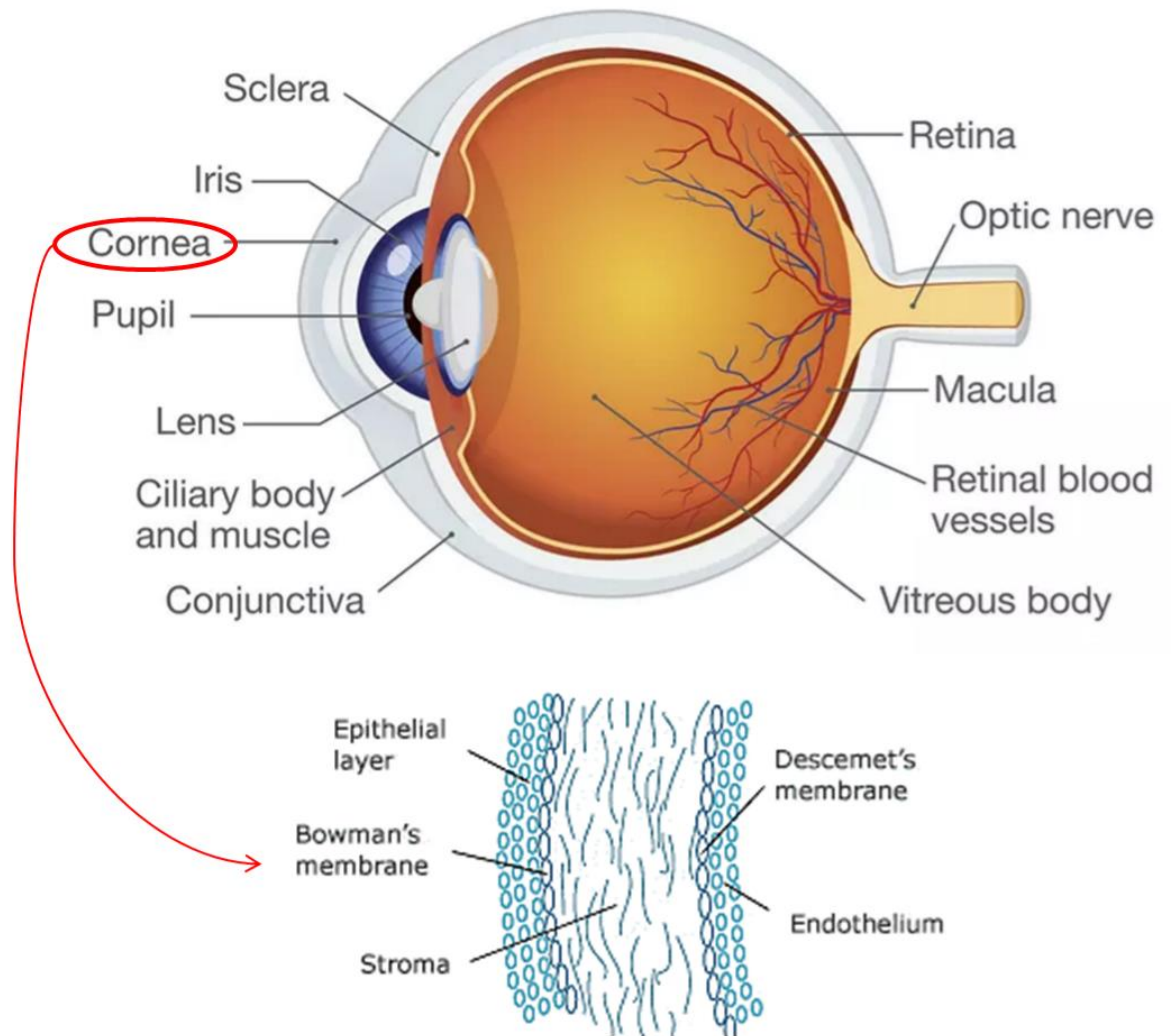


**Figure 1.1** Structures of the Eye. Upper image is a cross-sectional view of the adult human eye indicating indicates conjunctiva, iris, pupil, cornea, sclera, choroid, optic nerve, retina and vitreous humor. Bottom image is the layers of the cornea; epithelium, Bowman's membrane, stroma, Descemet's membrane, and endothelium(Excimer Clinic, 2020; Aboutkidshealth.ca, 2019)

The human cornea main functions are (i) to transmit and focus most of the light onto the retina with minimum scatter and optical degradation, and (ii) to protect the structures inside the eye. The cornea is a transparent avascular tissue comprised of five layers, stratified epithelium, Bowman's membrane, stroma, Descemet's membrane, and endothelium (Meek and Knupp, 2015). These five layers are composed of cellular and acellular components. Epithelial cells, endothelial cells, and keratocytes are the cellular components of the cornea, while the acellular components include glycosaminoglycans and collagen (Sridhar, 2018).

The epithelial layer is constituted of a non-keratinized, stratified, 5 to 7 layered squamous epithelium that makes 10% of the total thickness of the cornea approximately 50  $\mu\text{m}$ . These cell layers are composed of three types of cells; superficial, wing and basal cells. 2-3 layers are made up of superficial cells, with a thickness of 2-6  $\mu\text{m}$  and diameter of 40-60  $\mu\text{m}$ . Wing cells, or thawing cells, represent 2-3 layers as well. The last single layer is composed of basal cells, which have a cuboidal shape. Basal cells are active mitotically and have abundant organelles, making them capable of mitosis. Basal cells are the source of superficial and wing cells. The epithelium as well presents differences in its centre and peripheral area. In the central area the epithelium is 5-7 layers and there are no melanocytes or Langerhans cells. In the peripheral area the epithelium is 7-10 layered and have melanocytes and Langerhans cells. This epithelium is separated from the stroma by the Bowman's layer, which is a condensation of collagen (type I and V) and proteoglycans (Ramos, Scott and Ahmad, 2015; Sridhar, 2018).

The stroma is a transparent, collagenous, dense keratocyte fibrocyte containing and avascular layer that makes 80-90% of the total corneal thickness. Stroma transparency is due to the precise organization of stromal fibres and extracellular matrix. Three types of collagen can be found in the stroma, type I VI and XII, which are arranged in parallel bundles called fibrils. The fibrils are organised in layers that are called lamellae, and 200-250 lamellae constitutes the human stroma. It is important to notice that the collagen fibrils within the cornea are narrower than in other connecting tissue, which gives the cornea transparency. The major cells found in the stroma are Keratocytes. Keratocytes are able to synthesize glycosaminoglycans and collagen molecules, while maintaining stromal homeostasis. The Descemet's membrane separates the stroma of the monolayer of endothelial cells and is made of collagen type IV and laminin (Meek and Knupp, 2015).

The endothelium is a single layer, comprised of endothelial cells that are metabolically active. These specialized cells transport water and nutrients to and from the stroma to maintain optimal hydration and prevent corneal oedema. From the 5 layers that form the cornea, the superficial layers (stratified epithelium, Bowman's membrane and superficial stroma) are continuous with the conjunctiva (Di Girolamo, 2011; Ramos, Scott and Ahmad, 2015).

The conjunctiva is a thin loose transparent tissue that coats the opaque sclera and its functions are immune and secretory related, carried out by the Langerhans cells and mucin-producing goblet cells, respectively. The conjunctiva is divided by 3 zones: the bulbar region that has the function of cover the surface of the eye, the forniceal region that separates bulbar from palpebral, and the palpebral region that lines the inner surface of the eyelids. The corneal epithelium is separated from the conjunctival epithelium by a narrow band of limbal epithelium that encircles the cornea. This limbal epithelium is a barrier between the opaque vascularized conjunctiva and the clear avascular cornea, and also contains the stem cells that renew the corneal epithelium, also called limbal stem cells (LSCs) (Yanoff and Sassani, 2015).

### **1.3. Stem cells in the human eye**

The stem cells in the human eye can be generally divided into two main areas, the stem cells in the cornea and the stem cells in the conjunctiva. The reason of this difference is that even though they are close to each other, the corneal epithelial cells and the conjunctival epithelial cells belong to distinct lineages arising from different cell populations. When comparing the derived cysts of the epithelial cells it can be seen that limbal and corneal contain stratified squamous-type epithelial cells while the conjunctival contains stratified columnar-type epithelial cells interspersed with periodic acid-Schiff staining cells with a goblet-like structure (Z.-G. Wei, 1996).

#### **1.3.1. Stem cells in the cornea**

Limbal stem cells are located in the basal layer of the limbal epithelium; the epithelium is constantly renewed to replace the cells that are being detached from the corneal surface. This process is explained through the XYZ hypothesis of corneal epithelial maintenance. The XYZ hypothesis describes that the mass of corneal epithelium does not change under normal circumstances and can be seen as the resultant of three separate, independent phenomena. The proliferation of the basal epithelial cells represents X, the contribution to the cell mass by centripetal movement of peripheral cells is Y, and the epithelial

cell loss from the surface is Z. Therefore the corneal epithelial maintenance can be defined by the equation of  $X + Y = Z$ , which states that cell loss must be balanced by cell replacement (Thoft et al. 1983).

The cell replacement previously mentioned is maintained by the stem cells that are located in the limbal epithelium with original studies demonstrating this first in 1989 (Cotsarelis et al. 1989). The limbus is a zone that is highly vascularized and protected with melanin pigmentation against UV-light (Kruse and Schlo, 2005). Studies demonstrate that there is presence of limbal epithelial cells in a quiescent state but with a high proliferative response to injury (Cotsarelis *et al.*, 1989; Li *et al.*, 2014; Ramos, Scott and Ahmad, 2015).

The limbal stem cells, in the limbal epithelium, have been hypothesized to exist in niches within the palisades of Vogt. The theory was first proposed back in 1971 (Davanger M, 1971) and posterior research supported this theory, being one of the most recent studies, the one developed by Li's group in 2014 in which they isolated limbal stem cells and compared them with stromal cells. The results showed that the limbal niche cells have a significantly greater capacity to support limbal epithelial stem cells than stromal cells (Li et al. 2014). The palisades of Vogt are characterised with numerous undulations, with limbal papillae that extends downward into the stroma. These structures fulfil two purposes. First, the invaginations allow the basal limbal cells to interact with the rich vascular network that provides nutrients. Second, they provide an increased surface area, which allows a higher concentration of limbal stem cells within a small surface. Two other niche-like structures have also been identified within the adult limbal zone. The first is called focal stromal projections and are finger-shaped projections of limbal stroma that penetrate through to the epithelium. And the second can be called limbal epithelial crypts, and are limbal epithelial invaginations that radiate 5 to 7 solid cords of cells either circumferentially into limbal stroma or peripherally into conjunctival stroma (Hersh *et al.*, 2000; Dua *et al.*, 2005; Di Girolamo, 2011). In the following figure 1.2 is displayed the limbal structure – palisades of Vogt in a human eye.

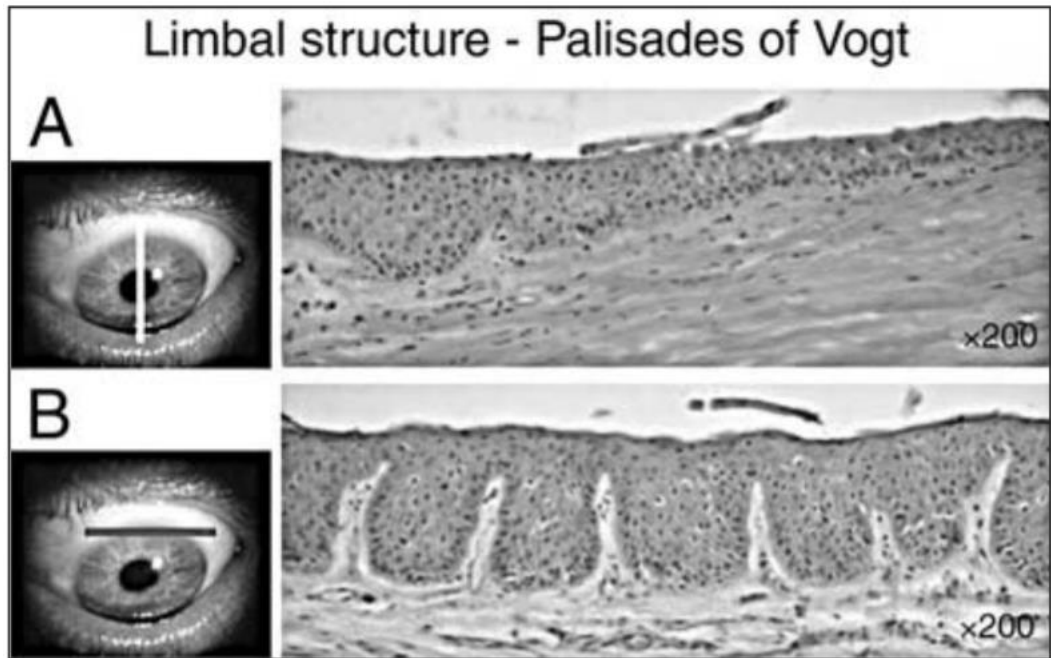


**Figure 1.2.** Haematoxylin-eosin staining showing palisades of Vogt limbal architecture by Chen. In A, a radial section can be seen, where corneal epithelial has five layers in the centre and 8-10 layers in the limbal area. In B a tangential section cut through the above section of the limbus, where can be seen the epithelial columns (Chen *et al.*, 2004).

To date, there are no definitive markers for these limbal stem cells. Putative positive markers, ABCG2 and p63 $\alpha$  can be highlighted, while for negative markers CK3 and CK12 can be mentioned as structural proteins found in the corneal epithelium (Kruse and Schlo, 2005; Ramos, Scott and Ahmad, 2015).

But it seems that the limbal zone is not the only reservoir of stem cells within the corneal epithelium. Recent studies in animal models have shown corneal epithelial maintenance without the input of the limbal zone, and self-maintenance of stem cells outside the limbal niche. These findings call to light the possibility of reservoirs of corneal stem cells that haven't been extensively described and that can be located at the central and peripheral cornea (Yoon, Ismail and Sherwin, 2014). For example, a study by Kameishi *et al.* showed remodelling of the rabbit corneal epithelium and basement membrane after 48 weeks without the presence of limbus (Kameishi *et al.*, 2014).

### 1.3.2. Stem cells in the conjunctival epithelium

Unlike the corneal localisation of stem cells, no current identified location of stem cells in the conjunctival epithelium has been completely accepted (Ramos, Scott and Ahmad, 2015). Some regions have been proposed, like the fornix region, the limbus, bulbar conjunctiva, the palpebral conjunctiva, and the mucocutaneous junction on the eyelid margin (Cotsarelis *et al.*, 1989; J. Pe'er, G. Zajicek, H. Greifner, 1996; Z.-G. Wei, T.-T. Sun, 1996; W. Chen, M. Ishikawa, K. Yamaki, 2003). It has also been suggested that conjunctival epithelial stem cells are located uniformly in the bulbar conjunctiva and the fornices (G. Pellegrini, O. Golisano, 1999). However, other studies point that the higher amount of conjunctival stem cells is found in the forniceal area (Z.-G. Wei, T.-T. Sun, 1996). The fornix may provide greater physical protection, intraepithelial mucous crypts, vasculature, and immune cells, features that are shared with other stem cells niches (Ramos, Scott and Ahmad, 2015). Rosalind Stewart studied in 2015 13 donor corneas and concluded that human conjunctival stem cells are predominantly located in the inferior forniceal areas and Medial Canthall. But more studies are needed as in her studies the age of the donors showed big impact in the potential to develop conjunctival stem cell-rich epithelium (Stewart *et al.*, 2015).

The markers for conjunctival stem cells are not clearly identified and there are only a few published studies in this area (R. P. Revoltella, S. Papini, A. Rosellini, 2007; A. Ramirez-Miranda, M.N. Nakatsu, S. Zarei-Ghanavati, C.V. Nguyen, 2011). The most commonly mentioned are ATP-binding cassette subfamily G member 2 (ABCG2) and the transcription factor p63. ABCG2 is a cell surface transmembrane transporter that is present in many adult stem cells, including limbal stem cells (Bunting, 2002). Conceptually, it may form a component of the molecular mechanisms by which long-lived stem cells reduce the potential for genomic damage over their extended lives, and their expression has been correlated with stem cell activity; p63 is a transcription factor that is known to be expressed by limbal stem cells and early transient amplified cells (Ramos, Scott and Ahmad, 2015; Stewart *et al.*, 2015).

Many of the previous findings and as well early testing of corneal treatments are made using animal models (Thoft, Friend and Murphy, 1979; Health, 2012; Ramachandran *et al.*, 2019). Medical research with animals is used when certain animals and humans share the

same illness. Due to this, rabbit is an animal that have been used for corneal research for a long time, but other animals like pig, cow, and mouse as well have been researched for this purpose (Grieve *et al.*, 2015; Understanding Animal Research, 2015). We will analyse this in the following section.

#### 1.4. Human corneal versus other animal species

For human eyes, two of the most used models are rabbit (Garner *et al.*, 1982; Biomaterials, 2007; Hitani *et al.*, 2008; Liang *et al.*, 2012; Kobayashi *et al.*, 2013; Griffith, Alarcon and Brunette, 2016) and pig (Brinkmann and Sc, 2000; Flueckiger *et al.*, 2005; Ang *et al.*, 2007; Lagali *et al.*, 2007; Elsheikh, Alhasso and Rama, 2008). In this research, we did not have access to human corneas (except for our short collaboration with LV Prasad in India (see Chapter 4)), and we used both rabbit and porcine cornea models. To understand our models it is important to know the differences between rabbit, pig, and human corneas.

The rabbit cornea has an horizontal diameter of  $13.41 \pm 0.34$  mm, a vertical diameter of  $13.02 \pm 0.30$  mm, and a thickness of approximately 0.41 mm, (Kaye, 1961; Bozkir *et al.*, 1997). The rabbit cornea is bigger than the human cornea that has in average 11.75 mm of horizontal diameter, and 10.55 mm of vertical diameter (Doughty and Zaman, 2000) and a thickness of approximately 0.535 mm (Bozkir *et al.*, 1997). The elastic modulus of the rabbit cornea is dramatically lower when compared to the human counterpart. This lower elastic modulus is due to the differences in the arrangement and spacing of the collagen (Jue *et al.*, 1986; Thomasy *et al.*, 2014). Regarding the relevance of limbal zone in rabbit eyes, rabbit cornea models have showed corneal regeneration with and without limbus present (Thoft, Friend and Murphy, 1979; Huang *et al.*, 2011; Kameishi *et al.*, 2014).

The porcine cornea also differs in size compared with the human cornea. Pig's corneas have a horizontal diameter of  $14.32 \pm 0.25$  mm, a vertical diameter of 12.00 mm, and a thickness of  $1.248 \pm 0.144$  mm (Sanchez *et al.*, 2011; Menduni *et al.*, 2018). When comparing the biomechanical properties between the human and pig cornea, they are similar only in tensile strength and the form of the stress-strain curve. But when comparing the stress-

relaxation properties of these corneas, they differ significantly. Considering this, porcine cornea is not comparable to a human cornea where viscoelastic behaviour needs to be considered; but if only tensile strength and stress-strain is consider, is an appropriate model to human cornea (Zeng *et al.*, 2001; Elsheikh, Alhasso and Rama, 2008). The limbal region in porcine eyes is more homogeneous distributed around the 360° of the eyes, which is more distributed when comparing to human's, where there are more crypts on the vertical axis rather than horizontal axis (Grieve *et al.*, 2015). Due to the distribution in the limbal region, getting tissue explants from this zone is more reliable when measuring the outgrowth, compared with explants from human cornea. In figure 1.3 is seen the human and porcine limbal morphology, where A is the human limbus and B is the porcine limbal.

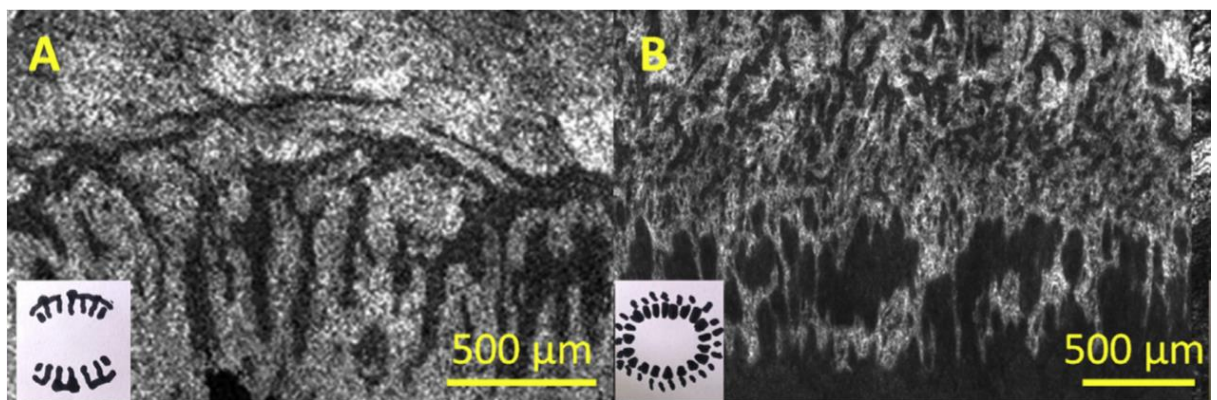


**Figure 1.3** Human and porcine limbal morphology extracted from Grieve et al research (Grieve *et al.*, 2015). En face FFOCM images, with illustrations of geometry of crypt structure and 360° distribution around the eye. A: Human, B: Pig.

Considering the similarities and differences between these 2 animal eyes and human eyes, it can be concluded that they are good candidates to be used as models to study corneal healing. Even though they have physical differences, biologically they hold key similarities (Lagali *et al.*, 2007; Pang, Du and Wu, 2010; Luo *et al.*, 2013; Ramachandran *et al.*, 2019).

## 1.5. Corneal Disease

Corneal disease is defined as visual impairment or blindness due to damage in the structure or shape of the cornea (Burton, 2009). The broad definition of corneal disease is what makes getting epidemiological data complicated and limited due to the wide variety of inflammatory and infectious disease involved (World Health Assembly, 2009). Corneal blindness can be defined as bilateral (both eyes affected) or unilateral (only one eye affected) (Buch, Vinding and Cour, 2001; Tarek Shaarawy, Mark B. Sherwood, 2009). Initially, it was reported in 2010 that 4.9 million people were affected by bilateral corneal blindness, but in 2016 a more precise study was made by Gain that reported that in 2016 the people affected by corneal blindness was nearly 10 million (Gain *et al.*, 2016). The prevalence of corneal blindness is not homogeneous in the world, as in India and Africa the people affected by corneal blindness represent a bigger percentage of total blind people (Oliva, Gulati and Schottman, 2012). Unilateral blindness is not registered in the WHO report, but Oliva's group estimate it was 23 million globally in 2010. Corneal scarring is as well the major source of permanent blindness in the world, as the complex pathophysiology of this disease is not completely understood (Chawla and Ghosh, 2018).

As mentioned earlier, the epidemiology aspect of corneal blindness can be due to a wide variety of diseases. It is important to mention that nearly 80% of people affected by corneal blindness could have been prevented. Corneal blindness is associated with poverty and is expected that as nutritional health and public sanitation improves globally, there should be a reduction of patients affected by corneal disease (World Health Assembly, 2009). The causes of corneal blindness can be separated in 7 groups (Burton, 2009):

- Infectious: Bacterial keratitis, Fungal keratitis, Viral keratitis, Trachoma, Onchocerciasis, Leprosy, and Ophtalmia neonatorum.
- Nutritional: Vitamin A deficiency (Xerophthalmia).
- Inflammatory: Mooren's ulcer, and Steven's Johnson Syndrome.
- Inherited: Corneal stromal dystrophies, and Fuch's endothelial dystrophy.
- Degenerative: Keratoconus.
- Trauma: Corneal abrasion, penetrating trauma, and chemical injury.

- Doctor-caused (iatrogenic): Pseudophakic bullous keratopathy.

To treat corneal blindness, corneal transplantation remains as the primary sight restoring procedure (Oliva, Gulati and Schottman, 2012). But, the primary issue with corneal transplantation is there is a considerable shortage of corneal graft tissue, being as extreme as only 1 cornea available for every 70 patients needing one (Gain *et al.*, 2016). In figure 1.4 can be seen a patient with bilateral corneal blindness.

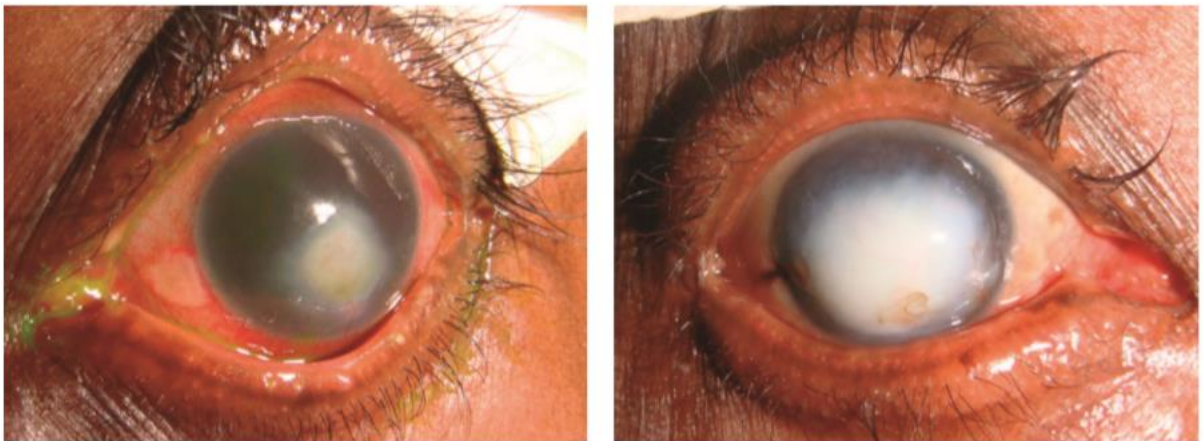


**Figure 1.4** Left and right eye of a patient affected by bilateral corneal blindness and the effect of corneal transplantation. In the left photo can be seen the left eye of the patient after weeks of receiving a corneal graft and starting to recover. In the right photo we see the right untreated eye with corneal blindness (Burton, 2009).

## 1.6. Corneal replacement surgical techniques

Corneal transplantation or keratoplasty is the most frequently used type of transplant in the world. As a transplant, it restores visual function to patients with severe damage in the cornea when they don't have any other option but to extract the damaged one for a new one (Gain *et al.*, 2016). The earliest use of Keratoplasty dates back to 1905, when Eduard Zirm did the first successful full-thickness penetrating corneal transplantation. Since then, keratoplasty have evolved to the point that the main concern about this technique is the availability of corneas in eye banks as they cannot match the worldwide demand (Tan *et al.*, 2012). In figure 1.5 is displayed that keratoplasty can be divided in 4 categories depending on the condition of the patient; full thickness opacity with poor endothelium, anterior stromal opacity with good

endothelium, posterior stromal opacity with good endothelium, and corneal decompensation with poor endothelium (Singh *et al.*, 2019).

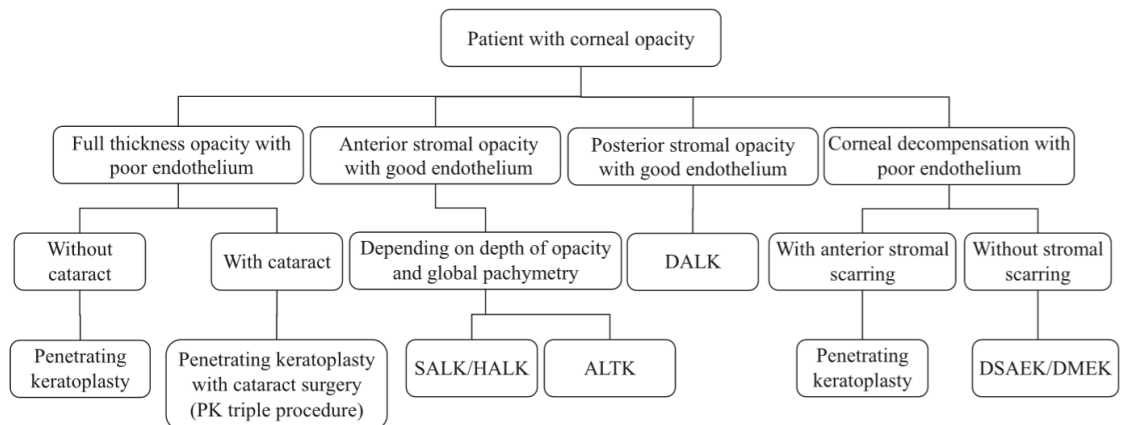


**Figure 1.5** Flowchart of the different keratoplasty indicated to patients depending on their corneal illness (Singh *et al.*, 2019). SALK, Superficial Anterior Lamellar Keratoplasty. HALK, Hemi-Automated Lamellar Keratoplasty. ALTK, Automated Lamellar Therapeutic Keratoplasty. DALK, Deep Anterior Lamellar Keratoplasty. DSAEK, Descemet Stripping Automated Endothelial Keratoplasty. DMEK, Descemet Membrane Endothelial Keratoplasty.

### 1.6.1. Penetrating keratoplasty

Despite the development and rapid adoption of new keratoplasty techniques, penetrating keratoplasty (PK) is still the most common corneal transplantation. Penetrating keratoplasty consist in replacing all 5 corneal layers in the patient and can be used for any indication (stromal or endothelial disease). It has good results in patients compared to other techniques due mainly that no lamellar corneal interface problems exist. Penetrating keratoplasty has some complications associated as well; it has a 20% of acute endothelial rejection after 5 years, endothelial failure is the major cause of transplant failure, and regular and irregular astigmatism is common in patients after surgery (Ramamurthi *et al.*, 2008; Rahman *et al.*, 2009; Patel, 2012; Tan *et al.*, 2012).

### 1.6.2. Selective lamellar keratoplasty

Selective lamellar keratoplasty is a corneal transplantation technique that involves the selective replacement of only the diseased layers of the cornea, trying to keep the healthy layers in it. Anterior lamellar keratoplasty (ALK) consists in replacing varying amount of stroma

layers, retaining the endothelium and Descemet's membrane. Even though anterior lamellar keratoplasty is a more technically demanding technique than penetrating keratoplasty, the risk of complications is lower than PK including transplant rejection (Tan *et al.*, 2012).

Superficial anterior lamellar keratoplasty (SALK) is a corneal transplant used mainly to treat corneal opacities involving anterior 30-40 percent of the cornea. This surgery is sutureless and replaces the host with a lamellar graft using fibrin glue. SALK is mainly indicated for superficial scars (Singh *et al.*, 2019).

Automated lamellar therapeutic keratoplasty (ALTK) is a technique used for treatment of anterior to midstromal corneal opacities. This technique makes use of microkeratomes for lamellar keratectomies, which makes more congruous lamellar dissection of the donor and host cornea. Due to the donor and host corneas have smooth opposing surfaces, the interface problems are reduced which improve the visual outcome (Vajpayee, Vasudendra and Titiyal, 2006).

Deep anterior lamellar keratoplasty (DALK) is a surgery performed when the patients are affected by deep anterior corneal opacities but have good endothelial function. This technique can be separated in two types, pre-Descemetic and Descemetic. Pre-Descemetic DALK is performed when the cornea is thin and exist a risk of perforation. Descemetic DALK is performed removing the complete stroma leaving only the Descemet's membrane (Singh *et al.*, 2019).

### **1.6.3. Endothelial keratoplasty**

Endothelial Keratoplasty (EK) is a technique that involves stripping the endothelium and Descemet's membrane from the host stroma, to later attach the donor tissue without sutures using air tamponade. The main complication of this technique is that the lamellar adhesion of the donor graft is unpredictable, resulting in various rates of dislocation (Tan *et al.*, 2012).

#### 1.6.4. Ocular surface transplantation and new surgical approaches

The ocular surface can be separated in two different mucosal epithelial, corneal and conjunctival. To maintain a healthy epithelium, corneal limbal stem cells are very important and the lack of these cells, also called limbal stem cell deficiency (LSCD) can result in acute injury. When this happens, the adjacent inflamed conjunctival epithelium covers the corneal epithelium with sub-epithelial fibrosis and vascularisation which results in corneal blindness (Tan *et al.*, 2012).

Different techniques have been used to treat corneal blindness or limbal stem cell deficiency (LSCD) including conjunctival limbal autografting (CLAU) technique and cultivated limbal epithelial transplantation (CLET) technique. These techniques are generally effective in long-term restoration of a damaged ocular surface but they have associated limitations (see below) which prompted the need of the development of new approaches (Sangwan *et al.*, 2012).

Conjunctival limbal autografting (CLAU) proposed by Kenyon and Tseng (Kenyon and Tseng, 1989) is an eye surgery approach that involves the transplantation of two donor lenticules, consisting of the limbus and adjacent conjunctiva, from the donor eye to later be fixed on the recipient ocular surface over amniotic membrane used as scaffold. Miri *et al.* showed that this technique was a safe procedure (Miri, Al-Deiri and Dua, 2010). The procedure consists in marking 2 clock-hours superior and inferior areas of the limbus (with a surgical marker pen), then mark 3x3 mm of the adjacent conjunctiva, then excised. They also address the limitations that this technique can have with the potential risk of donor site infection and decompensation of donor corneal epithelium, as some cases that were reported as unilateral corneal blindness were in fact bilateral (Miri, Said and Dua, 2011).

Considering the limitations of CLAU technique with patients that have bilateral corneal blindness, Pellegrini and her group proposed the cultivated limbal epithelial transplantation (CLET) technique. In this technique cells are cultivated from a 1 mm<sup>2</sup> biopsy sample of the limbus of the healthy eye. After 16 days of this procedure, a graft is generated from confluent secondary cultures mounted on either petrolatum gaze or a soft contact lens (Pellegrini *et al.*,

1997). Although this technique has been found to be effective for the treatment of limbal stem cell deficiency, the occurrence of immune rejection is still present. Immune rejection in CLET surgery facilitate cell death and failure of ocular surface reconstruction, and cannot be avoided as it is due to the expression of mature major histocompatibility class II molecules on cultivated limbal epithelial cells (Qi *et al.*, 2013). The rejection that was analysed by Qi showed that they were consistent with the T-cell mediated rejection phenomenon when comparing impression cytology and the allogeneic corneal epithelial cells are the target of the immune system (Qi *et al.*, 2013).

When compared these two techniques, CLET resulted in providing better vision and clinical results with less stromal scarring when compared to CLAU. The pro-inflammatory cytokine IL-8 was found to decrease more rapidly in the eye with CLET than CLAU. Also it is hypothesised that the almost immediate epithelialization achieved by CLET was due to the cultivated epithelial sheet in the amniotic membrane surface; the substrate may have contributed to faster ocular rehabilitation (Ang *et al.*, 2007). Despite this, the costs involved in using this technique, considering that needs specialised expertise and a licensed laboratory for the 2 weeks culture, are highly expensive (in 2010 reported to be 10,300 pounds per sheet), therefore, limbal tissue transplants are still the gold standard (Miri, Al-Deiri and Dua, 2010).

Sangwan and MacNeil proposed in 2012 the simple limbal epithelial transplantation (SLET) as a third option that could combine both existing techniques and, at the same time, avoid some of their drawbacks. This technique involves the direct transplantation of a small limbal fragment from a donor eye to the recipient eye (Sangwan *et al.*, 2012) (figure 1.6.). To perform this, a 2x2 mm area of the superior limbus is marked in the donor eye, to later incise the conjunctiva and subconjunctiva to reach the limbus. After reaching it, a dissection is done to remove 1 mm of the limbus, to later be excised and placed in a balanced salt solution. After placing the small limbal fragment in the salt solution, the recipient eye is prepared. A 360° peritomy is performed in the recipient eye and its vascular pannus covering the cornea is removed, cauterising the bleeding points. Later, a human amniotic membrane graft is fixed over the now bared ocular surface with fibrin glue. The donor small limbal fragment is taken out and cut into 8 to 10 small pieces gently. The small pieces, epithelial side up, are fixed with fibrin glue on the human amniotic membrane graft and distributed around it forming a circular shape

avoiding the visual axis (Sangwan *et al.*, 2012). In figure 1.6 can be seen the clinical photographs of this SLET technique for a clearer visualisation.

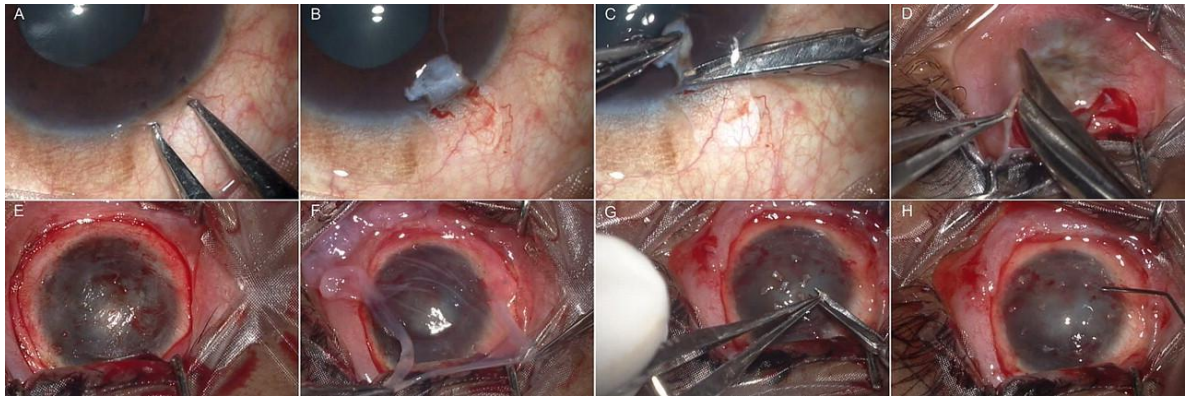


**Figure 1.6** Clinical photographs showing the SLET technique by Sangwan and his group. **A** an area is selected in the superior limbus of the donor eye of approximately 2x2 mm. **B** sub-conjunctival dissection of 1 mm into the clear cornea. **C** limbal tissue is excised. **D** Peritomy is performed in recipient eye. **E** fibrovascular pannus is excised. **F** human amniotic membrane graft is fixed with fibrin glue to the bare ocular surface. **G** the limbal tissue excised from donor eye is cut into 8 to 10 small pieces. **H** the limbal tissue pieces are fixed to the amniotic membrane with fibrin glue (Sangwan *et al.* 2012).

After this surgery, a soft bandage contact lens is placed on the recipient eye and one drop of 2.5% povidone-iodine is applied in donor and recipient eye, followed by overnight patching. The post-operative care includes ciprofloxacin 0.3% eye drops, prednisolone acetate 1% eye drops, and carboxymethyl cellulose 0.5% eye drops (Sangwan *et al.*, 2012).

It has already been demonstrated that when comparing SLET technique with CLAU technique in terms of safety, efficacy, and clinical outcome, both techniques are equally effective in achieving a stable ocular face; but, SLET requires minimal donor tissue compared to CLAU and therefore is the preferred option (Arora, 2017).

In 2016, Vikas Mittal and his group performed SLET in children (less than 15 years old) and did a follow up of these cases. The children were affected by severe unilateral in acute and late phases of chemical injury. In their results can be seen that after the first SLET performed in the children there was only a 25% of success rate, but after a second SLET was done the success rate improved to 100%. The most likely reason reported for this is that the chemical burns were grade 6 with an extensive limbal stem cell deficiency. The ocular surface remained stable for 60 months pointing towards the long-term efficiency of this procedure. Finally, it is interesting to highlight that the success rate reported for the CLAU technique in chemical

injuries is of 46.7% and is lower in child than in adults, making SLET technique a very promising treatment for limbal stem cell deficiency (LSCD) in children (Mittal *et al.*, 2016).

Sayan Basu and his group analysed the clinical outcome of 125 cases of unilateral chronic ocular surface burns that were treated with SLET technique during 2010 to 2014. With an average follow up of 1.5 years, 95 of 125 eyes maintained a successful regenerated stable corneal surface without infection, progressive conjunctivalization, development of persistent epithelial defect, or need to repeat SLET. This study shows that SLET is a promising technique compared to the previous ones and with a large amount of patients suffering a hard to treat injury (Basu *et al.*, 2016).

Other promising results were obtained by Arya and his group when treated a 14 years old patient with hydrochloric acid injury and a 63 old patient with severe dry eyes. Both patients after 4 weeks of the SLET technique being used on them were presenting a completely epithelialized, avascular and stable corneal surface (Arya *et al.*, 2016). Also it was reported that SLET achieved good outcomes in a case of ocular surface thermal burn with a patient that presented a molten metal ocular burn (Das, Basu and Sangwan, 2015).

Finally, two new surgical techniques are getting attention lately to improve the outcome of keratoplasty, these are Intra-operative optical coherence tomography (iOCT) and Femtosecond laser-assisted lamellar keratoplasty (FALK). iOCT is a technique that provides continuous feedback of operative surgical manoeuvres helping in the precision in techniques like selective lamellar keratoplasty. FALK is a technique that improves the accuracy of the cuts needed in these precise surgeries, which implies a better alignment of tissues that reduce post-operative problems like astigmatism and epithelial healing (Singh *et al.*, 2019).

## 1.7. Corneal scaffolds

As it has been mentioned before, the main problem to treat corneal blindness has always been the availability of donor corneas. Therefore, the use of scaffolds as cell carriers has been the next step in treating corneal disease. So far, the Human Amniotic Membrane

(HAM) has been the gold standard in this aspect, but new scaffolds with different features have been developed to deal with amniotic membrane limitations.

### 1.7.1. Amniotic membrane

Human amniotic membrane (HAM) is a thin semitransparent membrane with a thickness of 0.2 to 0.5 mm. Three main layers compose HAM, which are the inner compact layer, middle fibroblast layer, and the outermost spongy layer. HAM is frequently used in the field of tissue engineering due to its advantages as a biological membrane and as well a cell carrier. The Amniotic membrane stimulates re-epithelialization through growth factors. HAM basement membrane has been reported to reduce inflammation by anti-angiogenic properties and anti-fibroblastic activity, preventing scarring. In corneal transplantation field, HAM acts as an extracellular matrix as is rich in collagen (I, III, IV, V, and VI), hyaluronic acid, laminin, proteoglycans, elastin, and fibronectin, providing similar features to the corneal epithelium and conjunctival when using as scaffold. Finally, HAM is a good scaffold for corneal regeneration from a mechanical point of view, as its toughness and elasticity provides protection and support to the epithelial cells, promoting the adhesion and migration of them (Le and Deng, 2019; Brouki *et al.*, 2020). It was reported by Vajpayee's group that amniotic membrane transplantation alone is enough for patients with partial limbal stem cell deficiency without the need of stem cell transplantation (Sharma *et al.*, 1998).

Although HAM has many positive properties as a scaffold for corneal regeneration and is the gold standard for this case, is far from being a perfect answer to the corneal deficit. Between the limitations involved in using amniotic membrane is that has been demonstrated that using HAM can cause immunological reactions in the host, which increase the risk of transmitting infections, especially intracellular pathogens that could lead to graft rejection. It is due to this issue that using fresh HAM is not recommended, and a more specialised process of collection and decellularization are needed. Adding these steps, needed to ensure the health of the patient, makes HAM a not easily worldwide option to have, and suffers of access limitations same as corneal donors (Dehghani, Rasoulianboroujeni and Ghasemi, 2018; Brouki *et al.*, 2020). Therefore, there is still a need to have a more trustworthy, easily-accessible option (Tan *et al.*, 2012).

### 1.7.2. Biological scaffolds aside of amniotic membrane

Biological scaffolds are membranes or grafts that can be obtained from animals, humans or derived from them. As amniotic membrane has its limitations, through the years different options have been explored.

Collagen-based carriers are naturally biocompatible and an obvious choice as scaffold considering that the main component of corneas is collagen. Collagen is easy to isolate and animal-derived are cost-effective options. But there are concerns when using animal collagen considering the purity of it and the immunological reaction that it can cause. It has been demonstrated that limbal epithelial stem cells can be successfully cultivated in collagen. When using collagen as hydrogel, it has weak mechanical properties due to the high water content. To improve the mechanical properties of collagen two techniques have been developed, chemical crosslinking and plastic compression (Feng *et al.*, 2014). Cross-linked collagen gel has been tested with positive results as the gel was optically clear and robust enough to withstand manipulation, as well as seeing cells growing on them (Parenteau-bareil, Gauvin and Berthod, 2010). On the other hand, plastic compressed collagen gels were made to increase the mechanical strength of the material by reducing its water content, resulting in cells growing in a more homogeneous way (Mi *et al.*, 2010).

A more advanced membrane using collagen hydrogel is Real Architecture for 3D Tissues (RAFT) which involves casting and setting collagen hydrogel in a predetermined shape before being compressed. Due to the compression, the water loss is fairly controlled and is highly reproducible (Levis *et al.*, 2015). The big limitation of this technology is that even though there is some level of control in the water loss, is not completely controlled, and therefore cannot be moved to patients yet.

Fibrin membranes have been investigated as well. Fibrin can be easily fabricated by combining thrombin and fibrinogen and is a degradable natural substrate. Using dishes to create layers of 1:1 fibrin resulted in confluent human limbal epithelial stem cells sheets in only two weeks (Rama *et al.*, 2001). This group further worked with this fibrin sheet in transplantation, having as a result of renewing the corneal epithelium in 76.6% of the eyes (Feng *et al.*, 2014).

Holoclar® is a technique that has been approved to be used in Europe and UK. Holoclar® works as follows: a biopsy is taken from a healthy limbus, and then the sample is transported to the company where the cells are cultured. In the company, a fibrin matrix is used to let the cell expand forming discs, and then the discs are transported back to the patients (Milazzo, De Luca and Pellegrini, 2016). The limitations in this techniques are clear though, the fact that involves the need to transport samples to Italy and back to the patient reduces the readiness of the technique as well as increasing its cost.

### 1.7.3. Synthetic Polymeric scaffolds

Considering the limitations of the amniotic membrane, and the high cost of the biological membranes, is that the use of synthetic polymer-based scaffolds has been explored. Polymers are generally easy to store and easy to work with. At the same time, due to the ease of access and handling, production to deal with the global need could be achieved faster this way. During the past 2 decades different polymers have been tested as scaffolds for corneal regeneration.

Some polymeric scaffolds for corneal regeneration are already in the market. Boston Keratoprosthesis® and AlpaCor® are artificial corneas. Boston Keratoprosthesis® is a synthetic cornea composed of poly-methylmethacrylate and is the most used keratoprosthesis in the world. Boston Keratoprosthesis® have a low failure time of less than 2 years and the rigidity of poly-methylmethacrylate could lead to increase pressure in the eye and thus generating glaucoma (Shanbhag *et al.*, 2018; Sinha and Gupte, 2018). Alphacor® on the other hand is a 2 phases poly(2-hydroxyethyl methacrylate). Alphacor® has fewer cases of complications when compared to Boston Keratoprosthesis®, but still, same as Boston Keratoprosthesis®, Alphacor® has a low survival rate of the implant (Juraskova *et al.*, 2011).

Leaving aside the polymeric options that are already in the market, other polymers have been used for corneal repair research. Polymethacrylate-based, Poly (ε-caprolactone)-based, and Poly(lactide-co-glycolide)-based membranes have been used with positive results.

Polymethacrylate-based membranes are synthetic but have been used in ophthalmic applications such as contact lenses. As hydrogel, it can be fabricated to be transparent. Human corneal epithelial cells and bovine keratocytes have been cultured in these membranes showing good attachment of the cells to the scaffold, as well as good proliferation (Rimmer *et al.*, 2007). But in this case complete re-epithelialization was not achieved, however, this was modified after coating it with collagen IV.

Poly (ε-caprolactone) or (PCL) is a biocompatible polyester that is already extensively used for bone, skin, and mesenchymal stem cell applications. PCL membranes can support the proliferation and attachment of conjunctival epithelial and limbal stem cells. The cells growing in PCL membranes have showed similar characteristics to same type of cells cultured in human amniotic membrane (Ang *et al.*, 2007; Kim, Kim and Park, 2018).

Poly(lactide-co-glycolide) or (PLGA) is a biodegradable and biocompatible copolymer that is approved for use in medicine by the Food and Drug Administration. PLGA scaffolds have been used in our research group with very positive results (Ortega, Ryan, *et al.*, 2013; Ortega, Sefat, *et al.*, 2014; Ramachandran *et al.*, 2019). After only two weeks of culture, rabbit limbal epithelial cells were able to form layers in the scaffolds. Another aspect important in using PLGA for corneal regeneration is its degradation time, where can be seen that PLGA disappeared after two months of culture (Sefat *et al.*, 2013).

Focusing in PLGA, previous work done by our group have demonstrated that PLGA 50:50 can be degraded completely in rabbit eyes after one month post-surgery (Ramachandran *et al.*, 2019). The way that PLGA was treated was by electrospinning it, creating a fibrous membrane that successfully created a microenvironment that supported cell outgrowth from the limbal explants. In the next section electrospinning will be defined, considering its advantages and its characteristics.

## 1.8. Electrospinning

For early research applied to health sciences is critical to reproduce conditions *in vitro* as similar to reality as possible. 2D conditions work well for yeast or bacterial growth, but they have shown to poorly simulate the conditions in living tissues in which cells are naturally

placed in 3D environments (Liu, Thomopoulos and Xia, 2012; Lei *et al.*, 2013). Electrospinning offers great potential in terms of 3D scaffold design providing mats of fibres in the region of the micro-nano scale which, to a certain extent, can simulate the native extracellular matrix (ECM) (Liu, Thomopoulos and Xia, 2012; Choi *et al.*, 2015). Electrospinning is an efficient technique to make scaffolds for 3D cell culture and for tissue engineering applications (Wendorff, Agarwal and Greiner, 2012).

Electrospinning allows production of micro and nanofibers with diameters down to a few nanometers from a broad range of polymers. The typical electrospinning set up comprises a syringe with a metal tip, a solution of a polymer in a solvent, a pump or mechanism to control the flow out of the syringe, a metallic collector or receptor of the fibres, and a high-voltage appliance (Wendorff, Agarwal and Greiner, 2012; Ding, Wang and Yu, 2018). In the following figure we can see a simplified electrospinning setting as previously described.

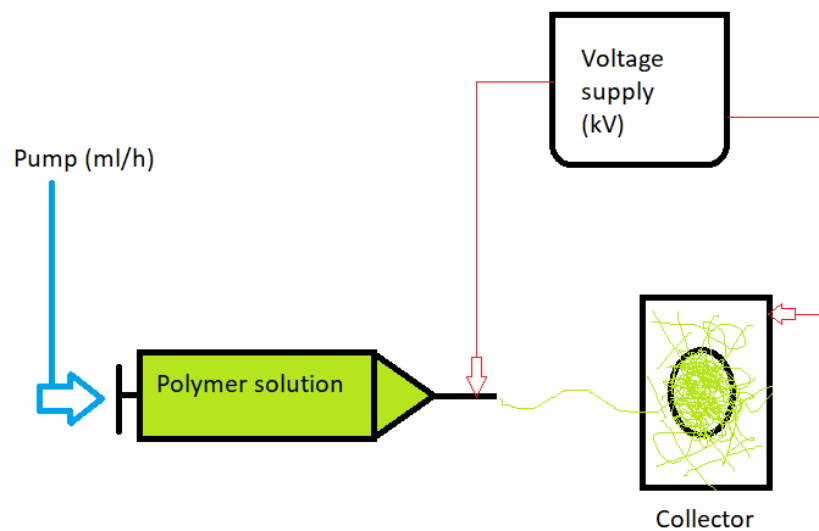


**Figure 1.7** Electrospinning set-up. The set-up consists of; a pump that will control the flow; the polymer solution that will be electrospun; a voltage supply which control the voltage of the electrospinning; and finally a collector where the fibres will land and create a scaffold.

Electrospinning works when a sufficient voltage is applied between the tip of the syringe acting as an electrode and a collector (or aluminium foil) acting as a counter-electrode. By the action of the voltage, the droplets that are being expelled of the syringe forming a point

of eruption known as Taylor cone. Depending on the molecular cohesion of the polymer solution, a stream can occur that will form a fibre when it dries in flight (Joachim H. Wendorff, Seema Agarwal, 2012).

It is important to note that electrospinning will vary depending of the working parameters used on it. These parameters are important to understand the nature of the electrospinning as well the conversion of polymer solutions into nanofibers. These conditions have been broadly divided into three; solution parameters, ambient parameters, and process parameters. Making variation in any of these 3 conditions involves changes in the morphology and diameters of the electrospun fibres and are presented in table 1.1 (Tong and Wang, 2010; Li and Wang, 2013; Khanlou *et al.*, 2014):

**Table 1.1** Overview of electrospinning parameters and their effects.

Parameters	Sub-parameter	Effect
Solution	Concentration	At low concentrations of polymer solution the electrospinning will form nano-particles, which is what is called electrospray. When the concentration is high, helix-shaped micro-ribbons can be observed instead of fibres (Li and Wang, 2013).
	Molecular weight	Lowering the molecular weight of the polymer will make the electrospinning form beads. At high molecular weights micro-ribbons can be observed (Li and Wang, 2013).
	Viscosity	In low viscosities, smooth and continuous fibers cannot be obtained. Hard ejections of polymer solution are detected with high viscosity (Li and Wang, 2013).
	Surface tension	Surface tension determines the boundaries of the electrospinning when all the other conditions are

		fixed. Changes in surface tension can lead to beaded fibers (Li and Wang, 2013).
	Conductivity	The solution conductivity is determined by the polymer and solvent. But the conductivity can be changed by adding ionic salts. Increasing the conductivity helps in reducing the beads in the fibers (Li and Wang, 2013).
Processing	Voltage	The voltage in the electrospinning process is crucial, as the voltage applied will form the Taylor cone. The effect of voltage in fibre diameter has been studied with different polymers, and some groups report no changes. But, some other groups have reported that higher voltages increase the electrostatic repulsive force favouring the narrowing of fibers (Li and Wang, 2013).
	Flow rate	Lower flow rates are usually recommended as the electrospinning solution will have enough time for polarization. While if the flow is too high, bead fibers and thick diameter of fibers can be seen (Li and Wang, 2013).
	Collectors	Collectors can vary in its shapes, and thus give complexity to the fiber alignments (Li and Wang, 2013).
	Distance	If the distance is too short, the fibers will not have enough time to solidify. And in the opposite, if the distance is too long, beads will be formed (Li and Wang, 2013).
Ambient	Temperature	With some polymers, increasing the temperature favour the formation of thinner fibres when there is a relationship between temperatures – viscosity (Li

		and Wang, 2013).
	Humidity	Low humidity can increase the solvent evaporation speed. On the other hand, high humidity can lead to thicker fiber diameter (Li and Wang, 2013).

Previously in our group, Dr. Ilida Ortega was able to electrospun PLGA (50:50) creating complex design mimicking limbal niches with positives results in cell outgrowth in them (Deshpande, Ramachandran, Sefat, *et al.*, 2013; Ortega, Sefat, *et al.*, 2014). Considering the positive results, we will keep using this polymer as our main polymer to create electrospun scaffolds for corneal regeneration.

It is important to considerer that creating a microenvironment with a good 3D-structure and porosity is not always the only factor that needs to be given by the cell carrier. Factors like stiffness, elasticity and degradability need to be controlled for achieving a successful cell response. In the following section the effect of stiffness will be highlighted and its effect in corneal cell growth.

## 1.9. Effects of stiffness of scaffolds in cell culture

It has been already mentioned how different cell cultures can behave when they are in a two dimensional (2D) culture versus their three dimensional counterpart. Between the differences that can be seen when compared 2D vs 3D culture is that cell morphology, proliferation rate, gene expression, and metabolic pathways are affected and 2D differs importantly when compared to *in vivo* conditions, which 3D is closer. The factors that make 3D cultures closer to *in vivo* conditions are many, however, the stiffness and composition of the microenvironment should be highlighted. These two factors have been demonstrated to affect cell morphology, signalling, cytoskeletal structure, and function and differentiation of normal and cancel cells (Breuls, Jiya and Smit, 2008; Peyton *et al.*, 2011; Xu *et al.*, 2019).

For corneal regeneration, it has been demonstrated that stiffness of the cell carrier plays a role as well. It was previously mentioned that human amniotic membrane is the gold standard as the scaffold to be used in corneal regeneration due to its mechanical properties, therefore knowing the effects of stiffness in corneal cells is fundamental for biomaterial design. The importance of keeping the mechanical properties in corneas have been explored, and in the case of decellularized corneas, the most important properties that need to be kept are tissue transparency and mechanical strength (Wilson *et al.*, 2013). But the importance of the mechanical properties of the membrane used as cell carrier are not only limited to basic support of cellular layers, but as well have been demonstrated its importance in the refractive effect of the cornea (Bao *et al.*, 2012).

The phenotype of human limbal epithelial stem cells is highly dependent of the mechanical properties of their substrates. Ricardo Gouveia and Che Connon have studied the biomechanical effect of the cornea and limbus with the limbal epithelial cells. In their findings, the limbus is softer (lower bulk modulus) compared to the centre of the cornea. The difference in stiffness between these two sections of the cornea is due that in the limbus is where the limbal epithelial cells mainly reside. Finally, they have concluded that it exists a phenotype-through-biomechanics correlation between the limbal epithelial stem cells and the stiffness and through this the cells could be modulated in its phenotype (Cardona *et al.*, 2017; Gouveia *et al.*, 2018, 2019).

It was mentioned that human amniotic membrane is the most often used option of a cell carrier for corneal regeneration. However, it has been analysed that the success rate of cornea regeneration using amniotic membrane as the cell carrier varies depending on the stiffness of this material (Chen *et al.*, 2012). Therefore using amniotic membrane increase variability in the reproducibility of results when used as a cell carrier. With this in mind, a more reliable membrane that can have reproducible mechanical properties is needed.

In addition, our group has closely interacted with representatives at L. V. Prasad Eye Institute (Hyderabad, India) for trying to achieve a better understanding of what is required in a membrane to be able to replace amniotic membrane as a cell carrier in SLET surgery. For this purpose, they had access to the electrospun PLGA scaffolds developed and tested

successfully in rabbit limbal explant models (Ortega, Deshpande, *et al.*, 2013; Ramachandran *et al.*, 2019). From these interactions it became clear that previous PLGA-based scaffolds presented high levels of brittleness and high stiffness after being delivered from UK to India. AM substitutes should be easy to handle for surgeons and able to resist minimum stress from handling in SLET surgery: finally, that the membrane should be highly hydrophilic since surgeons will wet it before use. Due to this, previous work developed in the group was not entirely successful in creating a cell carrier that could replace the amniotic membrane, mainly because the mechanical properties of previously developed electrospun membranes were too stiff and hard to handle by surgeons.

### **1.10. Findings from literature review and motivation for the project.**

Various approaches have been tested to improve the quality of life of the population affected by corneal blindness. Even though SLET has shown good results compared to previously established surgical techniques, the use of amniotic membrane is not an optimal option. There are disadvantages in using amniotic membrane as a graft material, for example, it does need to be harvested and banked under tissue banking conditions to reduce the risk of bacterial infections and its availability is reduced, among other possible associated Ethical issues (Feng *et al.*, 2014). Therefore a solution involving an easier accessible option is required.

One approach that has been explored in our group is the use of Poly (lactide-co-glycolide) or PLGA as a surface for limbal explant culture. The advantages of PLGA are (i) its degradation time can be controlled by varying the ratio of PLA and PGA (and it can achieve degradation rates comparable to those experienced when using the amniotic membrane) and (ii) it has been already approved for medical use in human. This minimises the time required to be tested and approved to be used as a biomaterial for cornea treatment (Ogunbanjo and Macneil, 2010).

Previously in our group electrospun PLGA scaffolds were proposed as an alternative to be used in SLET technique for the replacement of the amniotic membrane. One of the

objectives was to introduce within the design of the corneal carrier microfeatured structures to mimic to a certain extent the limbal region of the eye (the limbal crypts). Mimicking stem cell niches is a strategy that aims to elucidate stem cell-regulatory mechanisms, harnessing their regenerative capacity *in vitro* (Donnelly, Salmeron-sanchez and Dalby, 2018). Stem cells niches are crucial for different cellular functions like adhesion, proliferation, and differentiation. Being able to successfully mimicking a stem cell niche has been one of the objectives in the development of new biomaterials for clinical use (Ravichandran *et al.*, 2009). In this work Poly (ethylene glycol) diacrylate (PEGDA) rings mimicking the shape of the limbus were used as templates to then produce via electrospinning a PLGA 50:50 electrospun matrix. Then, rabbit limbal explants were placed on the models and re-epithelisation of rabbit wounded corneas was achieved. The study also reported that the microstructures included in the scaffolds influenced cell migration and directionality. Therefore it was shown that the 3D macrostructure of the carrier plays an important role in influencing cell behaviour and in enhancing, to a certain extent, cell maintenance (Deshpande, Ramachandran, Sefat, *et al.*, 2013; Ortega, Sefat, *et al.*, 2014).

However, because of medical regulations we needed to keep the solvent content in the the PLGA scaffolds to a minimum. Since the solvent acted as a softener the scaffolds became too brittle and stiff once the solvent was completely removed for use in the clinics of L. V. Prasad Eye Institute (Hyderabad, India). Therefore modifying the mechanical properties of these scaffolds is needed, but without modifying the advantages of the scaffolds, like their excellent properties for cell outgrowth and their degradation time. We have explored that PCL has been used as a corneal graft with positive results, so maybe a combination of different polymers, without affecting the biological properties of the scaffolds, can be an option (Kim, Kim and Park, 2018). Electrospun scaffolds made of PLGA and PCL have been done previously with positive cell outgrowth in other cell types, which is promising to see their effect on limbal epithelial stem cells (Subramanian, Maheswari and Sethuraman, 2012; Zhao *et al.*, 2016).

## 1.11. Aim and objectives

The aim of this project is to design and manufacture microstructured and mechanically-controlled electrospun corneal membranes to be used as future amniotic membrane substitutes.

To achieve these aim, we have divided our work in 3 chapters;” Production of a mechanically tailored electrospun scaffold that can be used as a cell carrier for corneal repair techniques”, “Bio-compatibility of mechanically tailored electrospun scaffolds using animal limbal explant model”, and “Exploring effect of topography in the manufacturing of electrospun scaffolds”

For the above 3 chapters the following objectives will be explored:

Chapter 2: Production of a mechanically tailored electrospun scaffold that can be used as a cell carrier for corneal repair techniques.

- 1.- Optimise electrospinning conditions for the manufacture of PLGA and PLGA plus PCL membranes .
- 2.- Characterise PLGA electrospun scaffolds mechanical properties, to determine its shortcoming as a good scaffold candidate for corneal repair.
- 3.- Analyse the effect of adding PCL to make PLGA-PCL blend electrospun scaffolds.
- 4.- Determinate an optimal PLGA-PCL concentration to make an electrospun scaffold that can be mechanically acceptable to be used in corneal repair techniques.

Chapter 3: Bio-compatibility of mechanically tailored electrospun scaffolds using animal limbal explant model.

- 1.- Optimise a protocol for limbal explant cell culture on electrospun scaffolds using rabbit and porcine explants.
- 2.- Compare cell outgrowth from limbal explants from rabbit and pig origin using fluorescence microscopy.

- 3.- Analyse and quantify cell outgrowth from limbal explants at different time-points of culture and at difference distances within the scaffold.

Chapter 4: Exploring effect of topography in the manufacturing of electrospun scaffolds.

- 1.- Manufacturing of collectors with different designs to develop topographically complex electrospun scaffolds.
- 2.- Preliminary assessment of topography complex electrospun scaffolds with specialists in L. V. Prasad Eye Institute using human limbal explants and studying key physical changes of the membranes (shrinkage) that can have an impact in their clinical use.
- 3.- Developing a reproducible and robust technique to analyse fibre orientation in complex electrospun scaffolds.

## Chapter 2: Modifying mechanical properties of electrospun PLGA membranes via the addition of Polycaprolactone

### 2.1.- Introduction

As mentioned in the literature review, the main problem to treat corneal blindness has always been the availability of donor corneas (Gain *et al.*, 2016). As a replacement, human amniotic membrane has been the gold standard as a cell carrier in corneal transplantation surgeries; however, it can also cause immunological reactions and transmit infections, therefore there is still a need for a better membrane (Sharma *et al.*, 1998; Tan *et al.*, 2012; Dehghani, Rasoulianboroujeni and Ghasemi, 2018; Brouki *et al.*, 2020). Different biological scaffolds and synthetic polymeric ones have been developed in recent years to try to tackle this need (this has been covered in the literature review) but none of them have been able to take the spot as the gold standard (human amniotic membrane). In the University of Sheffield the approach has been to use PLGA as a cell carrier due to scaffolds made of this polymer showing good results in epithelial tissue repair (Deshpande, Ramachandran, Sefat, *et al.*, 2013). The positive point of using PLGA is that the degradation rate is fast and tuneable. The original objective of the cornea research team at Sheffield was to have a cell carrier that could be degraded between 4 to 6 weeks, which was possible with PLGA 50:50 (Ortega, McKean, *et al.*, 2014; Ortega, Sefat, *et al.*, 2014). These scaffolds were tested in animal studies (rabbit) where corneal repair was achieved (Ramachandran *et al.*, 2019), and a simplified version of this was used in a safety in-man study in India (data being prepared for publication). Although the electrospun scaffolds developed in Sheffield were able to show good results as corneal cell carriers, surgeons at L.V. Prasad eye institute noticed that the scaffolds were brittle, and therefore not an optimal cell carrier until that aspect is fixed.

Scaffold brittleness is something that was not observed when working with them in Sheffield laboratories. The initial electrospun scaffolds in Sheffield were made using dichloromethane (DCM) as solvent, while the ones sent to L.V. Prasad eye institute were made by the Electrospinning Company using hexafluoroisopropanol (HFIP) (Ortega, Ryan, *et al.*, 2013). HFIP and DCM have very important differences when considering the stability of the

electrospinning process as well as the possible remnant solvents in the manufactured electrospun membranes. The European Medicines Agency and the U.S. Food and Drug Administration indicate in their guidelines that the maximum amount of DCM must be 600 ppm, while for HFIP must be kept as low as possible. Information for HFIP specific permitted levels is difficult to identify, however, for the scaffolds that the group developed for the previous in-man study, this solvent needed to be kept under 1% concentration. To decrease remaining HFIP, the scaffolds made by the Electrospinning Company were vacuumed extensively to be able to remove the HFIP from the scaffolds. Another possible factor that may have impacted the scaffolds sent to India is that PLGA scaffolds were affected by temperature changes and humidity (as reported by L.V. Prasad Eyes Institute). Electrospun membranes are stored in freezer conditions ( $-4^{\circ}\text{C}$  and under) with desiccant, as this way they do not show degradation and their mechanical properties are not affected (Deshpande, Ramachandran, Sefat, *et al.*, 2013). On the other hand, it is important to highlight that membranes were submerged in a saline solution (in theatre) prior to be placed on the human wounded corneas. This is a very important point to take into account since, as we will emphasize later on this chapter, the mechanical properties for wet and dry scaffolds can change significantly.

From previous work published in the group, we know that PLGA electrospun scaffolds are good cell carriers for limbal stem cell outgrowth from corneal limbal explants, but the mechanical properties of these scaffolds are not optimal. One way to improve our membrane mechanical properties is by combining PLGA with another polymer with well-known and desired characteristics (Powell *et al.*, 2009; Ann *et al.*, 2011; Chou and Woodrow, 2017). We propose in this research the addition of Polycaprolactone (PCL) which is a polymer well known for its low Young modulus mechanical properties, and is also an approved polymer used in medical applications (Powell *et al.*, 2009; Ann *et al.*, 2011; Chou and Woodrow, 2017). Additionally, PCL has been used before to explore corneal treatment (Salehi *et al.*, 2017; Kim, Kim and Park, 2018; Rose *et al.*, 2019). With the addition of PCL, we aim to develop an electrospun scaffold that will have improved mechanical properties to be used as a cell carrier for SLET surgery.

## 2.2.- Aim

The aim of this project is to produce a PLGA-PCL electrospun scaffold with mechanically tailored properties that can be used as a cell carrier for corneal repair techniques and thus, mimicking and replacing amniotic membrane in corneal treatments. We hypothesise that the inclusion of PCL within the electrospinning process will decrease the stiffness of the electrospun membranes thus maintaining their biological properties.

Specific objectives:

- 1.- Identify electrospinning conditions for PLGA and PLGA plus PCL that are reproducible and material-efficient.
- 2.- Characterise PLGA electrospun scaffolds' mechanical properties to determine its shortcomings as a good scaffold candidate for corneal repair.
- 3.- Analyse the effect of adding PCL to make PLGA-PCL blend electrospun scaffolds.
- 4.- Determine an optimal PLGA-PCL concentration to make an electrospun scaffold that can be mechanically acceptable to be used in corneal repair techniques.

## 2.3.- Materials and Methods

### 2.3.1.- Materials

In table 2.1 there is a list of all the chemicals and reagents used in this chapter with their respective supplier, and in table 2.2 the biological tissues used.

**Table 2.1** Chemicals and reagents used

<b>Chemical / Reagent</b>	<b>Supplier</b>
Dichloromethane	Fisher Chemical
Dimethylformamide	Fisher Chemical
Poly(lactic-co-glycolic acid) 50:50	Purac
Poly(lactic acid)	Sigma – Aldrich
Polycaprolactone	Purasorb / Corbion
Propanol-2-ol	Fisher Chemical

**Table 2.2** Biological tissues used

<b>Biological tissue</b>	<b>Source</b>
Rabbit Cornea	Eyes of wild rabbits hunted in United Kingdom. The Wild Meat Company.
Human amniotic membrane	Cervical tissue obtained under Ethical Approval from the South Yorkshire Research Ethics Committee 08/H1310/35. Preserved in PBS at a temperature of -20 <sup>0</sup> C

### 2.3.2.- Electrospinning

#### a) Electrospinning solutions

Poly (lactic-co-glycolic acid) 50:50 (PLGA) and Polycaprolactone (PCL) were mixed and used in different PLGA:PCL weight ratios (99:1, 95:5, 90:10, 85:15, 80:20, 70:30 respectively). To dissolve the polymers, a solvent solution of 25% Dimethylformamide (DMF) and 75% dichloromethane (DCM) was used. The solvent to polymer solution ratio was 80:20 in weight. Table 2.3 shows the recipes for 10 grams of electrospinning solution. Finally, polymers were mixed with the solvent solution in glass vials using magnetic stirring overnight and used the next day to avoid evaporation.

**Table 2.3** Electrospinning solutions

Solution	PLGA (g)	PCL (g)	DCM (g)	DMF (g)	Total (g)
Pure PLGA	2	0	6	2	10
99% PLGA 1% PCL	1.98	0.02	6	2	10
95% PLGA 5% PCL	1.9	0.1	6	2	10
90% PLGA 10%PCL	1.8	0.2	6	2	10
85% PLGA 15% PCL	1.7	0.3	6	2	10
70% PLGA 30% PCL	1.4	0.6	6	2	10

To get initial electrospinning conditions, PLLA (Polylactide acid) was also electrospun to compare with PLGA. In that case, PLLA was made under the same conditions of 20% polymer – 80% solvent, with the same DCM:DMF proportion.

## b) Electrospinning set-up

Polymer solutions were loaded into 1 mL syringes and vertically electrospun at a flow rate of 0.5 mL/h, voltage applied of 18kV, and the distance from the tip of the needle to the collector was 14 cm. 2.5 mL of solution were electrospun to create a scaffold sheet. The manufacturing took place at room temperature. After electrospinning, membranes were stored in a freezer (-18 °C) in sealable bags with desiccant inside (desiccant sachet 10g, silica gel with humidity indicator – orange gel). The electrospinning setup can be seen in figure 2.1

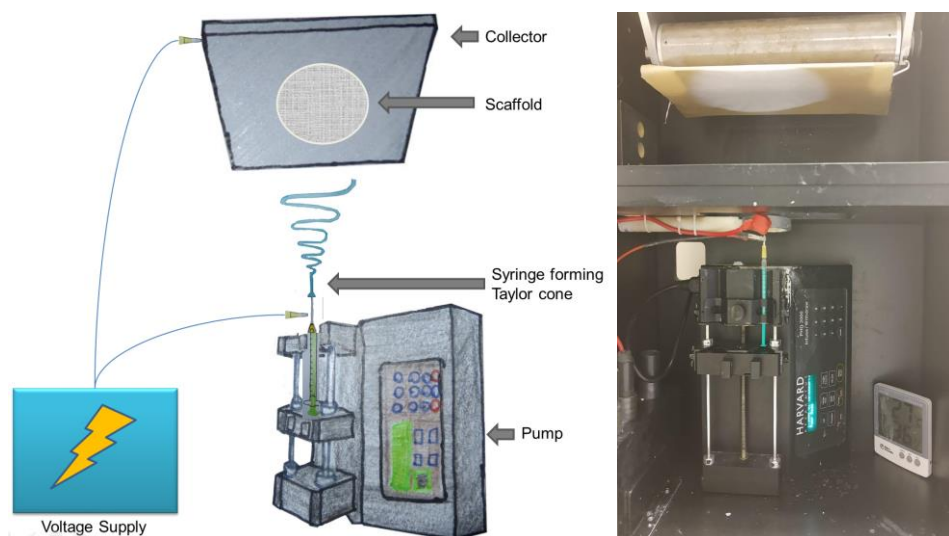


**Figure 2.1** General vertical Electrospinning set up. Left image is a schematic representation of the electrospinning set up used. Right image is the set up photography.

## 2.3.3.- Rheology

The viscosity of the electrospinning solutions was measured using an oscillation strain sweep assay. This was done in the different polymer solutions to obtain their storage and loss modulus using a rheometer at 25 °C (Anton Paar MCR 301 Rheometer, airline pressure of 5 bar). For the strain sweep assay the conditions were: 62.83 rad/s, initial 0.01%, final 1%, 6 pt/dec, and leaving a tolerance band of 3%.

### 2.3.4.- Tensile Testing

To compare the mechanical characteristics of our scaffolds we used a unidirectional tensiometer (EnduraTEC ELF3200 BOSE). The scaffolds were cut into strips and the length and width were measured before cutting, thickness was also measured using a micrometer (MITUTOYO, Digimatic, 25 mm Max Measuring Range, 0.001 mm Graduations). The corneal samples were obtained using the procedures shown in section 3.2.4, corneas were extracted and cleaned to later cut into strips of 12 mm x 5 mm for mechanical testing. From the data collected, the Young's modulus, the Ultimate tensile strength (UTS), and the strain at the UTS were calculated. Due to machine difficulties, we later changed from the EnduraTEC machine to Hounsfield H100KS (Tinius Olsen) with a load cell of 100 kN. In figure 2.2 is displayed an example of how the scaffold sample is measured in the tensiometer.



**Figure 2.2** Strip of a PLGA scaffold being tested in the tensiometer.

### 2.3.5.- Fibrin Glue coating

PLGA electrospun scaffold was coated with fibrin glue to analyse if this fibrin glue modified its mechanical properties. Fibrin glue was made by combining thrombin (2.5 U/ml) with

fibrinogen (18.75 mg/ml). The membranes were coated by adding first 100 µl of thrombin using a micropipette, to then add 100 µl of fibrinogen on the 100 µl of thrombin. The combination of thrombin and fibrinogen (now fibrin glue) was rapidly scattered on the surface of the membrane using the tip of the micropipette.

### **2.3.6.- Extraction-Capillary Gas Chromatography**

Remnant solvent concentration was measured in different electrospun membranes using Multiple Headspace Extraction-Capillary Gas Chromatography (Perkin-Elmer Autosystem XL gas chromatograph with HS40XL headspace autosampler; Column: Phenomenex ZB-624 (30 m x 0.32 mm, 1.8 µm film thickness)) hydrogen was used as carrier gas (7 psi) and then compared with the maximum amount permissible by EMA (European Medicines Agency) and FDA (U.S. Food and Drug Administration). The conditions of the gas chromatography were as follows: GC oven program: 40°C for 5mins, ramping to 200°C at 40°C/min, staying at 200°C for 1min; Autosampler mode: multiple headspace extraction (5 injections); Vial temperature 200°C; Vial thermostat time: 60 min; Autosampler pressure (hydrogen): 15psi; Vial pressurisation time: 1 min; Injection time: 0.04 min; Withdrawal time: 0.2 min; Needle and transfer line temp: 205°C; GC injector: split mode at 220°C; Detector: flame ionisation (FID) temperature: 250°C.

### **2.3.7.- Differential Scanning Calorimetry**

To analyse the thermal properties of the membranes, differential scanning calorimetry was used (TA instruments DSC25 with autosampler and RCS90 chiller accessory). Nitrogen was used as purge gas at 50 mL/min. The sample method was as follows: 25°C to 230°C at 10°C /min, then 230°C to -90°C at 10°C /min, and finally -90°C to 230°C at 10°C /min. The samples had a weight of approximately 2 mg.

### **2.3.8.- Scanning Electron Microscopy**

The electrospun membranes were characterised in different conditions after gold coating them using an Edwards Sputter Coater S150B (Edwards, UK). Fibre diameters were examined using Scanning Electron Microscopy (SEM) (Tescan Vega3 LMU Scanning Electron Microscope) and imageJ software (National Institutes of Health). To measure the fibre diameter of every scaffold conditions, 5 images were taken in  $\times 5000$  magnification. After the images were collected, ten prominent fibres of each photo were selected and their diameter was measured. The diameter measurement was done using imageJ software and using a scale bar provided in the SEM image.

### **2.3.9.- Studying differences between dry and wet scaffolds**

To fully understand the mechanical properties and morphology of the electrospun scaffolds we develop, it is necessary to study them in both dry and wet conditions:

Dry conditions are a representation of how the scaffold is stored. Dry conditions are defined as using the scaffold directly from storage ( $-18^{\circ}\text{C}$  in sealable bags with desiccant as described previously) and using it as soon as possible to avoid the effects of humidity on them.

Wet conditions are a more accurate representation of how the scaffold will be used in theatre (as clinicians wet the scaffold before transplanting it into the patient). Wet conditions are defined when the scaffolds are submerged in PBS and left in incubator conditions ( $37^{\circ}\text{C}$ ). For early assessments of humidity and temperature damage into the scaffolds, these were left in wet conditions overnight. While for degradation essay the scaffolds were left in wet conditions for up to 3 months.

### 2.3.10.- Statistical analysis

GraphPad Prism 7 software was used for one-way ANOVA analysis with p value <0.05 in consideration for statistical significance.

## 2.4.- Results

### 2.4.1.- Optimising electrospinning conditions

PLGA 50:50 have been largely used in electrospinning to get scaffolds of relatively fast degradation (Deshpande, Ramachandran, Sangwan, *et al.*, 2013; Keles *et al.*, 2015). Taking from the previous work made by our group, getting new PLGA 50:50 electrospun scaffolds to use as a model and set up to make later modifications was needed. Our first step then was to reproduce our conditions as similarly as we could, compared to the last work made by our group (Ortega, Ryan, *et al.*, 2013). These conditions were: gold coated ring collectors in a metallic plate covered in aluminium; 4 insulin syringes (Blunt ended 0.8 cm inner diameter needles) on a syringe pump loaded with 2.5 ml of PLGA solution each; Flow rate of 30  $\mu$ l/min; voltage of 15 kV; and distance of 15 cm (Ortega *et al.*, 2014).

The set up used was PLGA 50:50 following the previous work in our group and as well compared to another polymer that easily electrospins like PLLA. When comparing the outcomes of the scaffolds sheets, PLLA looks more homogeneous and with no visible droplets of polymer agglomeration as can be seen in big quantities in PLGA sheets. Considering this different electrospinning result, it was necessary to see if different results can be seen at microscopy level. In figure 2.3 an SEM comparison of these 2 scaffolds is shown.

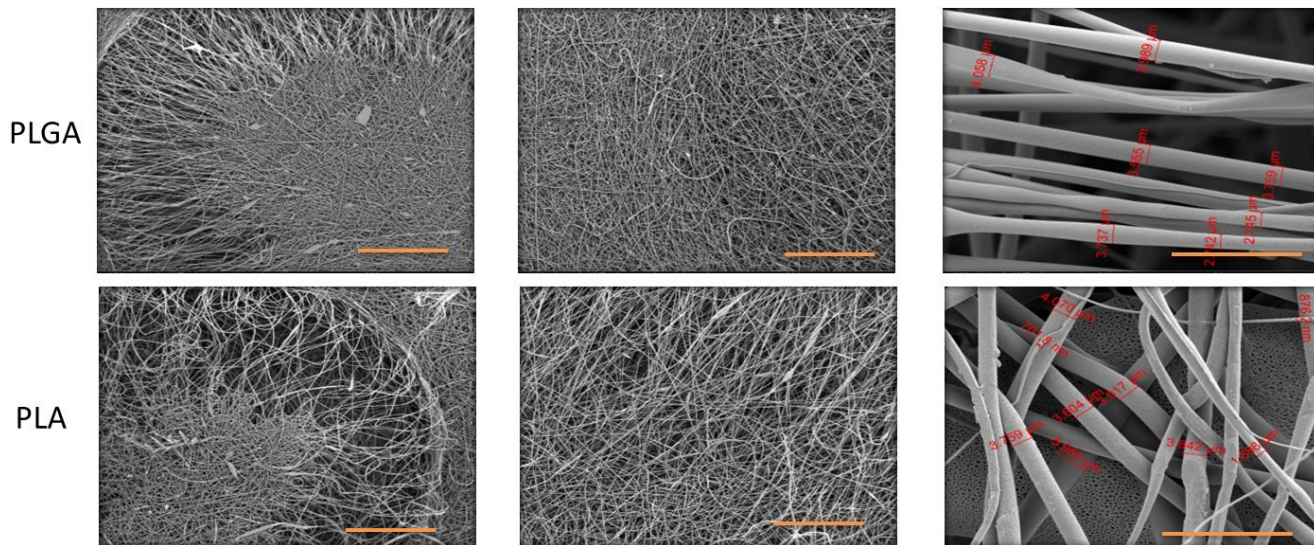


**Figure 2.3** Scanning electron microscopy on PLGA and PLA scaffold. Scale bar in the first two images from left to right represents 500  $\mu\text{m}$ , while the scale bar in the third image represents 20  $\mu\text{m}$ .

In the previous figure we can see a comparison between PLGA and PLA scaffolds (without agglomerations). From left to right it can be seen 150x, 1000x, and 5000x, having in this last one the diameter of the fibres marked in the figure. In these photos we can see well-formed microfibers in both polymers. We can see in 2.3 that diameters of the fibres in PLGA 50:50 vary from 2.74  $\mu\text{m}$  to 4  $\mu\text{m}$  with well-defined fibres, while PLA varies from 1.9  $\mu\text{m}$  to 3.9  $\mu\text{m}$ . In this stage of the research we are just comparing and exploring working conditions, so no further analysis of comparing these polymers were made.

As we are looking for optimal working conditions, we can see in the previous figures that PLGA electrospun scaffolds were made, but with an important amount of agglomerations, which are not desired as will make unreliable reproducible conditions, especially for mechanical properties as those agglomerations will affect the microfeatures in the scaffolds. Therefore, new conditions for electrospinning this polymer were needed to reduce these droplets. In table 2.4 there is a summary of the conditions that were tested to electrospun PLGA 50:50 in Kroto Research Institute set-up (previously seen in figure 2.3).

**Table 2.4** Different conditions used to electrospun PLGA 50:50

<b>Voltage (kV)</b>	<b>Flow rate (uL/min)</b>	<b>Observations</b>
15	30	<b>Agglomeration</b> of polymer solution at the end of the tips. Losing a considerable amount due to polymer droplets.
17	30	<b>Agglomeration</b> of polymer solution at the end of the tips but now in form of branches but <b>forming fibres</b> . Losing in droplets (less than previous condition) and beads in collectors
12	30	<b>Not forming fibres</b> at all, just droplets.
17	40	<b>Forming fibres</b> but also losing a considerable amount of polymer in form of droplets.
20	40	<b>Forming fibres</b> . Forming branches, but smaller than second condition. Scaffold attached to collectors looks good, but having issues peeling it off.

For the conditions tested in table 2.4 following characteristics remained fixed: the distance between the tip to the collector was 15 cm and the solution of PLGA was 20% weight in Dichloromethane. Voltage was changed between 15 kV to 20 kV, and flow rate between 30  $\mu$ L/min to 40  $\mu$ L/min. The way of assessing the results was visual, comparing the previous scaffolds made and shown in figure 2.3 with the new developed ones. From the conditions described in the table, the scaffold manufactured using 20 kV and a flow rate of 40  $\mu$ L/min was the most reliable. With these conditions the loss of polymer by droplets was low and the collectors were covered in quite a fast time (one hour of electrospinning). On the other hand, these conditions showed problems regarding peeling of the scaffold off the collectors, the scaffold being strongly tied to the collectors and also brittle (which means that every attempt to remove the scaffold ended up breaking it). Therefore, 17 kV and 30  $\mu$ L/min were chosen as

working conditions, which still showed a bit of polymer loss by droplets, but let us peel off the scaffold without problems.

Due to laboratory relocation, the electrospinning was changed to a vertical set up as can be seen in figure 2.1 in the School of clinical Dentistry of the University of Sheffield. As the same conditions were not possible to reproduce (different orientation and syringe capacity), a new visual analysis was done and the new conditions that had been in use in this new setting are described as follows: PLGA 20% in 60% Dichloromethane and 20% Dimethylformamide, a distance between the tip and the collector of 14 cm, 18 kV and a flow rate of 0.55 mL/h. With these new conditions, and using non-wax baking paper to cover the metallic plate collector, we were able to have reproducible conditions that do not create visible agglomerations and no polymer solution is wasted as all is electrospun into the collector. In the figure 2.4 are displayed SEM images of the electrospun scaffolds with this final electrospinning condition, showing clear fibre structures.

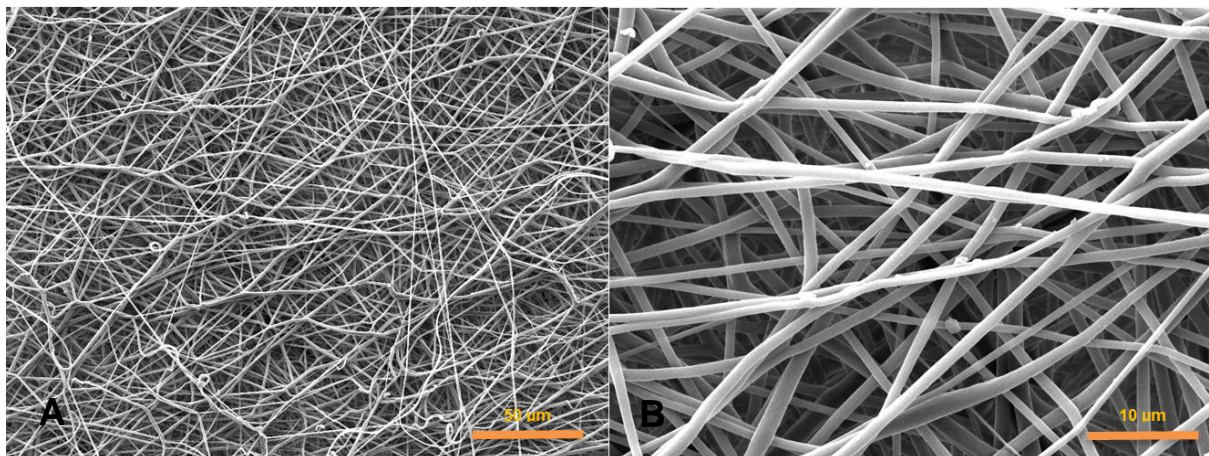


**Figure 2.4** Scanning electron microscopy on PLGA scaffold under final set up conditions. A is the electrospun scaffold at x1000 and B is at x5000.

#### 2.4.2.- Studying possible plasticising effects of PCL

One of the main objectives of this research was to be able to modify the mechanical properties of our scaffolds. Therefore, and considering the previous work made by our group, we introduced a plasticizer agent to the PLGA 50:50 scaffolds that we knew can be electrospun under the previous conditions (2.4.1). PCL is a polymer that has been used extensively for electrospinning (Thi

and Lee, 2010; Chou and Woodrow, 2017), but as well has interesting mechanical properties that we are looking to include in our scaffolds (Powell *et al.*, 2009), with low values of stiffness and higher elongation % compared to PLGA.

PLGA and PCL electrospun blends have been explored before, usually dual rotating them in separate syringes forming one scaffold (Thi and Lee, 2010; Ann *et al.*, 2011), but also mixed together using HFIP as solvent (Chou and Woodrow, 2017). Considering the high reproducibility of our electrospinning conditions we decided to add the PCL to the PLGA in the same electrospinning syringe, instead of electrospinning them separately as had been previously explored with our solvent selection with PCL (Santocildes-romero *et al.*, 2016; Paterson *et al.*, 2017). The addition of PCL will be done respecting the amount of polymer vs solvent that has been used previously (20% polymer and 80% solvents) and was described in 2.3.2.

In figure 2.5 we can see the electrospun scaffolds made out of the combination of PLGA and PCL, using as comparison a pure PLGA electrospun scaffold.

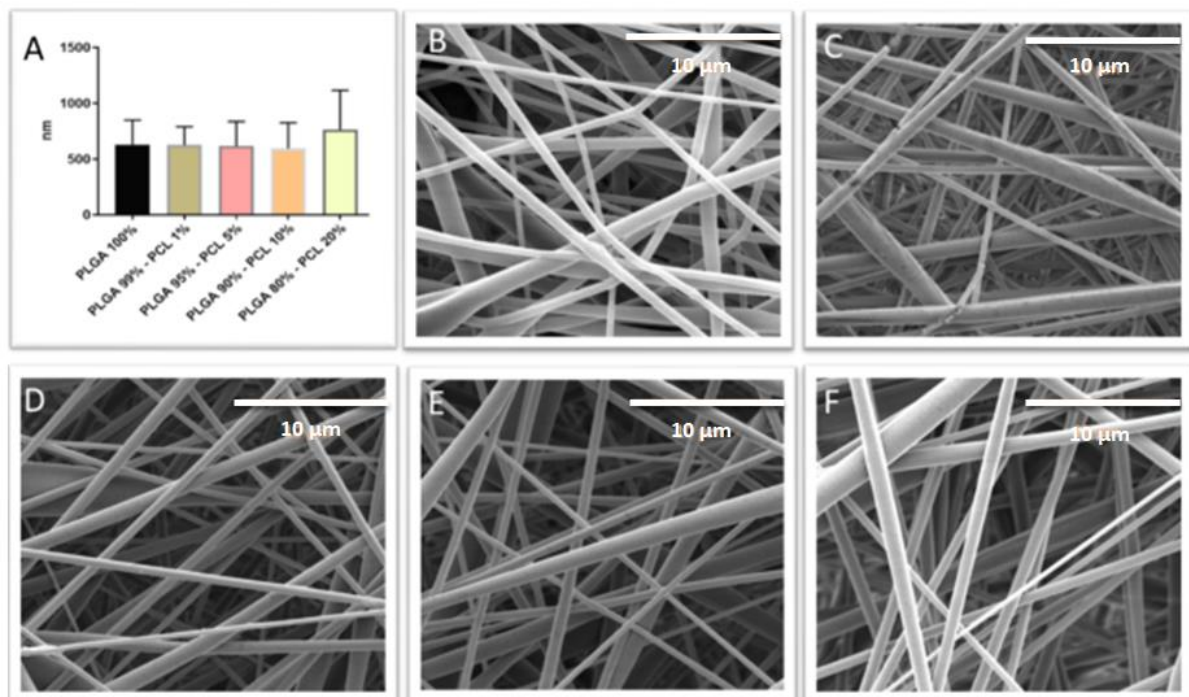


**Figure 2.5** A- Fibre diameter comparison between electrospun scaffolds of PLGA with different amount of PCL added. N=1, n=30. No statistic difference can be appreciated between the average fibre diameter ( $P < 0.05$ ). B- SEM image of scaffold 100% PLGA. C- SEM image of scaffold PLGA 99% - PCL 1%. D- SEM image of scaffold PLGA 95% - PCL 5%. E- SEM image of scaffold PLGA 90% - PCL 10%. F- SEM image of scaffold PLGA 80% - PCL 20%.

In figure 2.5 we can see different blends of PLGA-PCL going from 99%-1% to 80%-20%. When comparing the morphology of these scaffolds, no statistical difference can be seen between the

fibre diameters in all of them ( $P < 0.05$ ). Additionally, visually we can see that all the fibres in the scaffolds look homogeneous, something interesting to note considering we are mixing two different polymers.

Once it was demonstrated that it was feasible to electrospin PLGA-PCL blends, without morphological differences, we defined the following blend conditions to be analysed in this research:

- Pure PLGA
- 99% PLGA – 1% PCL
- 95% PLGA – 5% PCL
- 90% PLGA – 10% PCL
- 85% PLGA – 15% PCL
- 70% PLGA – 30% PCL

#### **2.4.3.- Rheology properties of different electrospun solutions**

As mentioned earlier, one of the reasons that lead to the brittleness of the previous PLGA scaffolds developed in Sheffield was that the solvent, or lack of this, changed the mechanical properties of the membrane. The role of the solvent in PLGA electrospun solutions have been explored previously (Liu *et al.*, 2017). In Liu study he concludes that solvents can influence the morphology and mechanical properties of the electrospun scaffolds by altering the properties of the PLGA solution. Considering this, a strain sweep test was made to the electrospinning solutions to see if there could be any appreciable difference between solutions by comparing their loss and storage modulus. The storage and loss moduli are responses of viscoelastic fluids to sheer stress. The loss modulus of a material or solution is the ratio of the viscous component of the stress and is the ability of the material or solution to dissipate stress through heat. The storage modulus on the other hand is an indication of the ability of the material or solution to store energy elastically. In figure 2.6 is displayed an oscillation strain sweep assay to the electrospinning solutions of the membrane conditions explained in table 2.3.

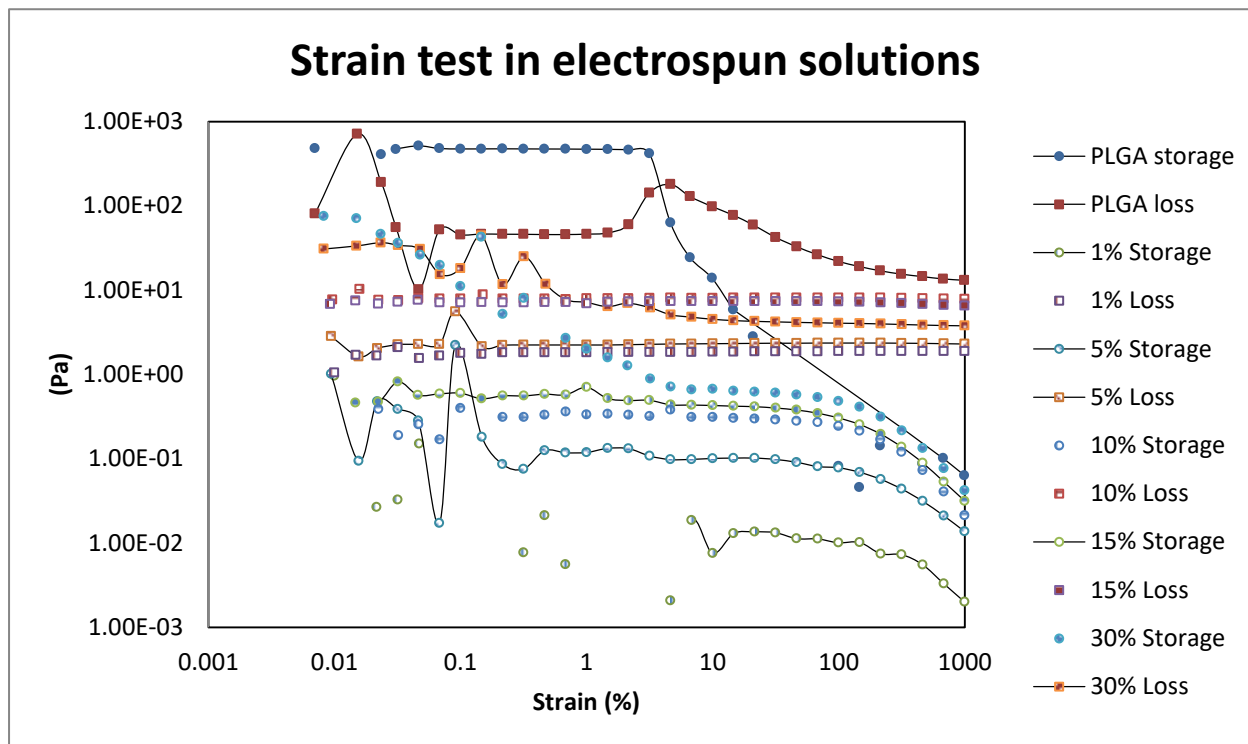


**Figure 2.6** Oscillation strain sweep assay to electrospinning solutions. Conditions were: 62.83 rad/s, initial 0.01%, final 1%, 6 pt/dec, and leaving a tolerance band of 3%, airline pressure of 5bar, and temperature 25°C. Two curves of data were obtained of each solution, storage and loss modulus.

Figure 2.6 displays the storage and loss modulus of the solutions of the six different polymer blends presented in 2.4.3. When the strain is between 0.001 and 100% the data for the polymers are not showing a clear pattern. Between 0.01 and 0.1% all the solutions have big differences in their data, as can be seen in their peaks. As the information of figure 2.6 does not show any pattern, the stress test was repeated twice on the same electrospinning PLGA solution which is showed in figure 2.7.

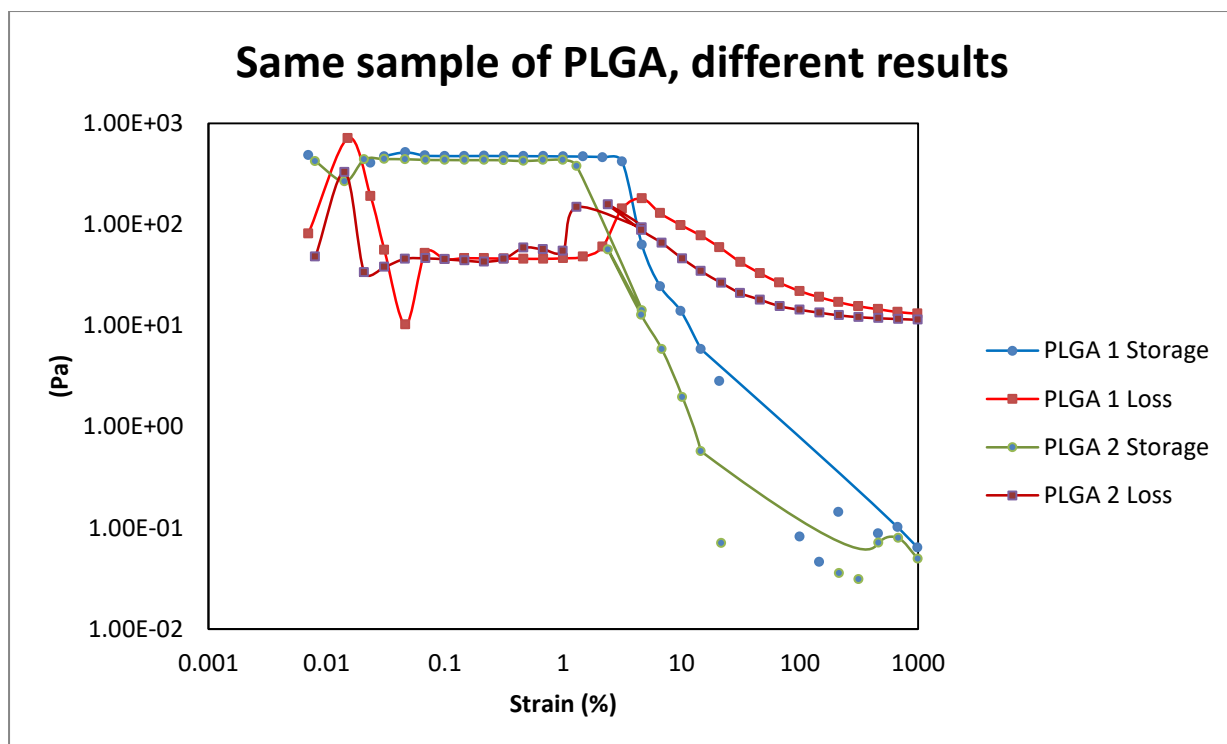


**Figure 2.7** Oscillation strain sweep assay to electrospinning solutions. Conditions were: 62.83 rad/s, initial 0.01%, final 1%, 6 pt/dec, and leaving a tolerance band of 3%, airline pressure of 5bar, and temperature 25<sup>0</sup>C. Same solution of PLGA was measured twice in the figure.

In figure 2.7, it can be appreciated that the same pattern is repeated that was seen in figure 2.6. The data between 0.01 to 0.1% does not have a clear read, explaining the peaks. Between 0.1 to 1000 % a better reading is shown, but still the differences between readings of the same sample are considerably large. These results can be due to the fact that the solutions were behaving mainly like solvents and the machine used is not so precise as to be able to get that specific information. At the same time, using polymer solutions of 20% polymer (PLGA and PCL) in DCM and DMF do not show clear differences between them at our concentrations.

#### 2.4.4.- Mechanical properties of scaffolds

##### a) Understanding mechanical properties of PLGA electrospun scaffold

As mentioned in the introduction and aims of this chapter, the mechanical properties of the scaffolds were the reason for not achieving an optimal scaffold for SLET surgery here in Sheffield. Our main aim is to be able to produce a scaffold that can be used in SLET surgery,

but before that, it is important to know what the mechanical properties of the PLGA are versus the cornea and the amniotic membrane. In figure 2.8 we can see a comparison between them, as well as the effect of adding fibrin glue in them, which is used in SLET surgery to coat the membrane so the explants can easily attach to it as a natural glue (Anita and Sandeep, KumarAbhiyan, KumarRaseena, 2005).

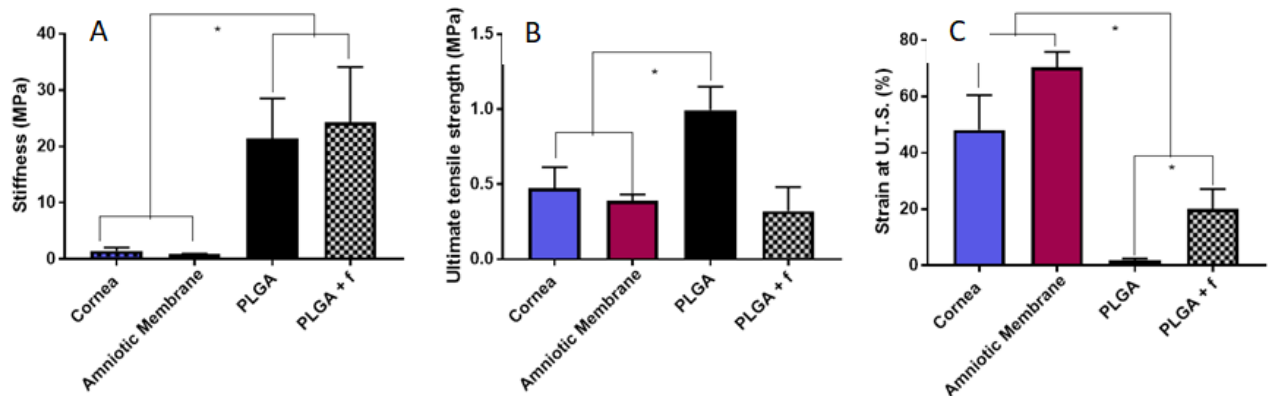


**Figure 2.8** Tensile testing for Cornea, Amniotic membrane and PLGA scaffold. From left to right: Stiffness, Ultimate tensile strength (UTS), and strain at U.T.S. Scaffold sample dimensions had a constant 8 mm length, width between 5 to 6 mm, and height between 0.14 to 0.18 mm. For analysis, dimensions were used to normalize data. Values are presented as average with standard deviation, n=6.

Figure 2.8 reveals the comparison between rabbit cornea, human amniotic membrane, and PLGA scaffolds (with and without fibrin glue). The results presented in the graphics were done with six replicates of each element.

In the graphs, what we wanted to see was a first approach of the mechanical properties that our early fabricated scaffolds were having. The figures are a first approach of measuring a characteristic that we will control more in the future of this research as part one of our variables. In figure 2.8 (A) the stiffness of each element is shown. Cornea and amniotic membrane have a low stiffness, with an average of 1.50 and 0.93 MPascal respectively. When using ANOVA compared to cornea values we can see that PLGA with and without fibrin glue have a significant difference when compared to cornea. When comparing the effect of fibrin glue in PLGA we do not see a significant difference (P=0.69).

In figure 2.8 (B) the Ultimate Tensile Strength (UTS) of each element can be appreciated. UTS represents the maximum strength of the material before failure. Cornea and amniotic membrane have an average of 0.47 MPascal and 0.39 MPascal respectively. When

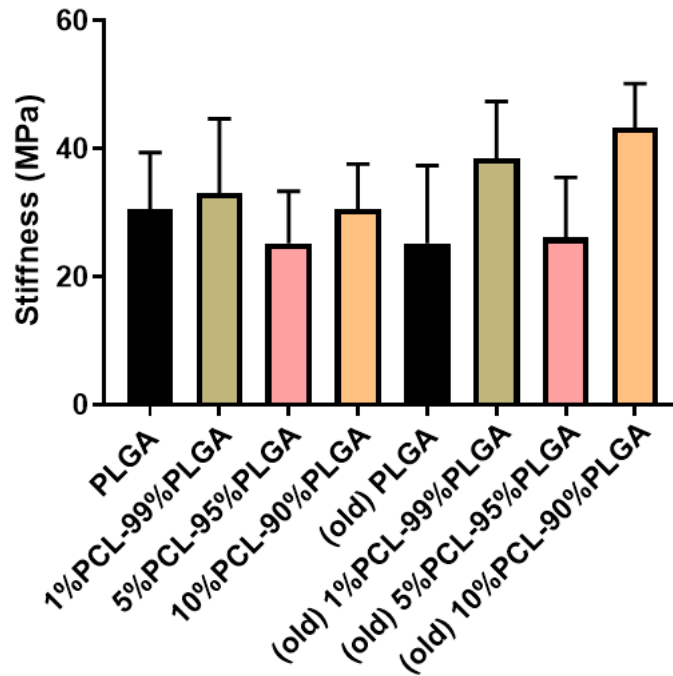
using ANOVA compared to cornea values we can see that there is only a significant difference between Cornea and PLGA. Fibrin glue has a significant effect on PLGA ( $P=0.01$ ).

Figure 2.8 (C) shows the strain at the UTS characteristic of each element. An ordinary one-way ANOVA compared to the cornea values was used with a 95% CI ( $P<0.05$ ). The mean of Cornea was 0.48 compared to the other results in having a significant difference with amniotic membrane and the scaffolds. When comparing PLGA with PLGA with fibrin glue using the T-student, we can see a significant difference ( $P=0.01$ ).

The effect of adding fibrin glue to the membranes was only significant in modifying the strain at UTS of the membranes. Considering our first aim is to achieve membranes with improved mechanical properties, we are going to focus in modifying the stiffness of the membranes without adding fibrin glue in the following analysis.

#### **b) Studying possible plasticising effects of PCL**

When the mechanical properties of PLGA were established, we started the comparison with the PLGA-PCL electrospun scaffolds. In the following figure 2.9, 4 polymer scaffold conditions were compared; PLGA, 1%PCL – 99%PLGA, 5%PCL – 95%PLGA, and 10%PCL – 90%PLGA. Also in figure 2.9, the polymer conditions are measured twice, as one month later after storage its stiffness was measured to see any relevant change in the mechanical properties.



**Figure 2.9** Stiffness for PLGA, 1%PCL – 99%PLGA, 5%PCL – 95%PLGA, and 10%PCL – 90%PLGA scaffolds at the start of the storage and two months later (old). Scaffold sample dimensions had a constant 8 mm length, width between 5 to 6 mm, and height between 0.14 to 0.18 mm. For analysis, dimensions were used to normalize data. Values are presented as average with standard deviation, n=6.

In figure 2.9, the stiffness of PLGA, 1%PCL – 99%PLGA, 5%PCL – 95%PLGA, and 10%PCL – 90%PLGA scaffolds can be seen. When using ANOVA, it can be appreciated that there is not a significant mechanical property change between the scaffolds at the start and one month later after storage ( $P < 0.05$ ). In dry conditions it can also be seen that small additions of PCL (<10%) seem to not significantly change the mechanical properties of the scaffolds as there is not a statistical difference between the scaffold conditions ( $P < 0.05$ ).

With the results of figure 2.9, and knowing that storage under  $-4^{\circ}\text{C}$  with desiccant is not affecting the mechanical properties of the materials under two months (Sefat *et al.*, 2013), we proceeded to analyse the effects of wetting the scaffolds. Considering the values acquired in figure 2.9, a bigger concentration of PCL is considered as well. In the following figure 2.10 is displayed PLGA, 1%PCL – 99%PLGA, 5%PCL – 95%PLGA, 10%PCL – 90%PLGA, 15%PCL – 85%PLGA, 30%PCL – 70%PLGA scaffolds in dry and wet conditions (overnight).

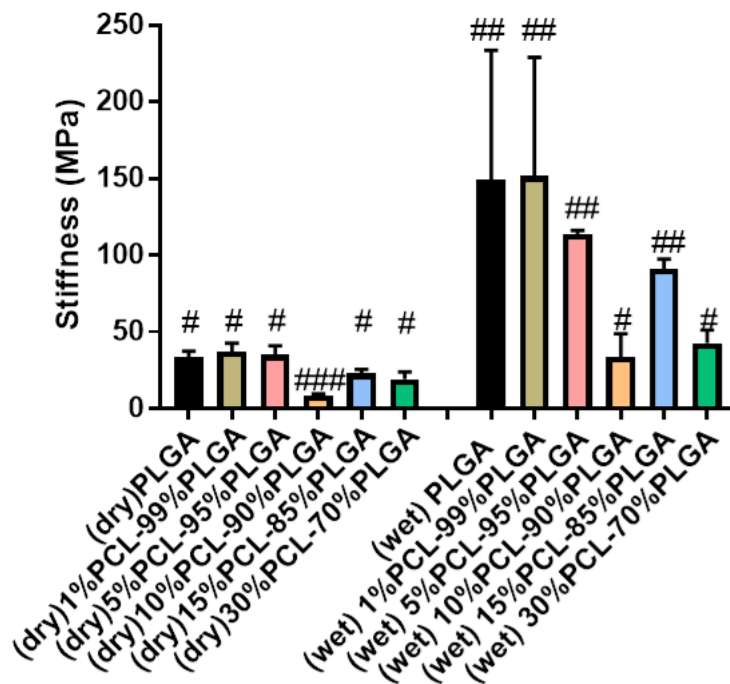


**Figure 2.10** Stiffness for PLGA, 1%PCL – 99%PLGA, 5%PCL – 95%PLGA, 10%PCL – 90%PLGA, 15%PCL – 85%PLGA, 30%PCL – 70%PLGA scaffolds in dry (storage) and wet conditions. Scaffold sample dimensions had a constant 8 mm length, width between 5 to 6 mm, and height between 0.14 to 0.18 mm. For analysis, dimensions were used to normalize data. Values are presented as average with standard deviation, n=6. Groups with the same amount of # are statistically similar to each other (p<0.05).

In figure 2.10 the stiffness of PLGA, 1%PCL – 99%PLGA, 5%PCL – 95%PLGA, 10%PCL – 90%PLGA, 15%PCL – 85%PLGA, 30%PCL – 70%PLGA scaffolds are displayed. Using ANOVA, we can see that the scaffolds have statistically significantly different mechanical properties between their dry and wet conditions, even after only one night of wetting (P<0.05). When compared to each other, in dry conditions only 10%PCL – 90%PLGA is showing significant differences compared to the other, which was not seen in the previous figure 2.9. When comparing their wet conditions, 10%PCL and 30%PCL have the lowest stiffness and therefore changes in their mechanical properties, but still significant (p<0.05). It is also noticeable that adding PCL is making an impact in reducing the stiffness of the scaffold when in wet conditions, compared to the impact it has when dry.

**c) Studying the effect of wetting on mechanical performance of PCL-modified electrospun membranes**

The changes seen due to wetting the scaffolds are significant in their stiffness, so we repeated these experiments twice but this time considering strain at UTS, UTS, and thickness of the scaffold. In figure 2.11 is displayed this analysis showing the strain at UTS, UTS, and thickness of the scaffolds. In figure 2.12 is shown the change in thickness of the scaffold before and after the wetting on them.

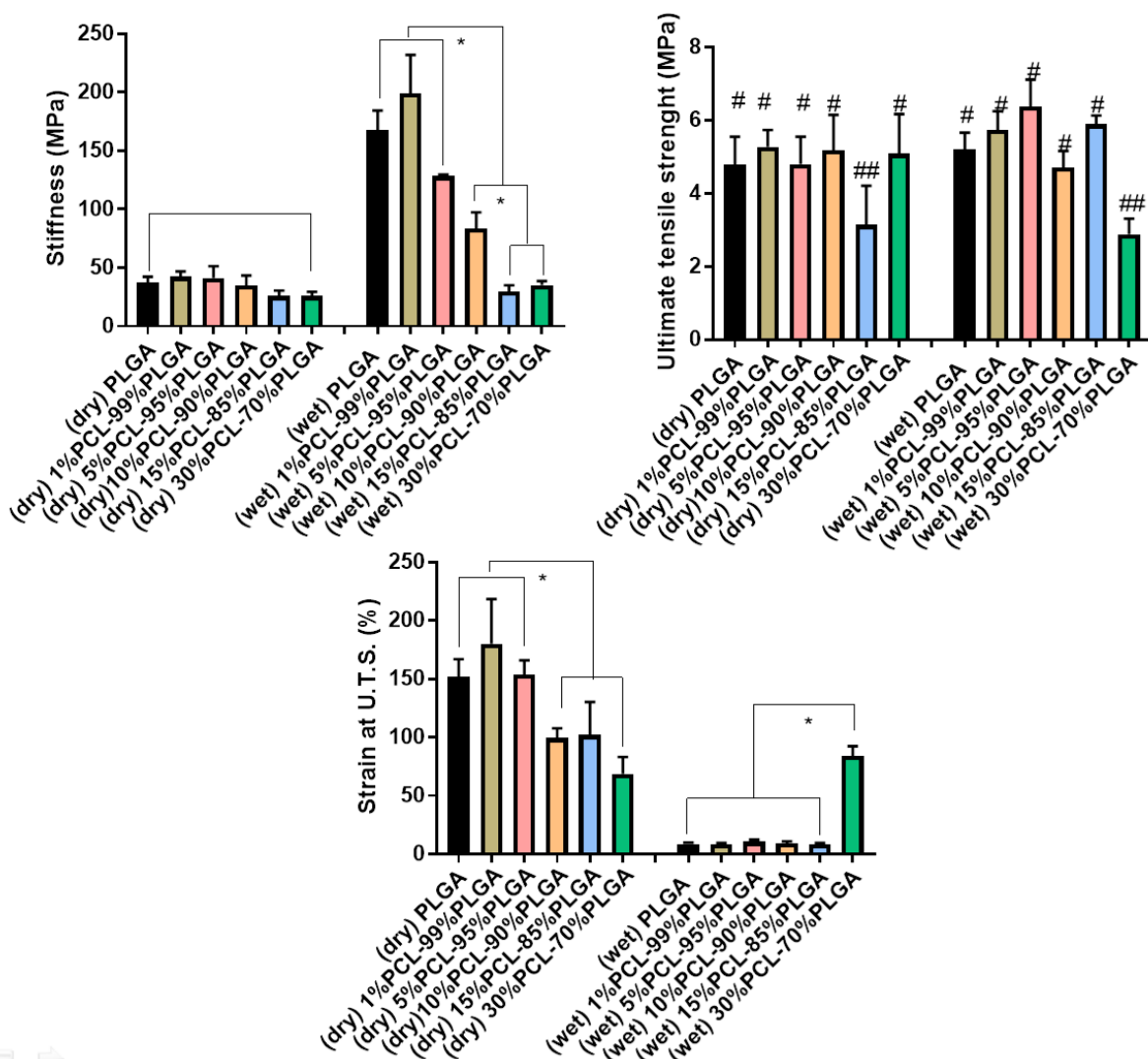


**Figure 2.11** Tensile testing for PLGA, 1%PCL – 99%PLGA, 5%PCL – 95%PLGA, 10%PCL – 90%PLGA, 15%PCL – 85%PLGA, 30%PCL – 70%PLGA scaffolds in dry (storage) and wet conditions. From left to right: Stiffness, Ultimate tensile strength (UTS), and strain at U.T.S. Scaffold sample dimensions had a constant 10 mm length, width of 10 mm, and height between 0.14 to 0.18 mm. For analysis, dimensions were used to normalize data. Values are presented as average with standard deviation, N = 2, n=6.

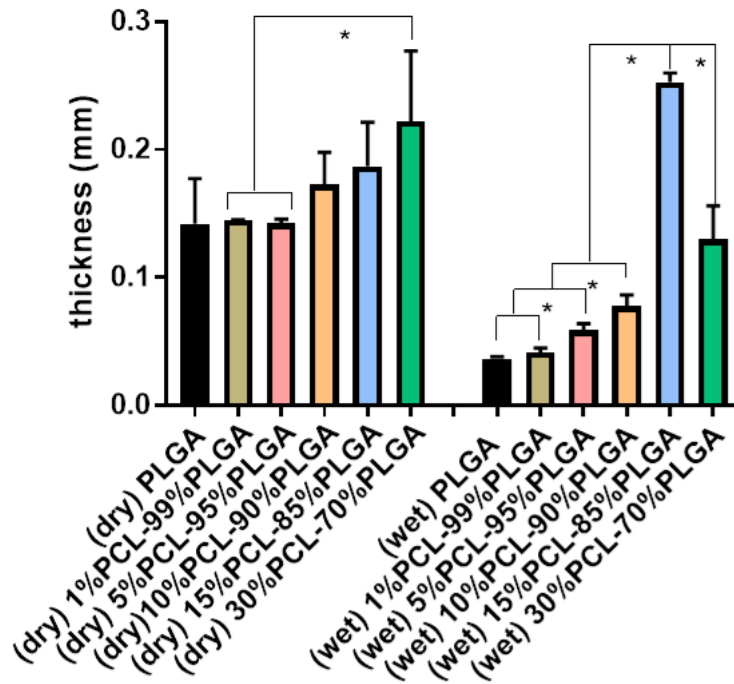


**Figure 2.12** Thickness for PLGA, 1%PCL – 99%PLGA, 5%PCL – 95%PLGA, 10%PCL – 90%PLGA, 15%PCL – 85%PLGA, 30%PCL – 70%PLGA scaffolds in dry (storage) and wet conditions. Scaffold sample dimensions had a constant 10 mm length, width of 10 mm, and height between 0.14 to 0.18 mm. For analysis, dimensions were used to normalize data. Values are presented as average with standard deviation, N = 2, n=6.

In figures 2.11 and 2.12 is displayed a comparison of the mechanical properties and thickness of the membranes in dry and wet conditions. The results show two measurement sessions with 6 replicates each time.

In figure 2.11 (left) is revealed the stiffness of the membranes in dry and wet conditions. Similar to what was see in figure 2.10, while there is not statistical differences between the stiffness of the dry membranes, wet conditions shows a clear tendency of less stiffness the more PCL is in the membrane. The most remarkable result in figure 2.11 is that once again 30%PCL – 70%PLGA membrane has a similar stiffness when dry and wet. As well, in figure 2.11 it can be seen that 15%PCL – 85%PLGA as well preserves its stiffness in dry and wet conditions, but these could be due to the folding issue which was detected in figure 2.12 in this membrane as in figure 2.10 15%PCL – 85%PLGA dry and wet conditions are statistically different.

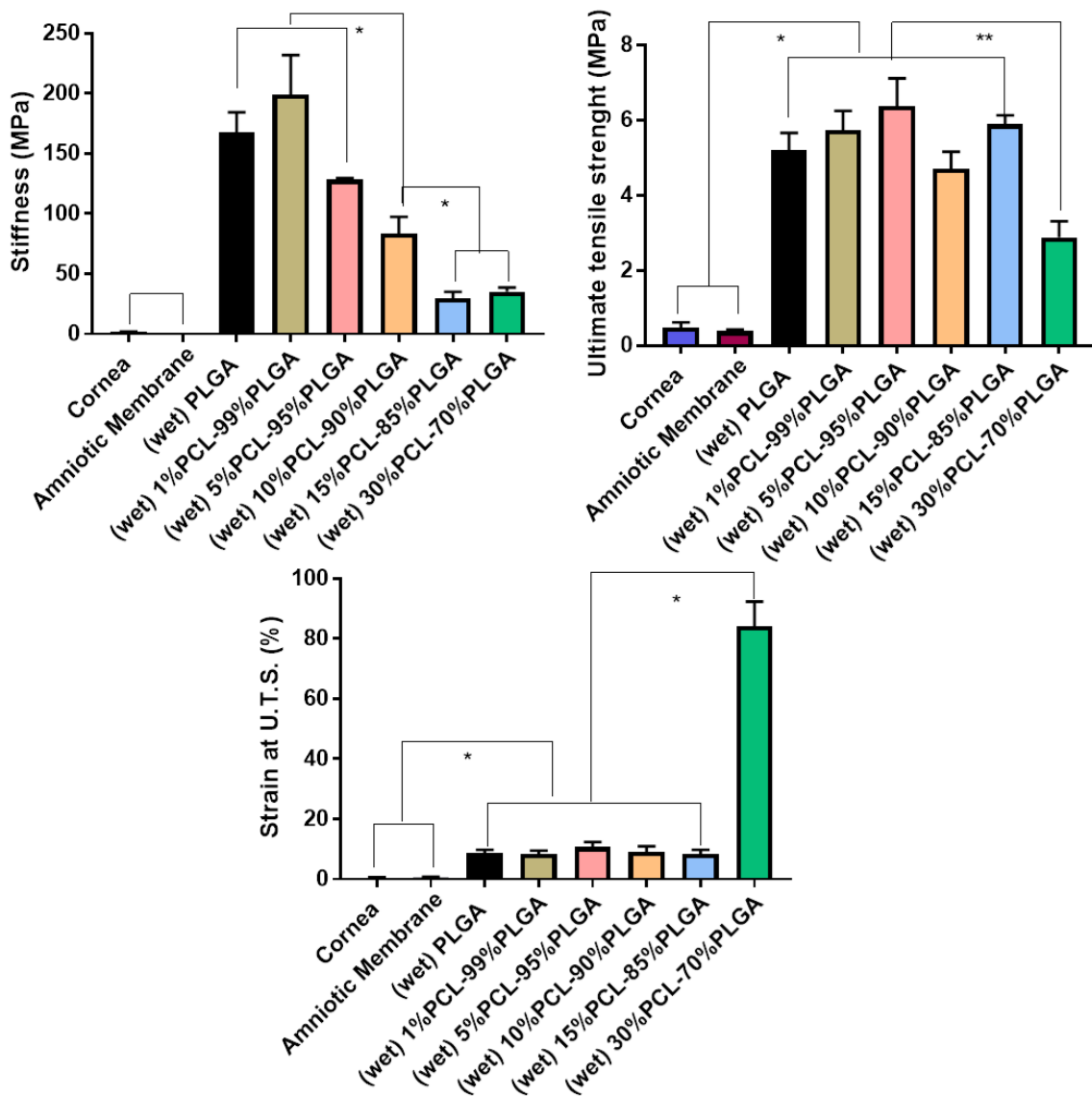
Figure 2.11 (right) shows the ultimate tensile strength in these membranes. Groups with the same amount of # are statistically similar to each other ( $p < 0.05$ ). PLGA, 1%PCL – 99%PLGA, 5%PCL – 95%PLGA, and 10%PCL – 90%PLGA do not present any statistical difference when dry or wet. 15%PCL – 85%PLGA presents an increase of its UTS when wet, but again, could be due to folding issues. 30%PCL – 70%PLGA on the other hand has a decrease of its UTS after an overnight in wet conditions.

Figure 2.11 (down) displays the strain at U.T.S. where in dry conditions we can separate the membrane in two groups. The first group consists of PLGA, 1%PCL – 99%PLGA, 5%PCL – 95%PLGA; and the second group consists of 10%PCL – 90%PLGA, 15%PCL – 85%PLGA, 30%PCL – 70%PLGA. The first group is statistically different than the second group, presenting a higher strain at U.T.S. than the second. In wet conditions however, all the conditions but 30%PCL – 70%PLGA present a dramatic decrease at the % of strain, while 30%PCL – 70%PLGA is able to preserve its properties.

Figure 2.12 shows the difference in thickness of the scaffolds before doing the mechanical testing. Measuring the thickness of the scaffold before doing the tensile test can give us hints of how the membranes are reacting to the liquid environment with temperature. In the case of PLGA, 1%PCL – 99%PLGA, 5%PCL – 95%PLGA, 10%PCL – 90%PLGA, and 30%PCL - 70%PLGA, a reduction in their thickness is displayed after being in wet conditions overnight. One option is that this could be due to the PLGA degradation in PBS buffer (liquid used). This theory is supported when comparing the thickness lost between pure PLGA scaffold versus the amount loss of 30%PCL – 70%PLGA, which even though presents a reduction in thickness, is not as extreme as the former. In the case of 15%PCL – 85%PLGA, and considering there should be some levels of degradation of PLGA, we theorise that what we are seeing is folding of the scaffold, which due to human error was not able to be controlled as well as with the other samples. Leaving aside 15%PCL membrane, we can see a tendency in the wet scaffolds of losing less thickness the more PCL added, once again supporting that PLGA dissolves very fast overnight in wet conditions. On the other hand, how can a scaffold that becomes stiffer are degrading at the same time? Considering the membranes are the same before and after being in wet/temperature condition. One option of this could be crystallization of the membrane. It is known that PLGA has an increased degradation rate at

higher crystallinity due to the loss of amorphous material and formation of voids during annealing. But these conditions of crystallinity were achieved at 115°C (Chye *et al.*, 2005). It would be interested to explore in future works if after wet/temperature some crystallization is seen in the membranes.

With these values in consideration, once again we will compare the values obtained with the values of the rabbit cornea and the amniotic membrane previously presented. For this comparison we will use only the wet results of the membranes, as the wet conditions are closer to how the membrane will be used in clinic. This comparison can be seen in the following figure 2.13.



**Figure 2.13** Tensile testing for cornea, amniotic membrane, and PLGA, 1%PCL – 99%PLGA, 5%PCL – 95%PLGA, 10%PCL – 90%PLGA, 15%PCL – 85%PLGA, 30%PCL – 70%PLGA scaffolds in wet conditions. Scaffold sample dimensions had a constant 10 mm length, width of 10 mm,

and height between 0.14 to 0.18 mm for the electrospun scaffolds, sample dimensions had a constant 8 mm length, width between 5 to 6 mm, and height between 0.14 to 0.18 mm for cornea and amniotic membrane. For analysis, dimensions were used to normalize data. Values are presented as average with standard deviation, N = 2, n=6. For cornea and Amniotic membrane N=1, n=6.

In figure 2.13 is displayed a comparison of the mechanical properties of rabbit corneas, amniotic membrane, and the manufactured membranes in wet conditions. The results show two measurement sessions with 6 replicates each time for the membranes, and one measurement session for rabbit and amniotic membrane with 6 replicates.

Figure 2.13 shows that even though we have successfully reduced the stiffness of our membrane, these values are still far from the low values of cornea and amniotic membrane. As well, this figure displays that the U.T.S. of the cornea and amniotic membrane is lower than the values achieved by our membranes. And finally, in figure 2.13 is revealed that our membrane possesses a bigger % of strain at U.T.S. than cornea and amniotic membrane. Combining the values of U.T.S. and strain at U.T.S. we have membranes that are harder to break than cornea and amniotic membrane.

#### **2.4.5.- Remnant solvent in scaffolds after electrospinning**

Gas chromatography was used to determine the remnant solvents in the electrospun membranes. The amount of DCM and DMF in the scaffolds made at different concentrations needs to be lower than 600 ppm and 880 ppm respectively as that is the maximum amount permissible by FDA and EMA (European Medicines Agency, 2016). 4 different polymer concentration electrospun scaffolds were measured, avoiding exposing the membranes outside their storage conditions for long periods of time. In table 2.5 it is shown that the concentration of DCM and DMF in parts per million (ppm) was considerably lower than the maximum amount permissible by the international agencies.

**Table 2.5** Remnant solvent in electrospun scaffolds using gas chromatography for concentration detection (ppm). Samples were stored in freezer (-4<sup>0</sup>C) without desiccant and measured before 4 hours after producing them. n/d means no detection.

Sample	DCM (ppm)	DMF (ppm)
PLGA	n/d	142.82
PLGA 99% - PCL 1%	0.05	49.28
PLGA 95% - PCL 5%	n/d	100.59
PLGA 90% - PCL 10%	0.04	63.7
CONCENTRATION LIMIT	600	880

#### 2.4.6.- Thermal properties in scaffolds

Differential scanning calorimetry was used to study the thermal profile of the membranes with different polymer concentrations. 7 different polymer concentration membranes were analysed. PLGA, as an amorphous polymer, presents a glass transition temperature (T<sub>g</sub>) but not a melting temperature (T<sub>m</sub>); while PCL has a melting temperature. Mixed polymer membranes present both conditions as can be seen in figure 2.14.

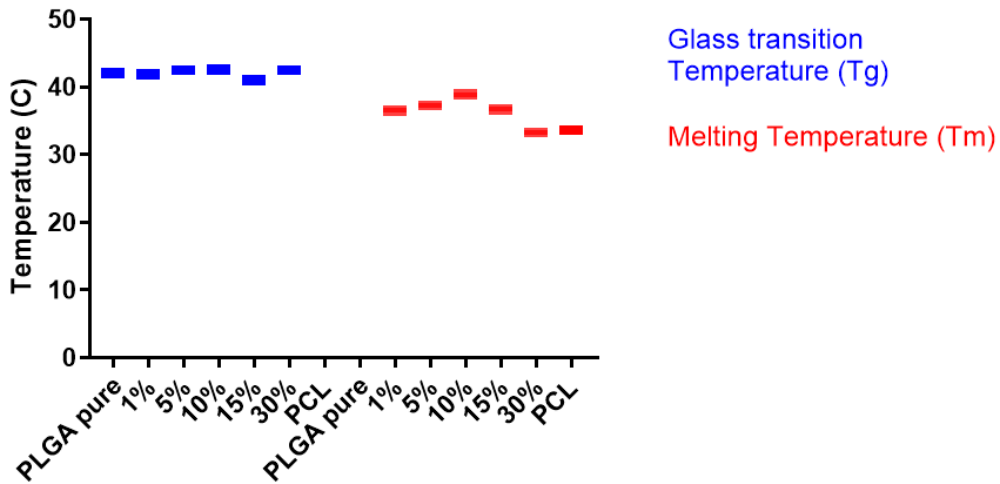


**Figure 2.14** Glass transition temperature and melting temperature of 7 different polymer membranes measured by TA instruments DSC25. Sample method: 25°C to 230°C at 10°C /min, then 230°C to -90°C at 10°C /min, and -90°C to 230°C at 10°C /min.

#### 2.4.7.- Scaffolds morphology and degradation

Scanning electron microscopy was used to analyse the scaffolds morphology and their degradation. To measure the degradation of the scaffolds, a piece of the scaffolds was submerged in petri dishes with PBS and then put together in an incubator at 37°C (wet conditions). Then, after one day and two months a sample was collected and analysed at X500 and X5000 magnification. The following figure 2.15 displays the changes in the scaffolds. When there was not any appreciable scaffold in the petri dish, no sample was collected.

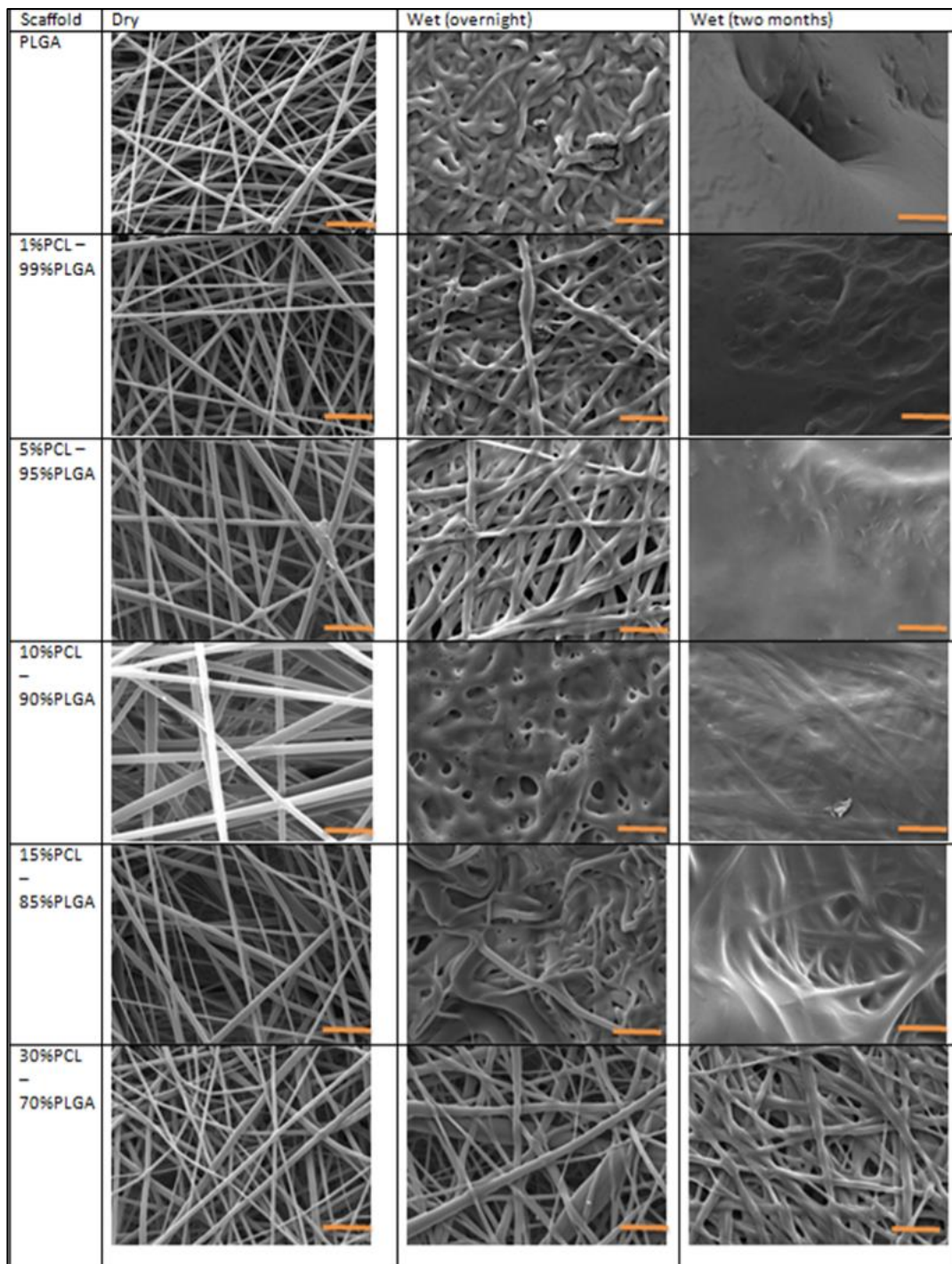


**Figure 2.15** Scanning electron microscopy of PLGA, 1%PCL – 99%PLGA, 5%PCL – 95%PLGA, 10%PCL – 90%PLGA, 15%PCL – 85%PLGA, and 30%PCL – 70%PLGA electrospun scaffold at x5000 magnification.in 3 period of times the photos were acquired; storage (dry), 1 day wet, and 2 months wet. Scale bar = 10  $\mu$ m.

Figure 2.15 displays the effects in the fibrous microenvironment of the membranes after overnight, two months, and three months in wet conditions. The images were acquired using Scanning electron microscopy at x5000 for a better view of the

fibrous composition. PLGA scaffold was completely dissolved after 2 months losing all its fibrous design. Figure 2.15 shows the effect of adding PCL in keeping the fibrous composition in the membranes. In the overnight images, it can be seen how the more PCL is added the more fibrous composition is kept. This is even clearer at two months. At two months 1%PCL – 99%PLGA and 5%PCL – 95%PLGA have lost their fibrous composition and have collapsed in a one layer membrane. On the other hand, in wet conditions at two months 10%PCL to 30%PCL kept their fibrous microenvironment, highlighting the fact that no visible change can be seen in 30%PCL – 70%PLGA membrane after two months in wet conditions.

## 2.5.- Discussion

This chapter investigated the option of creating mechanically tailored electrospun scaffolds using combinations of PLGA and PCL polymers. As mentioned in the introduction, previous work developed in Sheffield laboratories was successfully able to deliver a fibrous PLGA membrane able to support limbal cell outgrowth (Deshpande, Ramachandran, Sangwan, *et al.*, 2013; Ortega, Sefat, *et al.*, 2014; Ramachandran *et al.*, 2019). Unfortunately, due to the way the manufacturing process was carried out, the membranes did not have the mechanical properties to make them suitable for clinical use. Due to this, the focus of this chapter was the manufacturing of electrospun membranes with mechanically tailored mechanical properties. Considering PCL as a polymer with plasticizer properties, we decided to make electrospun membrane with different PCL:PLGA ratios (PLGA, 1%PCL – 99%PLGA, 5%PCL – 95%PLGA, 10%PCL – 90%PLGA, 15%PCL – 85%PLGA, and 30%PCL – 70%PLGA). The ratios selected were using in consideration that we did not wanted to have an electrospun scaffold with more PCL than PLGA due to PCL having a longer degradation time than PLGA (Dunnen *et al.*, 1996; Jansen *et al.*, 2004; Meek and Jansen, 2008). 1% and 5% PCL conditions were added to measure if small amounts of PCL can create differences in the mechanical properties of the membranes.

In our group, PLGA has been electrospun using two different solvents, DCM and HFIP. When using DCM as a solvent, the weight percentage of polymer on solvent has been between 20% to 25%, while with HFIP it has been between 10% and 20% (Ortega, Deshpande, *et al.*, 2013; Ortega, Ryan, *et al.*, 2013). As electrospinning solutions, and under their electrospinning conditions, HFIP showed better results in creating electrospinning solutions of suitable viscosity for electrospinning (Ortega, Ryan, *et al.*, 2013). Considering that PLGA (50:50) can be electrospun with different solvents, Chen compared electrospinning this polymer with 3 solvents; HFIP, DCM, and TCM (trichloromethane). Using electrospinning conditions of a flow rate ranging between 0.6 to 1.2 ml/min and voltage ranging between 15 to 20 kV, they obtained that when using HFIP as a solvent the resulting electrospun fibres were always narrower than when using the other solvents (Chen *et al.*, 2019). The reason for the good results electrospinning using HFIP as a solvent is that this polymer shows strong hydrogen

bonding properties for better dissolving, and thus it is easier for the solutions to be stretched by external electrical forces (Chung, Moghe and Montero, 2009). In this research, it is also presented that flow rates below 0.6 ml/min might not create fibres as they would break from overstretching, which is something that did not happen in this research even though the membranes were manufactured with a flow rate of 0.5 ml/hr. Chen as well mentions that DCM as a solvent fails to create an electrospinning solution with low variability in the fibre diameter. To fabricate our membranes, we mixed DCM with DMF, which has previously shown good results in creating reliable electrospinning solutions with PCL (Santocildes-romero *et al.*, 2016; Paterson *et al.*, 2017) and PLGA (Boncu, Ozdemir and Guclu, 2020). The mixture of DCM and DMF, plus our electrospinning conditions, made us able to manufacture membranes with different blends of PLGA:PCL that present a similar microenvironment, as can be seen in figure 2.5 where the fibre diameter is not statistically different when comparing different the conditions. It is important in this research to achieve comparable microenvironments between the membranes so any difference in the mechanical properties will be due to polymer composition rather than physical differences of the fibre characteristics. Additionally, considering the previously explained limitations of the membranes developed in this group, the solvent solution plays a key role in deciding if the membranes need to be vacuumed or not. Vacuuming the samples resulted in losing the plasticizer effect of the solvent (Amato *et al.*, 2018). In table 2.5 it is displayed that, in our case, the amount of remnant solvent is lower than the limits of remnant solvents stipulated by EMA and FDA, and therefore can be used in clinical applications without vacuuming them (European Medicines Agency, 2016).

Oscillation strain sweep assay have been used before to study PLGA electrospun solutions (Liu *et al.*, 2017). In these results, different weight proportions of polymer to solvent were analysed using a combination of tetrahydrofuran (THF), DMF and Chloroform. PLGA solutions show a decrease in their storage modulus as the oscillation strain increases, which is the same noted in our electrospun solutions (figure 2.6). However, as seen in figure 2.7, there is a big variability in our results even when analysing the same sample. This is mainly due to the electrospinning solution behaving as a solvent and the equipment we used for this analysis not being precise enough to measure these types of solutions.

Using DSC to study PLGA – PCL materials was used by Cameron group to identify if their blend foam changed its thermal properties compared to the pure state of both PLGA and PCL (Southgate, Cameron and Baker, 2009). In their results, PLGA preserved its glass transition temperature in the blends, same as PCL kept its melting temperature. Similarly, our results, regardless of the similarities observed in the microenvironments of the scaffolds, maintain the glass transition temperature and melting temperature of PLGA and PCL in their pure states respectively.

PLGA electrospun membranes are a good candidate for corneal regeneration application, as these membranes are degraded in one to two months in corneal models (Deshpande, Ramachandran, Sefat, *et al.*, 2013; Ramachandran *et al.*, 2019). However, the degradation in these cases has been analysed with cells on them. In figure 2.10, we wanted to study the changes in the membrane by submerging it in a buffer solution at 37°C, separating the cellular degradation effect. On the other hand, PCL has a slow degradation in biological samples, as implants made of this polymer can stay 3 years in the body (Sun *et al.*, 2006). Also, when using as a copolymer, changes can be seen in its degradation time. Poly(DL-lactide-ε-caprolactone) or PLA<sub>85</sub>CL<sub>50</sub> has been analysed, and it was observed that this copolymer degraded completely within 12 months without forming crystals (Dunnen *et al.*, 1996). Whereas other co-polymers of PCL, like poly(DLLA-ε-CL), had not been able to degrade after 24 months implanted in subjects (Jansen *et al.*, 2004; Meek and Jansen, 2008). In addition, when using PCL as a blend with Polyglyconate (Maxon) in a 1:3 proportion, a 6 week elongation of the degradation process was seen in the electrospun scaffold (Schindler *et al.*, 2013). In the same year, Trombetta's group investigated how to control the degradation rate of electrospun PCL scaffolds by blending it with poly(N-vinyl-2-pyrrolidone) (PVP). In this research, different levels of PVP modified the degradation rates of the electrospun scaffolds as the faster degradation of one of the polymers (PVP) was causing nanoporosity in the fibres and thus speeding up the process of degradation (Kim *et al.*, 2013). In our degradation assay, we do not see degradation of the fibres after 2 months in the condition with more PCL, however, more time for analysis would be interesting to see if the nanoporosity reported by Trombetta can be seen in our blended membranes. In the following chapter, the biological impact that the electrospun membrane could have on the limbal cell culture is explored, but it is important to

note from figure 2.15 that the degradation in these scaffolds is different, being 30%PCL – 70%PLGA, the scaffold conditions that preserve its microenvironment after 2 months in wet conditions.

Once reliable electrospinning conditions were found, the addition of a possible plasticising effect and its effects on the electrospun scaffold were studied. In this research PCL was used as a plasticizer, this is due to PCL having been extensively used in electrospinning and having low values of stiffness, making it a good candidate (Powell *et al.*, 2009; Ann *et al.*, 2011; Chou and Woodrow, 2017). PLGA, when electrospun with DMF, had a stiffness of roughly 250 mPa, and a strain at U.T.S. of approximately 72%, which is the same stiffness when compared with a PLGA scaffold made with HFIP as a solvent (Joo *et al.*, 2014; Chou and Woodrow, 2017). In our research, as can be seen in figure 2.7, PLGA membranes have a stiffness of approximately 38 mPa (dry) and 167 mPa (wet). A reason for achieving a lower stiffness compared to other electrospun conditions could be that in our case we do not have to vacuum the membrane, therefore they still preserve the plasticizer effect of the solvents; as well it has been reported that crystallization of a polymer can be suppressed when there is rapid solvent evaporation (Kim *et al.*, 2005). PLGA and PCL have been electrospun together before with positive results, but using HFIP as a solvent and a flow rate of 1.2 ml/hr (Chou and Woodrow, 2017). Chow's research shows that there exists a relationship between the stiffness of the scaffold and the polymer composition, with the more PLGA in the membrane being stiffer, reaching a stiffness of approximately 250 mPa, while pure PCL membrane is below 50 mPa. In our case, the PCL we used in this research has an average molecular weight of 70,000 g/mol; while in Chou's and Ann's PCL was of 80,000 g/mol, and in Powel's was 40,000 g/mol. In our results, with a different solvent, we can also perceive this tendency of PCL reducing the stiffness of the membranes even with the different molecular weight when compared to Chow's research. In 2.10 and 2.11 can be seen the effect of PCL reducing the stiffness of the membranes, but this effect is more noticeable when the membranes are in wet conditions. 30%PCL – 70%PLGA showed interesting mechanical properties, as when it is in dry or wet conditions it has similar stiffness, being approximately 26 and 35 mPa respectively. With these results we have obtained our objective of developing a manufacturing technique that lets us mechanically tailor our membranes. Although the results obtained here of mechanical

properties are positive and we were able to reduce the stiffness of the membranes, they are still far from the approximate values of corneal stiffness (1.5 mPa) and amniotic membrane (0.9 mPa). Additionally, pure PCL electrospun membrane can reach even lower stiffness values of approximately 3.8 mPa (Croisier *et al.*, 2012). Considering that one of the negative observations made by the surgeons of L.V. Prasad Eye Institute was the stiffness and brittleness of the scaffold, 30%PCL – 70%PLGA shows promise as a membrane as with a low stiffness and a high strain at UTS, meeting the requirements for the intended application.

## 2.6.- Conclusion

Electrospun scaffolds were made in a 20% polymer 80% solvent ratio. The electrospinning conditions had a flow rate of 0.5 mL/h (8.3  $\mu$ l/min), voltage applied of 18kV, and a distance of 14 cm. These electrospinning conditions created homogeneous PLGA and PCL:PLGA scaffolds in a reproducible way. Using DCM and DMF as solvents produced a lower amount of remnant solvents in the scaffold than the maximum permissible by EMA and FDA. Electrospun scaffolds with different amounts of PCL:PLGA show similar fibrous microenvironments but preserve their thermal properties of PLGA and PCL. Adding PCL shows statistical differences in the stiffness of the membrane for blends with 10% or more PCL on it, an effect that is increased when the membranes are analysed in dry and wet conditions. From the membranes blended analysed, 30%PCL - 70%PLGA is able to maintain its mechanical properties in wet/warm and dry condition, making it a good candidate to be used by clinicians as allow us to deliver a material to surgeons that is reliable and they can handle with the current protocols in theatre. This membrane conditions also possess a high strain at UTS and low stiffness, making it resistant to mechanical stress and non-brittle.

## Chapter 3: Studying limbal explant behaviour on electrospun scaffolds with controlled mechanical properties

### 3.1.- Introduction

Electrospun membranes are porous and fibrous 3D scaffolds that are able to offer culture conditions closer to the *in vivo* environment, replicating to a degree the structure of the extra cellular matrix (ECM) (Place, Evans and Stevens, 2009). When using 3D culture conditions, factors like stiffness and composition of the microenvironment (which have shown to play a key role in cell behaviour) can be studied in a more realistic manner (Breuls, Jiya and Smit, 2008). In the case of corneal cell culture, studying decellularized membranes has shown that their stiffness is a relevant factor when providing support of cellular layers and being involved in the refractive effect of the cornea (Bao *et al.*, 2012; Wilson *et al.*, 2013). Additionally, the cornea has different levels of stiffness that vary from its centre to the limbal area. These different levels of stiffness affect and could modulate the corneal cell fate, providing a phenotype-through-biomechanics correlation between the epithelial stem cells and the mechanical properties of the membrane (Cardona *et al.*, 2017; Gouveia *et al.*, 2018, 2019). In essence, these studies report an increasing gradient of stiffness from the limbal area towards the centre of the cornea which is intimately related with limbal stem cell differentiation.

The amniotic membrane is well-known for its biocompatibility and also because of its desirable mechanical properties and ease of handling. Although HAM can be identified as the gold standard for corneal cell-delivery; presenting high variability in its stiffness, something which should be considered. As it is a human tissue, it is subjected to patient variability which has a very high impact on membrane properties (importantly biomechanical properties) which can limit the success rate of corneal regeneration (Chen *et al.*, 2012). The electrospun membranes fabricated in this research overcome the variability problem since they can be manufactured to a high degree of reproducibility, maintaining controlled mechanical properties, however, it is important to note that our membranes are stiffer than amniotic membrane.

Different animal model corneas have been used *in vitro*, rabbit eyes being the most utilised (mainly due to their accessibility and ease of use). When comparing the human cornea

to the rabbit cornea we find that rabbit corneas are dramatically softer, which is due to the arrangement and spacing of the collagen (Bozkir *et al.*, 1997; Thomasy *et al.*, 2014). On the other hand, porcine corneas have a uniform and continuous limbus and a similar tensile strength to human cornea (Zhang *et al.*, 2011; Grieve *et al.*, 2015; Menduni *et al.*, 2018). When comparing these two animal models, they have different size and mechanical properties, however it has not been described if these differences can affect cell outgrowth from limbal explants on membranes, which is something we will explore in this chapter.

In this research, different mechanically tailored electrospun membranes were manufactured to further understand the effects that changes in the mechanical properties of the scaffolds could have in corneal cell outgrowth. In the previous chapter, we focussed on the manufacturing and characterisation of these membranes as well as on understanding their mechanical properties so we could modify their handleability. It has been reported that electrospun membranes made of PCL (Kim) or made of PLGA (Sheffield) on their own support the growth of limbal stem cells (Ortega, Deshpande, *et al.*, 2013; Sefat *et al.*, 2013; Kim, Kim and Park, 2018), but the electrospinning conditions reported in these pieces of research were different to ours and they resulted in the production of membranes with thicker microfibrils. Combining PCL with other materials for limbal cell culture has also been reported with mixed results, as it has shown positive results when combined with decellularized amniotic membrane, but a negative effect when blended with gelatine (type B from bovine skin) (Zhou *et al.*, 2019; Sanie-jahromi *et al.*, 2020). Considering the effects of the stiffness and microenvironment of a 3D scaffold, it is necessary to test the cell outgrowth of the blended PLGA-PCL membranes with corneal cells and corneal limbal explants. Therefore, in this chapter we will investigate limbal explant outgrowth on the mechanically tailored membranes. Initially, we will compare the electrospun PLGA membranes with 10%PCL – 90% PLGA, being 10%PCL membrane the first condition that showed different mechanical properties than the PLGA membrane in chapter 2.

### 3.2.- Aim

The aim of this chapter is to study limbal cell outgrowth on PCL-modified mechanically tailored electrospun scaffolds using animal limbal explants.

Specific objectives:

- 1.- Optimise the protocol for limbal explant cell culture on electrospun scaffolds using rabbit and porcine explants.
- 2.- Compare cell outgrowth from limbal explants from rabbit and pig origin using fluorescence microscopy.
- 3.- Analyse and quantify cell outgrowth from limbal explants at different time-points of culture and at difference distances within the scaffold.

### 3.3.- Materials and Methods

#### 3.3.1.- Materials and cells used

In table 3.1 there is a list of all the chemicals and reagents used in this chapter with their respective supplier. In table 3.2 can be seen the cell source used.

**Table 3.1** Chemicals and reagents used

<b>Chemical / Reagent</b>	<b>Supplier</b>
Dulbecco's Modified Eagle's medium (DMEM)	Sigma – Aldrich
Ham's F-12	Sigma – Aldrich
Fetal Calf Serum (FCS)	Sigma – Aldrich
Penicillin Streptomycin (Pen Strep)	Sigma – Aldrich
Amphotericin B	Sigma – Aldrich
Insulin	Sigma – Aldrich

Insulin	Sigma – Aldrich
Epidermal Growth Factors (EGF)	R&D Systems
Povidone – Iodine	Ecolab
Trypsin	Sigma – Aldrich
Dimethyl sulfoxide (DMSO)	Sigma – Aldrich
Formaldehyde	Sigma – Aldrich
DAPI	Sigma – Aldrich
Phalloidin	Sigma – Aldrich
Triton-X	Sigma – Aldrich
Hexamethyldisilazane (HMDS)	Sigma – Aldrich
Ethanol	Sigma – Aldrich
Glutaraldehyde	Sigma – Aldrich

**Table 3.2** Cells used

<b>Cells</b>	<b>Source</b>
Rabbit Limbal Epithelial Cells	<p>A) Isolated from eyes of wild rabbits hunted in United Kingdom. The Wild Meat Company.</p> <p>B) New Zealand white rabbits, all females. Eyes were donated from another experiment where rabbits were treated with aristolochic acid for 150days (used to induce kidney fibrosis) and then with an antibody for 3</p>

	months. This treatment does not affect the eyes of the rabbits.
Porcine Limbal Epithelial Cells	Porcine eyes were obtained from R B Elliot and Son Limited.

### 3.3.2.- Animal limbal explant isolation

Porcine and rabbit eyes were obtained from (RP Elliott abattoir, England) and the Wild Meat Company (Blaxhall, England) respectively. Animal eyes were collected in sealed containers with PBS, keeping cold temperatures with ice around the containers. The eyes were disinfected using 3% Videne antiseptic solution (Ecolab). Later the corneas were extracted and disinfected in solutions of Videne and washed with PBS. The disinfected corneas were placed in corneal limbal media (1:1 DMEM + Glutamax: Ham's F12, 10% fetal bovine serum, 1 U ml<sup>-1</sup> penicillin, 100 mg ml<sup>-1</sup> streptomycin, 2.5 µg ml<sup>-1</sup> amphotericin, 10 ng ml<sup>-1</sup> of EGF and 5 µg ml<sup>-1</sup> of insulin (Ortega et al., 2013)) overnight to observe any contamination before using them. After overnight (rabbit) or 48hours (pig) without seeing contamination on them, the limbus was minced to be used for culture. In table 3.3 can be seen the CLE medium recipe, and in figure 3.1 is displayed the animal limbal explant isolation.

**Table 3.3** CLE medium recipe for 500 mL.

Component	Volume (mL)	Final concentration
DMEM	219	
Ham's F12	219	
Pen Strep	5	100 U/mL
Amphotericin B	5	2.5 µg/mL
EGF	0.0025	2.5 ng/ml
Insulin	2.5	5 µg/mL
FCS	50	10%

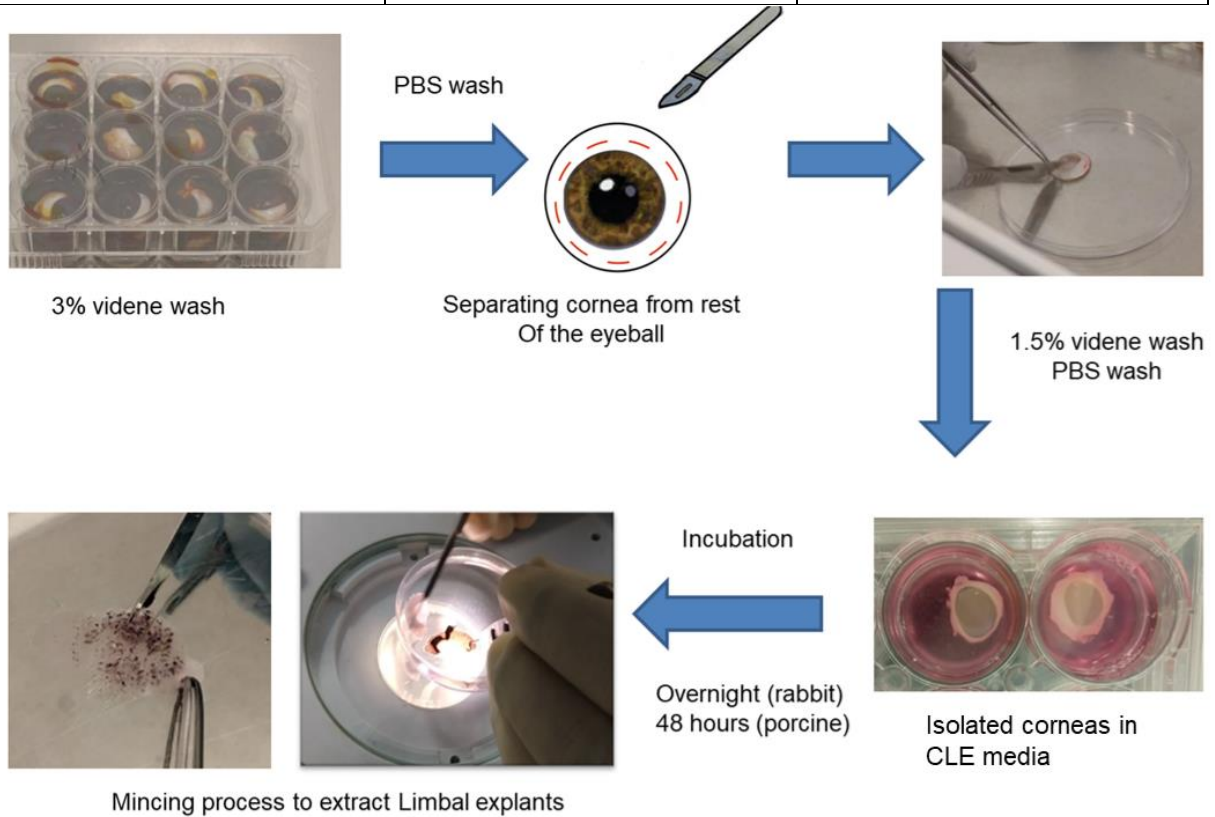


**Figure 3.1** Animal limbal explant isolation process. In the top left of this figure is displayed the animal eyes being cleaned in a 3% videne solution. After a PBS wash, the cornea is separated from the rest of the eyeball and washed in 1.5% videne solution and PBS. The extracted cornea is submerged in CLE media and then put inside an incubator overnight (for rabbit) or 48 hours (for pig). After the incubation time, with no contamination, the limbus is separated from the rest of the cornea and minced to get explants, as can be seen in the bottom left of the figure.

### **3.3.3.- Animal limbal epithelial cell culture**

This procedure is used after cleaning the eyes to keep a stock of epithelial limbal cells. Clean eyes are immersed in 1.5% iodine solution for 60 seconds and washed with PBS. Then the cornea is cut out and separated from the scleral button. From the removed cornea, the limbal area is extracted (the limbus can be described as the junction between the transparent cornea with the white sclera). The limbal area is chopped into small pieces to later scrape the limbal cells out of them and collect them in a well (of a 6 well plate) with RLE medium. The media with cells is spun at 1000 rpm for 5 minutes, counted in a Neubauer chamber, and then seeded into a T25 flask containing irradiated 3T3s. The media was changed when the colour of it changed from pink to a pale yellow (2 days).

### **3.3.4.- Animal limbal explants seeding into membranes**

For seeding the explants into the membranes, sterile electrospun membranes were put in the centre of 35 mm petri dishes and fixed in position with autoclaved metal rings. 3 explants were then located on the membrane simulating the scaffold and left to dry for 30 minutes to stimulate a natural fixing of the explant with the membrane in the incubator. After the fixing time, media was added until covering the membrane and explants and put back in the incubator. The media was changed every 3 days. Figure 3.2 shows this process of seeding into the membranes.

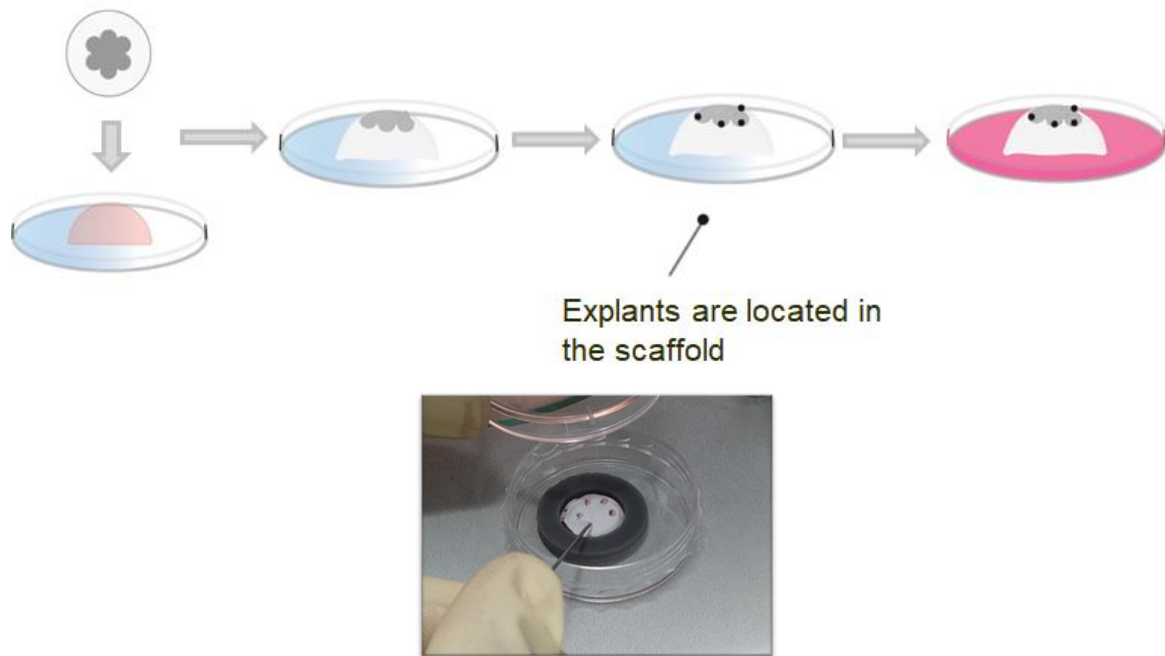


**Figure 3.2** Animal limbal explants seeding into electrospun scaffolds. In the top is displayed a schematic representation of this process. An electrospun scaffold is positioned in the middle of a p35 petri dish to then seed the explants, and then adding media. In the bottom can be seen the process of adding explants to a scaffold

### 3.3.5.- Cell outgrowth on electrospun scaffolds and staining techniques

Cell outgrowth from animal explants was studied using 4 different microscopies, Inverted Olympus Fluorescent Microscope, Zeiss Z1 Lightsheet Microscope, and Tescan Vega3 LMU Scanning Electron Microscope. Inverted fluorescent microscopy, and light sheet microscopy were used to analyse the cell outgrowth and these techniques were compared to know which one would give us a better understanding of the outgrowth in the electrospun membrane. SEM was used to see changes in the electrospun membrane when there is cell outgrowth on them.

To analyse cell outgrowth under fluorescent and lightsheet microscopes, the samples were stained with DAPI and Phalloidin TRITC. To do this staining, the samples were washed three times with PBS to completely remove the media. Then, enough Triton-X (1%) was added to the samples to cover them (approximately 1.5 mL depending on the curvature of the scaffold) for 30 minutes. After the time passed, the samples were once again washed three

times with PBS to completely remove the PBS. Now that the samples were clean, they were fixed using 3.7% formaldehyde solution (approximately 1.5 mL depending on the curvature of the scaffold) overnight in fridge conditions. Later, the samples were washed three times with PBS to remove the formaldehyde. Once the washes were complete, a solution of DAPI and Phalloidin TRITC was added to the samples, once again covering them depending on their curvature for 1 hour. Finally, the samples were washed two times with PBS and left with PBS for imaging purposes.

To analyse cell outgrowth in SEM, a Hexamethyldisilazane (HMDS) staining protocol was used. To start this protocol, the samples were washed with PBS three times to remove the media. Then, the samples were covered in Glutaraldehyde solution (2.5%) for 1 hour. After this time had passed, the samples were washed once again three times with PBS. Later, the samples were washed once more, but this time with distilled water. After the samples were washed with distilled water, they underwent a dehydration protocol with ethanol inside a fume cupboard. The dehydration protocol consisted of submerging the samples for 15 minutes in different concentrations of ethanol, starting at 35%, 60%, 80%, 90%, and ending at 100%. After dehydration, and still inside the fume cupboard, the HMDS treatment was made. The HMDS treatment consisted of submerging the samples in a 1:1 ethanol:HMDS solution for 1 hour, to then wash them twice in 100% HMDS. After that, HMDS was removed from the samples and left to air-dry in the fume cupboard for 1 hour. Finally, after the samples were dry, they were gold coated for imaging.

### **3.3.6.- Analysing and quantifying cell outgrowth on electrospun scaffolds**

Using the protocol of epifluorescence and microscopy described in 3.3.5, and as well with 2 weeks of culture on the membranes, a quantification of the outgrowth was made using the following steps:

1. Localise in the epifluorescence images the explant and outgrowth from it for every condition of membrane.

2. Visually separate the explant from the outgrowth with a line.
3. Using the scale bar as a reference, create eight squares of  $100\ \mu\text{m} \times 100\ \mu\text{m}$ . These squares will be used to separate eight sections of cellular outgrowth as representations of the total cellular outgrowth from the explant. Four squares will be positioned at  $100\ \mu\text{m}$  distance from the explant, while the other 4 squares will be positioned at  $500\ \mu\text{m}$  distance from the explant.
4. Count all the cells (blue DAPI stains) in the squares.
5. Repeat this process in all the images and get the averages to compare the average cell outgrowth in every membrane.

This protocol was repeated but instead of using two groups of 4 squares at different distances, 6 squares in a distance from 0 to  $300\ \mu\text{m}$  from the explant showing cell outgrowth were picked as well. Figure 3.3 display an example of this protocol.

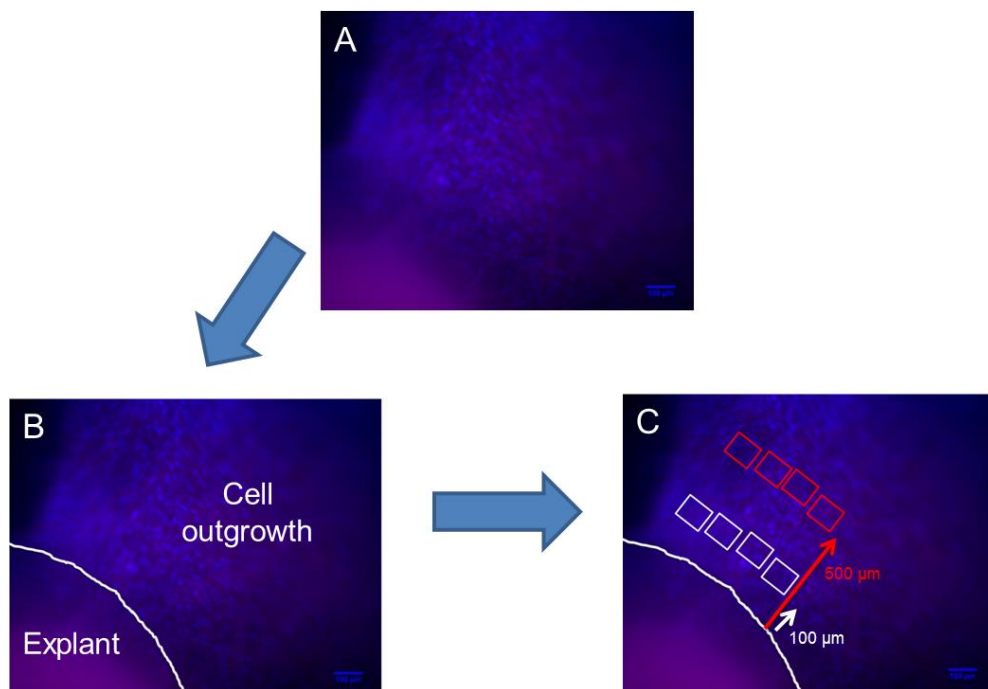


**Figure 3.3** Process of creating the squares that will be used to measure the average cell outgrowth in the membranes after 2 weeks of culture. A is the epifluorescence image of cellular outgrowth from an explant on an electrospun membrane. B shows a white line to separate visually the explant from the outgrowth. C displays the 8 squares that will be used to measure the average cell outgrowth on the membranes, where 4 of them are at  $100\ \mu\text{m}$  from the explant (white) while the other four are at  $500\ \mu\text{m}$  from the explant (red).

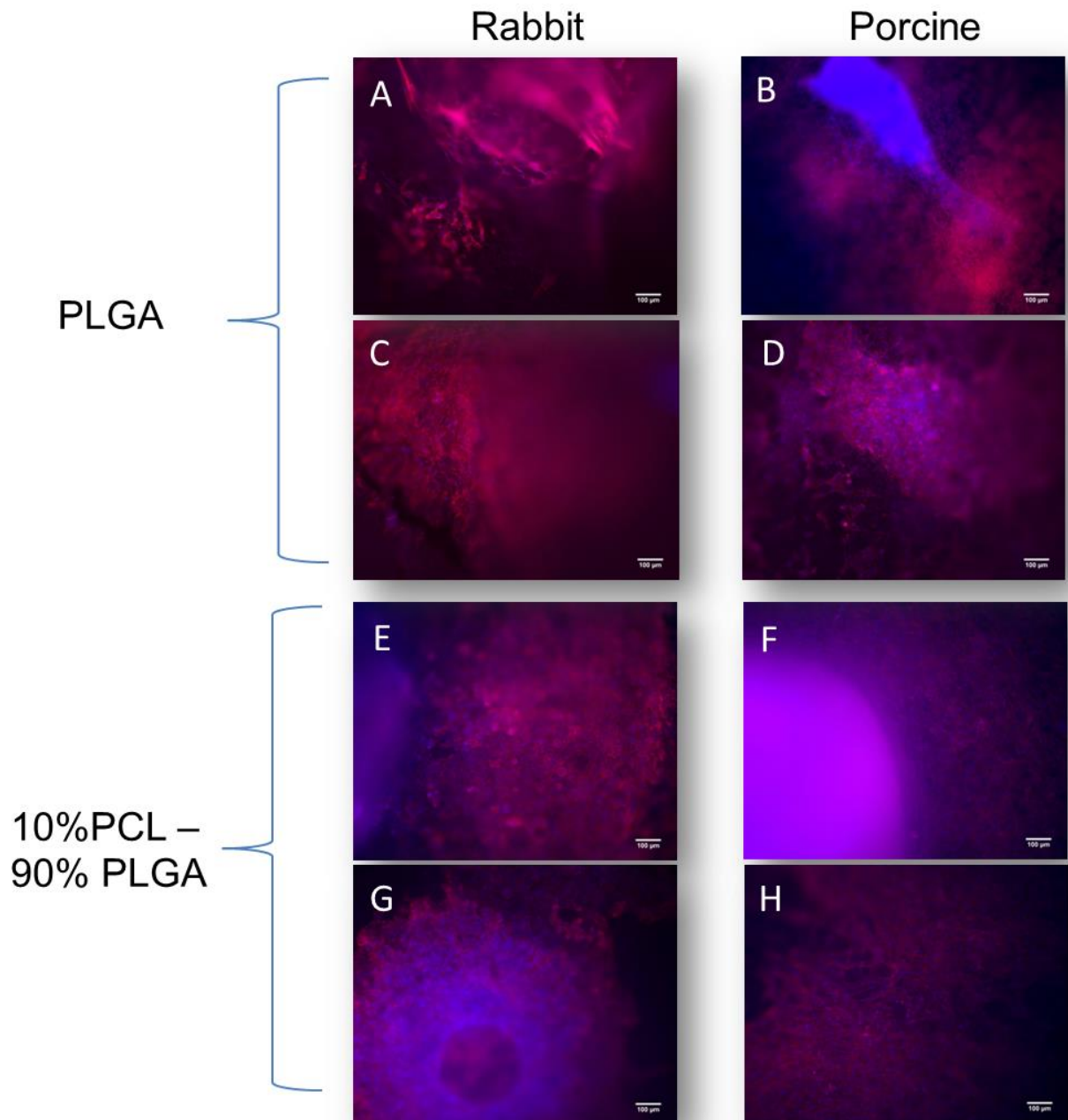
### **3.3.7.- Statistical analysis**

GraphPad Prism 7 software was used for one-way ANOVA analysis with p value <0.05 in consideration for statistical significance.

## **3.4.- Results**

### **3.4.1.- Rabbit limbal explants v/s porcine limbal explants**

Two animal sources were used; rabbit and porcine eyes (table 3.1.2). As mentioned in section 1.4, rabbit eyes have been used in corneal research extensively. Previously in this group, rabbit limbal explants were utilized to test electrospun scaffolds (Deshpande, Ramachandran, Sefat, *et al.*, 2013)(Ortega, Sefat, *et al.*, 2014). Although the protocols of using rabbit eyes as an animal model to study corneal outgrowth from limbal explants have been successfully used in this group, securing a reliable source of them has been challenging, as the main source of rabbit eyes were obtained by the company through wild hunting. Taking into consideration the reliability of the rabbit eyes, and as well the reliability of the condition they were in, it was needed to explore other options of animal eyes. Due to this, it was decided to move to a porcine model, which as mentioned in section 1.4, is a model well identified with a homogeneous limbal zone. Using the protocols 3.3.2, 3.3.3, and 3.3.4 limbal explants were isolated and cultured into electrospun scaffolds. For analyzing biocompatibility in the mechanically tailored electrospun scaffolds, only two scaffold conditions were analyzed and compared, pure PLGA and 10%PCL – 90%PLGA as the latest is the first condition to show mechanical properties changes with minimum amount of PCL added (2.5). In figure 3.4 can be seen a comparison of using these 2 animal sources.



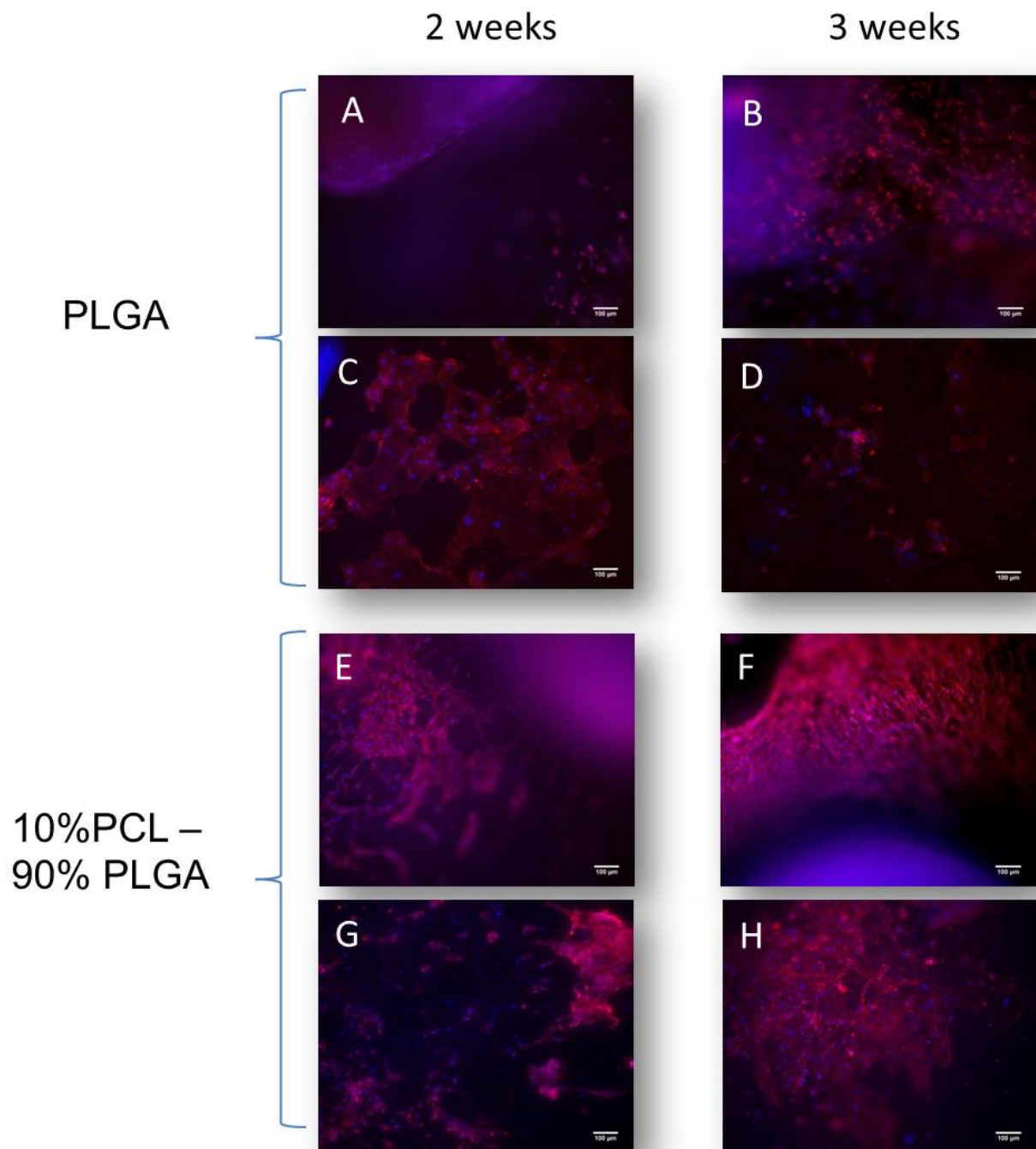
**Figure 3.4** Comparison of rabbit limbal explant culture with porcine limbal explant culture on 2 types of electrospun scaffolds after 3 weeks of culture. Column ACEG is rabbit explants, Column BDFH is porcine explants. Rows AB and CD are PLGA electrospun scaffolds, while rows EF GH are 10%PCL – 90%PLGA. In rows AB and EF are shown the limbal explant and the outgrowth from it. Rows CD and GH shows the outgrowth in the scaffolds. Staining used is DAPI – Phalloidin TRITC. Scale bar = 100 μm.

Figure 3.4 displays a comparison between the limbal explant outgrowth on electrospun scaffolds of two sources of animals, rabbit (ACEG) and pig (BDFH). 2 electrospun scaffold conditions were used, PLGA (ABCD) and 10%PCL – 90%PLGA (EFGH). The images were acquired using epifluorescence microscopy and staining the samples with DAPI and Phalloidin TRITC. In the figure, we can see that with both sources of animal explants, a healthy outgrowth in the electrospun scaffolds is detected. As well, when comparing the two scaffolds, no

appreciable difference can be seen, in both cases the outgrowth is clear. Then, and considering getting porcine limbal explants is more reliable than rabbits, we moved forward using porcine explants.

### **3.4.2.- Studying cell outgrowth at 2 and 3 weeks of culture on scaffolds**

With a more reliable source of animal explants achieved, it was decided to study the time needed for culture of the explants in the electrospun membranes. We know due to previous work developed in this group that PLGA electrospun membranes stay one month in the eye and in vitro before starting to disappear completely (Sefat *et al.*, 2013; Ramachandran *et al.*, 2019). However, considering that in this research different membranes are being compared, it is better to compare cell outgrowth in an early stage than membrane breakdown. In 3.4.1 we used 3 weeks as culture time and significant outgrowth was observable. In the following figures (3.5, 3.6, 3.7) 2 weeks and 3 weeks of culture will be compared with 3 microscopy techniques; epifluorescence microscopy, light sheet microscopy, and SEM respectively.



**Figure 3.5** Comparison of porcine limbal explant culture on 2 types of electrospun scaffolds after 2 and 3 weeks of culture using epifluorescence microscopy. Column ACEG is 2 weeks culture, Column BDFH is 3 weeks culture. Rows AB and CD are PLGA electrospun scaffolds, while rows EF GH are 10%PCL – 90%PLGA. In rows AB and EF are shown the limbal explant and the outgrowth from it. Rows CD and GH shows the outgrowth in the scaffolds. Staining used is DAPI – Phalloidin TRITC. Scale bar = 100  $\mu$ m.

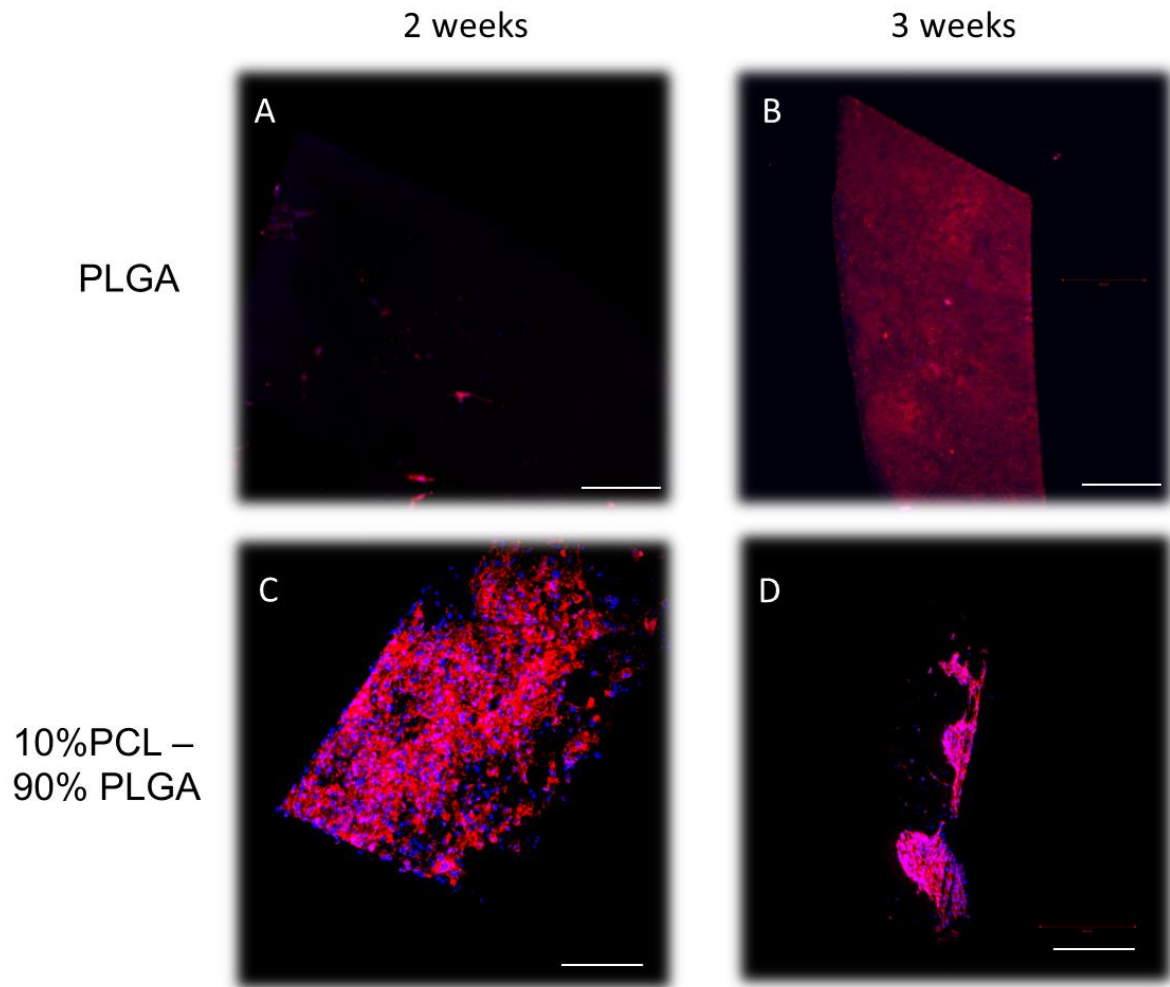


**Figure 3.6** Comparison of porcine limbal explant culture on 2 types of electrospun scaffolds after 2 and 3 weeks of culture using light sheet microscopy. Column AC is 2 weeks culture on scaffolds. Column BD is 3 weeks culture on scaffolds. Culture.staining used is DAPI – Phalloidin TRITC. Scale bar = 200  $\mu$ m.

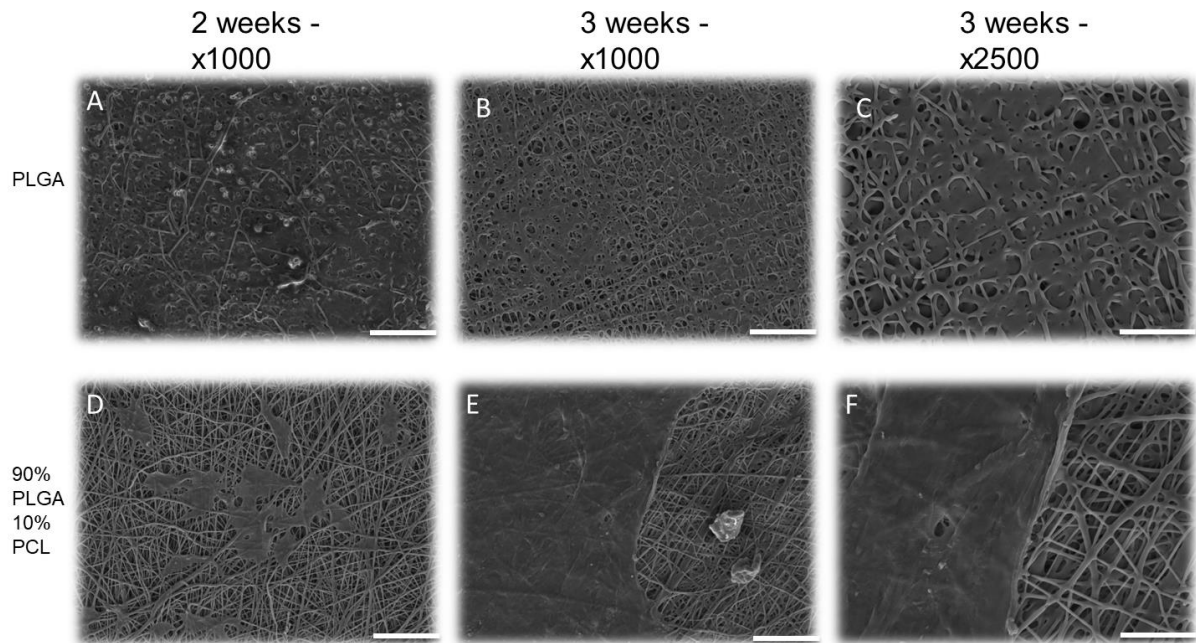


**Figure 3.7** Comparison of porcine limbal explant culture on 2 types of electrospun scaffolds after 2 and 3 weeks of culture using S.E.M. Images A and B are limbal outgrowth at 2 and 3 weeks in PLGA respectively. Images D and E are limbal outgrowth at 2 and 3 weeks in 10%PCL – 90%PLGA respectively. C and F are zoomed images at x2500 to appreciate better the outgrowth at 3 weeks in PLGA (E) and 10%PCL – 90%PLGA (F). Culture staining was done using HMDS staining protocol. Scale bar in ABCD = 20  $\mu$ m, in EF = 50  $\mu$ m.

Figure 3.5 shows the limbal stem cell outgrowth from limbal explants at 2 and 3 weeks of culture on the membranes. A, B, C and D is cell outgrowth on an electrospun PLGA membrane; while E, F, G and H is cell outgrowth on an electrospun 10%PCL – 90%PLGA membrane. A and B show outgrowth from the explant, where the explants have an intense purple colour due to being strongly stained by DAPI and phalloidin. C and D show the cell outgrowth on the membrane in a distance between explants. These 4 images show cell outgrowth from the explants through the electrospun PLGA membrane, with no clear difference in the amount of outgrowth between 2 or 3 weeks of culture. Similarly, E and F show outgrowth from the explant but in an electrospun 10% PCL – 90% PLGA membrane. While G and H show the cell outgrowth on the membrane in a distance between explants. Comparably to what was seen with the PLGA membranes, a clear cell outgrowth from the explants can be seen in the 10% PCL – 90% PLGA membranes. A quantitative method to compare the outgrowth is needed to allow us to differentiate the amount of outgrowth between 2 and 3 weeks, as well as between the membranes, as with these images it is hard to visually detect a difference.

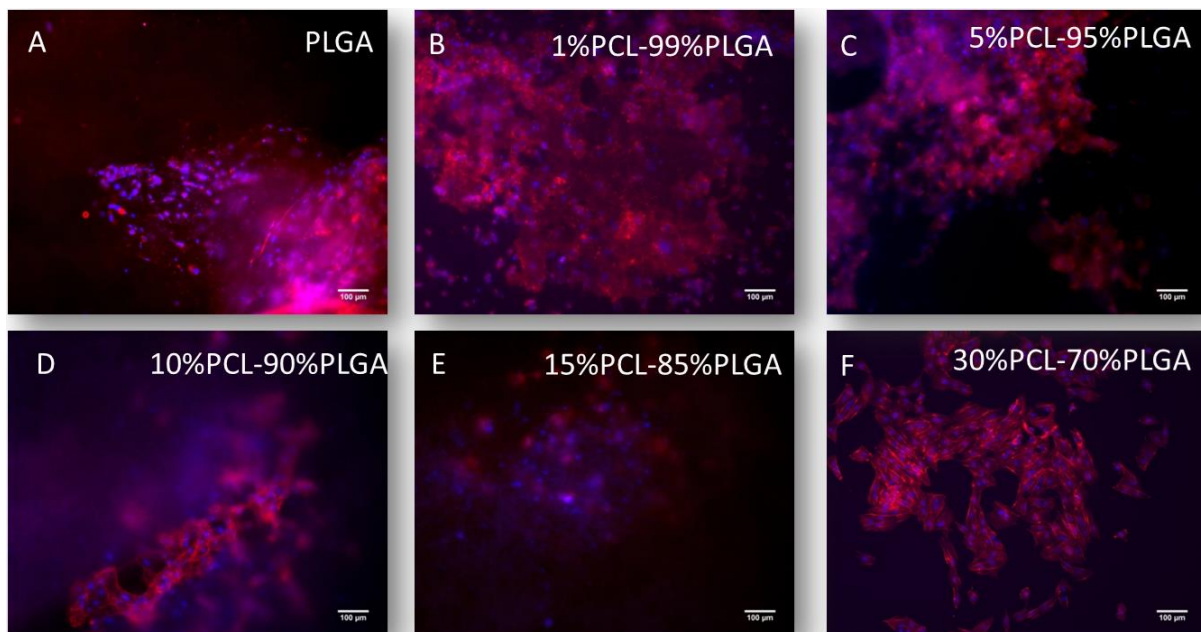
Nevertheless, epifluorescent microscopy with DAPI and Phalloidin stains showed to be a simple and effective methodology to see limbal cell outgrowth from explants on electrospun membranes.

Figure 3.6 displays the cell outgrowth in PLGA and 10% PCL – 90% PLGA membranes using light sheet microscopy. For these images, a section of no more than 1 mm width of the membranes was chosen. The section selected in each membrane was between the explants on the membrane, as equidistant as possible. In A and B some cell outgrowth can be seen, but not as much as the one detected through epifluorescence. On the other hand, in C and D a clear cell outgrowth can be seen on the 10% PCL – 90% PLGA electrospun membrane. In the case for image A, and considering that cell outgrowth was detected using epifluorescence microscopy, we hypothesize that the section selected of the membrane for this analysis was not close to a explant seeding area as no clear outgrowth is seen.

Figure 3.7 reveals the cell outgrowth in PLGA and 10% PCL – 90% PLGA membranes using SEM. With SEM, we can see in the figures not only the cell outgrowth, but as well how the membranes have been affected through the explant culture. In A, B and C can be seen that with this microscopy technique it is hard to detect the cell outgrowth over the electrospun fibres after 3 weeks as the morphology of these fibres had changed. On the other hand, in D, E and F the cell outgrowth can clearly be differentiated over the electrospun fibres.

### **3.4.3.- Porcine explants in mechanically tailored scaffolds (2 weeks of culture)**

In 3.4.2 it was demonstrated that 2 of the electrospun membranes were suitable as cell carriers for limbal stem cells as through 3 different microscopy techniques we have seen cell outgrowth from limbal explants. The next step is to expand the analysis to all the membrane conditions and compare the cell outgrowth in each of them. In figure 3.8 can be seen the limbal stem cell outgrowth in the 6 different membrane conditions after 2 weeks of culture.



**Figure 3.8** Porcine limbal explant culture on mechanically tailored scaffolds after 2 weeks of culture. A: PLGA; B: 1%PCL – 99%PLGA; C: 5%PCL – 95%PLGA; D: 10%PCL – 90%PLGA; E: 15%PCL – 85%PLGA; F: 30%PCL – 70%PLGA. Staining used is DAPI – Phalloidin TRITC. Scale bar = 100  $\mu$ m.

Figure 3.8 shows limbal stem cell outgrowth from porcine limbal explants in 6 different electrospun membrane conditions after 2 weeks of culture. Similarly to what was seen in figure 3.5, in all the membrane conditions can be seen cell outgrowth on the membranes after 2 weeks of culture.

#### 3.4.4.- Quantification of cellular outgrowth on the membranes

3.4.3 showed outgrowth in all the membranes without seeing any difference in the amount of outgrowth between them. Using the protocol explained in 3.3.6, 6 sections of outgrowth on the membranes were selected and calculated an average outgrowth per electrospun membrane as is shown in figure 3.9. The membrane 30%PCL – 70%PLGA presented as well cell outgrowth in the other side of the membrane (side not seeded with explants) and is represented in the figure as 30%PCL – 70%PLGA (inv).

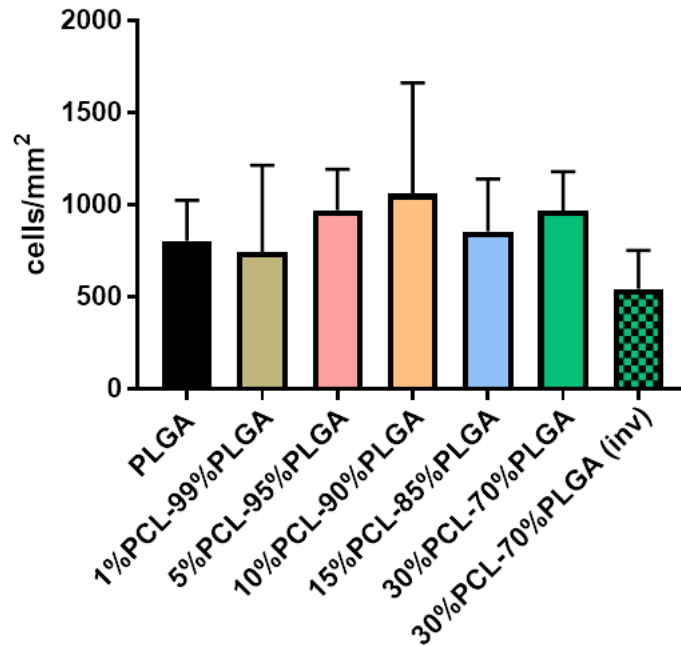


**Figure 3.9** Average cell outgrowth from porcine limbal explants on mechanically tailored scaffolds after 2 weeks of culture. In the case of 30%PCL – 70%PLGA cell outgrowth was visible on the other side of the membrane as well (the one where the explants were not seeded), so they were measured as well. N=3, n=18.

In figure 3.9 is displayed the average cell outgrowth of porcine limbal explant culture on our membranes after 2 weeks of culture. As previously described in 3.3.6, with our methodology we are selecting 6 squares representative of cell outgrowth in the images obtained from epifluorescence microscopy to get these results. These 6 squares are selected from a distance to the explant from 0 to 300  $\mu\text{m}$ . As previously seen in 3.8, the cell outgrowth in every membrane is comparable and not being affected by the polymer composition of our blended electrospun scaffolds. No statistical difference can be seen in the cellular outgrowth on different membranes ( $p > 0.05$  between them). It is important to notice that in the case of 30% PCL – 70% PLGA cellular outgrowth was clearly identified on the other side of the membrane, suggesting that the cell outgrowth in that membrane did not only grow across the surface of the membrane, but as well into it.

Considering the results shown in 3.9, we also studied the cell outgrowth at two distances from the explants, 100 and 500  $\mu\text{m}$ , which is shown in figure 3.10.

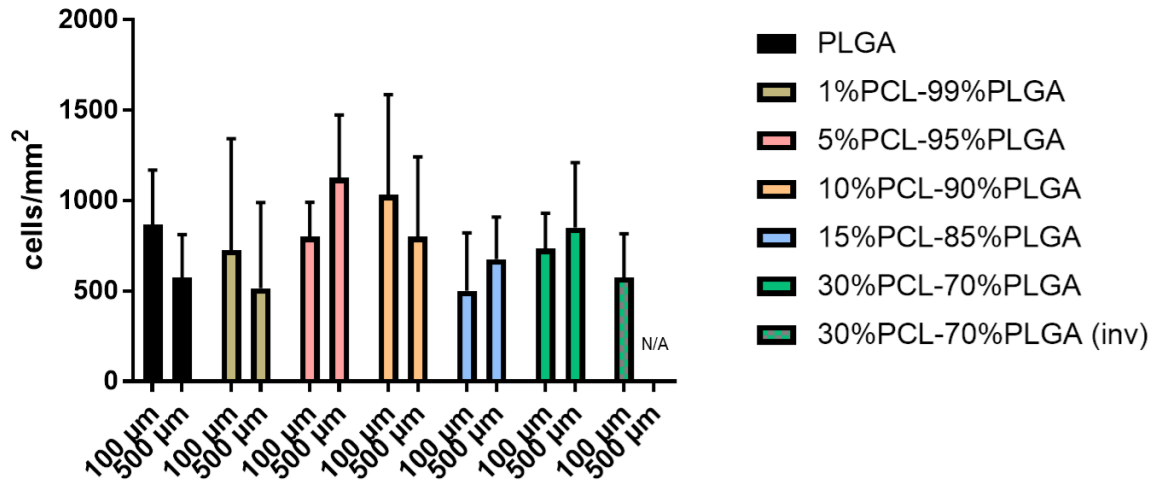


**Figure 3.10** Average cell outgrowth from porcine limbal explants on mechanically tailored scaffolds after 2 weeks of culture at two distances from the explant (100 and 500 µm). In the case of 30%PCL – 70%PLGA cell outgrowth was visible on the other side of the membrane but a distance from the explant was not defined, so for comparison purposes it was only selected as data for 100 µm. N=3, n=12.

Figure 3.10 reveals that there are no statistical differences between measuring the explant cell outgrowth at 100 or 500 µm distance from the explant. For 30%PCL – 70%PLGA (inv) we only considered 100 µm as the measured distance as the outgrowth we are highlighting is the cell outgrowth that went through the membrane to the other side of the scaffold, directly below the explant on the seeding side. No statistical difference can be seen in the cellular outgrowth at different distance ( $p > 0.05$  between them)

Due to the COVID-19 global pandemic, this experiment was realized only once in triplicates. However considering the variability of the results, more repetitions are needed to obtain a more certain average of cell outgrowth in each electrospun scaffold blend. Another factor to take into account when working with limbal explant culture is the quality and size of the explants seeded into the membranes (Kethiri *et al.*, 2017). One of the limitations in our work is to avoid using fibrin glue to fix the explants to the membranes, making it hard to strongly fix the explants to the membranes. Although the explants are fixed through the culture, they are unlikely to stay attached after the numerous washes of the DAPI-Phalloidin staining needed for microscopy.

### **3.4.5.- COVID-19 Considerations**

As briefly explained in 3.4.4, the global pandemic COVID-19 affected us in this chapter to be unable to achieve more quantitative data regarding the cell outgrowth on our electrospun membrane conditions (PLGA, 1%PCL – 99%PLGA; 5%PCL – 95%PLGA; 10%PCL – 90%PLGA; 15%PCL – 85%PLGA; 30%PCL – 70%PLGA). As well it affected us in doing cultures with porcine corneal fibroblasts which we previously isolated. More details about this impact are reported in appendix A.

### 3.5.- Discussion

The relevance of cell carriers or membranes for corneal regeneration has been demonstrated since 1998 when it was shown that patients with partial LSCD amniotic membranes were able to have corneal regeneration without stem cell transplantation (Sharma *et al.*, 1998). Since then, and due to the limitations of amniotic membrane as a cell carrier, different approaches have been studied that were covered in the literature review (Brouki *et al.*, 2020). Membranes made of PLGA and PCL are the ones that come to our attention due to the fast degradation of PLGA, and the mechanical properties of PCL. PLGA membranes as cell carriers for limbal stem cells have been studied in the University of Sheffield for more than 8 years with positive results supporting the growth of limbal epithelial cells and their transfer to the cornea (Deshpande *et al.*, 2011; Deshpande, Ramachandran, Sangwan, *et al.*, 2013; Ortega, Deshpande, *et al.*, 2013; Sefat *et al.*, 2013; Ramachandran *et al.*, 2019). Electrospun PLGA membranes have shown that after 2 to 4 weeks they start breaking down losing 75% of their weight by 6 weeks, with PLGA with a higher molecular weight breaking down slower than its lower molecular weight counterpart (Deshpande, Ramachandran, Sangwan, *et al.*, 2013; Sefat *et al.*, 2013). When comparing these results with the PLGA membrane in this research two differences can be noted; first the fibre diameter in these researches is higher than the one manufactured by us, and secondly, the molecular weight of our PLGA has an average of 70,000 g/mol versus the 153,000 g/mol and 44,000 g/mol used by Sefat and Deshpande. Regardless of these differences; the electrospun PLGA membrane manufactured by us worked as a cell carrier, showing clear cell outgrowth from the limbal explants from two animal sources. As well, in figure 3.7 we can see that the electrospun PLGA membrane is losing its microenvironment features after 3 weeks of culture, similar to what was previously reported. Additionally, and considering what was seen in figure 2.15, we know that the PLGA membrane we manufactured is completely broken down in 3 months just by water and temperature effects. It would be interesting for future work to extend the cell culture to two months to see differences in the break down time to see if our manufacturing differences affect this aspect as well.

In the case of membranes made with PCL, several studies have been made using this polymer, as even though it has a long degradation time, its biocompatibility is desired as it does

not induce any immunological reactions after degradation (Ang *et al.*, 2006; Sharma *et al.*, 2011). PCL as an electrospun membrane for human corneal cells has been used in random or aligned orientation, but the fibre orientation did not show any difference in the adherence and proliferation of the corneal cell lines (Sta *et al.*, 2017). In Sta's research as well they combine PCL with poly glycerol sebacate (PGS) and chitosan reducing the hydrophobicity of the membranes, but no significant change in the proliferation was seen. Radially aligned PCL membranes have shown that they can guide the main collagen and cellular actin filament in the extracellular matrix (Kim, Kim and Park, 2018). PCL as a membrane has proven to keep its adhesion, proliferation and differentiation of the cultivated limbal cell properties even when mixed with antimicrobial agents like cefuroxime (CF) or titanium dioxide (TiO<sub>2</sub>) (Trcin *et al.*, 2020). In our research, as seen in figure 3.8, a similar proliferation and adhesion can be seen in our different PLGA-PCL blends, which is expected considering both PLGA and PCL have shown good results as cell carriers for limbal stem cells.

PCL membranes combined with other membranes for limbal stem cell culture have been explored as well. Composite membrane of PCL with decellularized amniotic membrane (dAM) has been studied with rabbit limbal stem cells (Zhou *et al.*, 2019). In this research the composite membrane of dAM-PCL maintains the immunomodulatory and pro-regenerative properties of dAM, but as well promotes the re-epithelialization in the repair site of the rabbit LSCD model with a reduced inflammation. These enhancements were due to the addition of PCL nanofibers as they stabilize and toughen the dAM to achieve a longer-lasting and durable membrane (Zhou *et al.*, 2019). While in the results presented in this chapter we were not able to measure and compare the cell outgrowth between the membrane conditions with different PCL additions, in figure 3.7 we can see that the membrane with 10% PCL preserved better its microenvironment compared to the pure PLGA membrane at the same time-point. On the other hand, a negative effect has been reported when PCL is blended with Gelatine (type B from bovine skin) as the blended membrane had higher levels of vascularization and inflammation compared to the pure PCL ones (Sanie-jahromi *et al.*, 2020).

Rabbit cornea and porcine corneas have different sizes, mechanical properties, and limbal structures in the eyes (Bozkir *et al.*, 1997; Huang *et al.*, 2011; Thomasy *et al.*, 2014; Grieve *et al.*, 2015; Menduni *et al.*, 2018). Regardless of these differences, figure 3.4 does not

show any difference between the outgrowth of both pig and rabbit limbal cell outgrowth, making them good candidates to study the cell carrier capacity of the membranes.

Regarding the explant cell outgrowth seen in figures 3.9 and 3.10, no statistical difference can be seen between the membrane blends. Although, as previously mentioned, due to COVID-19 we could not do this experiment three times, which would have helped to reduce the variability in the results, the amount of outgrowth in the membranes are comparable. Theoretically, as seen in the previous works cited, the cell outgrowth of the blends should not be affected by the cellular adhesion of the cells to the membrane, as both PLGA and PCL have shown good adhesion to limbal stem cells (Deshpande *et al.*, 2011; Sta *et al.*, 2017). On the other hand, in chapter 2 we saw that the addition of PCL improved the degradability in water of the membranes, which can be seen as well in figure 3.7. Another factor to consider in the variability of the results is the quality and size of the limbal explants seeded into the membranes. Vivek's group in L.V. Prasad Eye Institute have worked with improving this aspect of the SLET surgery and found out that explants from live biopsy have an 80% growth potential, versus the 40% growth potential of cadaveric ones, which is the type of explants we used (Kethiri *et al.*, 2017).

One membrane condition that is relevant to highlight is 30%PCL – 70%PLGA. In figure 3.9 and 3.10 this membrane shows that the cell outgrowth does not only proliferate on the surface, but also through it as cell outgrowth can be seen in the opposite side of the explant seeding in the membrane. One of the reasons for this can be explained back in figure 2.15, where it was shown that this membrane blend condition was able to preserve better its fibrous microenvironment, therefore making it easier for the cells to outgrowth through the membrane. An interesting future work regarding this type of membrane would be to try it in a wounded cornea model (Ortega, Deshpande, *et al.*, 2013), where its capacity to provide a better outgrowth through the membrane could have a positive impact in the cornea regeneration.

### 3.6.- Conclusion

Limbal cell outgrowth was studied on PLGA-PCL electrospun membranes. Using rabbit or porcine limbal explants on the electrospun membranes did not show any difference in the capacity of the membranes as cell carriers. PLGA and PLGA-PCL membranes showed outgrowth from limbal explants at 2 and 3 weeks with no statistical difference in the amount of cell outgrowth between them. 30%PCL – 70%PLGA showed cell outgrowth as well on the other side of the membrane that was not seeded, showing that the cell outgrowth went through the membrane in this blend condition. Finally, all mechanically tailored membranes developed in this research showed a good capacity as cell carriers of limbal corneal cells.

## Chapter 4: Introducing complexity within electrospun membranes via the incorporation of defined 3D-microfeatures

### 4.1.- Introduction

In the previous chapters we have explored the mechanical properties of our newly developed membranes and the feasibility of using them as cell carriers for the use of limbal explants as an epithelial cell source. These results are preliminary but generally positive and indicate that our mechanically modified membranes are potential candidates to be used in SLET surgery. Another relevant aspect to take into account for the fabrication of synthetic membranes is the effect of the underlying topography on cell behaviour. The importance of the 3D micro-structure of the cornea has been consistently reported as it affects some of its key features; including tissue transparency, mechanical strength, refractive effect and the phenotype of limbal epithelial stem cells (Bao *et al.*, 2012; Wilson *et al.*, 2013; Gouveia *et al.*, 2017; Kim, Kim and Park, 2018). Our group in Sheffield has previously worked on the fabrication of a new electrospun microfabricated membrane with targeted and controlled topography that incorporated complex microfeatures and that tried to emulate the limbal stem niches in the limbus (Ortega, Deshpande, *et al.*, 2013; Ramachandran *et al.*, 2019). Stem cell niches are known to be well-defined physical spaces that harbour stem cells in specific tissues; these niches are of high complexity and have the ability to keep stem cells in their undifferentiated state (Bao *et al.*, 2017; Prina *et al.*, 2020). In the cornea, these niches or specialized microenvironments are normally called epithelial crypts and the maintenance of the epithelium relies on the stem cells that reside on them (Prina *et al.*, 2020). These crypts are located in the limbus, which has shown to contain delimited functional areas that house the limbal crypts and that are called Palisades of Vogt (Cotsarelis *et al.*, 1989; Ramos, Scott and Ahmad, 2015). The limbal zone is located between the corneal epithelium and the conjunctival epithelium; opposite to the cornea, the limbus is highly vascularized and due to its morphology is able to protect the limbal stem cells residing in it (Katikireddy and Ula, 2014; Singh, Shukla and Ramachandran, 2015; Yanoff and Sassani, 2015). The limbal zone in a human eye can be seen clearly in the following image 4.1.

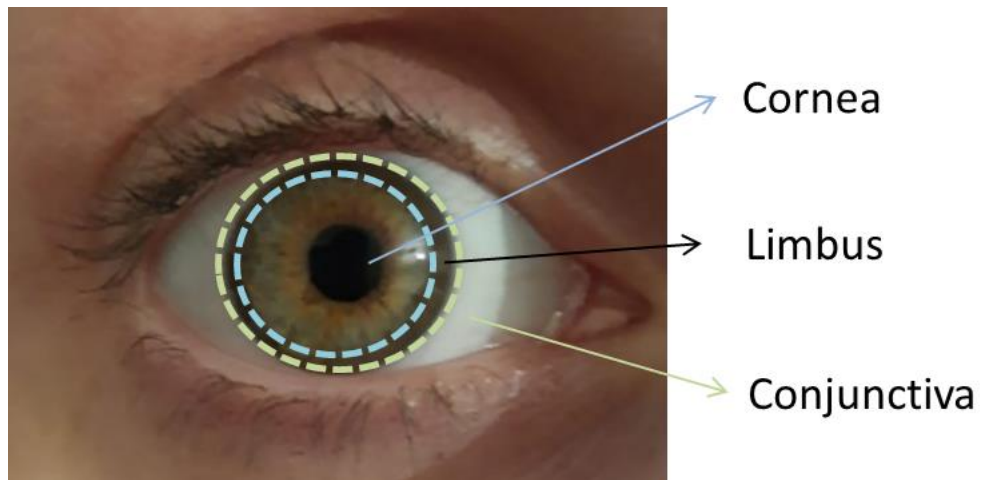


**Figure 4.1.** Human corneal limbus. A frontal view of the human eye showing the cornea, the limbus, and the conjunctiva.

As highlighted above, previous work developed in UoS was directed to the creation of electrospun membranes with microniches that simulate the protective environment of the Palisade of Vogt (Ortega, Deshpande, *et al.*, 2013; Ortega, McKean, *et al.*, 2014). In this research, corneal cell lines were seeded to the artificial microniches and this showed that the loaded cells were able to form a multi-layer epithelium when placed on *ex vivo* corneal models for up to 4 weeks. Additionally, the membranes with microniches and coated with fibronectin showed 50% more cell outgrowth than membranes without microniches (Ortega, Deshpande, *et al.*, 2013).

The previous designs were mimicking the stem cell niches, which are 100-200  $\mu\text{m}$  sized pockets (Ortega, Deshpande, *et al.*, 2013). In conjunction with L.V. Prasad Eye Institute we developed an alternative approach. Instead of making stem cell niches directly in the scaffold, they were mostly interested in creating retaining pockets for limbal explants, and this enabled limbal explants to recreate the limbal stem cell niches directly. The explants they normally use in theatre are of approximately 500 -1000  $\mu\text{m}$  and our first attempt to include microfeatures was based on the manufacture of synthetic niches of around 350-500  $\mu\text{m}$  (Kethiri *et al.*, 2017).

The topography of the membrane is important as we have explained above, however the intrinsic microstructure should also be considered. The cornea is a complex tissue and as highlighted in previous chapters, its mechanics play a key role in directing cell behaviour. For example, collagen fibre alignment and orientation in the cornea has shown to modulate tissue

transparency and refractive effect (Bao *et al.*, 2012; Wilson *et al.*, 2013). In this sense, considering fibre orientation is key for the development of a new membrane and measuring fibre alignment is a very important task that can be intricate. Different approaches have been developed to analyse the impact of fibre orientation on cell growth (Yan *et al.*, 2011; Kim, Kim and Park, 2018; Fernández-pérez *et al.*, 2020), but to our knowledge there are no available protocols to consistently measure a complex structure with more than just one orientation in it.

In this chapter we explore the manufacture of a more surgically-orientated suitable membrane design that can incorporate topographical cues that can be implemented in electrospun membranes to be used in SLET surgeries. It is important to highlight that in 2018 we were granted funding from “MeDe innovation secondment scheme” that allowed me to travel to Hyderabad (India) and interact directly with the specialists at L.V. Prasad Eye Institute (LVPEI). We had fruitful discussions about design and suitability of a membrane for them which we implemented in part of the designs highlighted in this chapter. Additionally, when incorporating complex morphologies within a membrane, it is important to ensure that we can appropriately make and characterise these structures with the correct tools. As reported by Ortega and Paterson the manufacture of intricate structures using substrates enabled the electrospinning to give way to a pool of fibrous structures that can be formed by aligned and randomly distributed fibre domains (Paterson *et al.*, 2017). These fibrous microstructures can be very complex and it is important to accurately measure and quantify the levels of alignment and fibre orientation on the membranes so future cell responses can be understood. In this chapter we propose a simple methodology of collector making involving 3D printing and metal casting with equipment we have available in the School of Clinical Dentistry. Finally, we present a simple and robust quantitative methodology to measure fibre alignment and orientation in different zones of an electrospun membrane using SEM images and the ImageJ software.

## 4.2.- Aim

In this chapter we aim to explore another important aspect in membrane design and manufacture which is the inclusion of micro and macro topographical cues within a fibrous membrane. We also aim to explore new ways to reliably quantify fibre alignment and distribution within complex structures, since we hypothesize this will be key for our future work which will comprise of the study of corneal cell biological responses on these types of new microstructured membranes. To achieve that we set the following specific objectives:

- 1.- Manufacturing of collectors with different designs to develop topographically complex electrospun scaffolds.
- 2.- Preliminary assessment of topography complex electrospun scaffolds with specialists in L. V. Prasad Eye Institute using human limbal explants and studying key physical changes of the membranes (shrinkage) that can have an impact in their clinical use. (Appendix C shows the ethic approval of this research)
- 3.- Developing a reproducible and robust technique to analyse fibre orientation in complex electrospun scaffolds.

## 4.3.- Materials and Methods

### 4.3.1.- Materials

In table 4.1 there is a list of all the chemicals and reagents used in this chapter with their respective supplier, while table 4.2 is for the biological tissues used.

**Table 4.1** Chemicals and reagents used

<b>Chemical / Reagent</b>	<b>Supplier</b>
Milling Wax	Bristol Cadcam
LabCAST®	Solidscape
Solidscape® Support material	Solidscape
Castable photopolymer resin	FormLabs
Sprue Wax	Bego
Sheramaster (Wetting agent)	Shera
SheraLiquid®	Shera
Sherafina-rapid®	Shera
Tilite Alloy	Talladium

**Table 4.2** Biological tissue used

<b>Biological tissue</b>	<b>Source</b>
Human corneas	Human corneas and human amniotic membrane was donated by L.V. Prasad Eye Institute in our visit to their institute. The tissues were donated by their patients and preserved through their standards. Full information about the ethical approval can be seen in appendix C.
Human amniotic membrane	

### 4.3.2.- Manufacturing collectors for electrospinning templating

#### a) Collector design:

The collectors were designed using the software Inventor Professional 2017 (Autodesk, USA). Once the Software is open, the new standard ipt option is selected. Later, in sketch the “start 2D sketch” is chosen and for then starting to draw the desired design in the XZ plane. Once the 2D sketch is done, the extrude option in 3D model is selected and the collectors are made and saved in stl file. The designs were created in consideration of the surgeon’s practical design input and are separated into two generations. The first generation of collectors was made to identify the best collector manufacturing technique and how the electrospinning works in it, as well as being used in India as a first trial (further explained in 4.4.1). The second generation was used to understand and study the fibre alignment in plane and hemispherical collectors. All the collectors have a diameter of 15 mm to be used as corneal cell carriers. An schematic representation of this process can be seen in figure 4.2.

#### b) Collector printing

b.1. Wax Drilling: Roland DMX-50 was the Dental Milling Machine used to drill the collector models on professional milling wax of 98 x 14 mm Blue.

b.2. Wax 3D printing: The 3D printer used was 3ZLab from Solidscape®. The stl file of the collector is loaded into the software 3zworks that will define how the print will look. The final version after using 3zworks is loaded into the 3D printer that should be warmed previously (usually left turned with a room temperature of around 20°C overnight). This printer uses LabCAST and Soliscape support material as waxes.

b.3. Resin 3D printing: The 3D printer used was Form 2 from FormLabs®. The stl file of the collectors is loaded in the FormLabs PreForm print preparation software. To be able to use the printed design into collectors, a castable photopolymer resin is used (product code RS-F2-CABL-02, FormLabs®). In this technique, the resin is cured layer by layer with a 250mW UV

laser. For our designs, the speed of printing selected was normal as high definition was not required due to their details being bigger than 25  $\mu\text{m}$ .

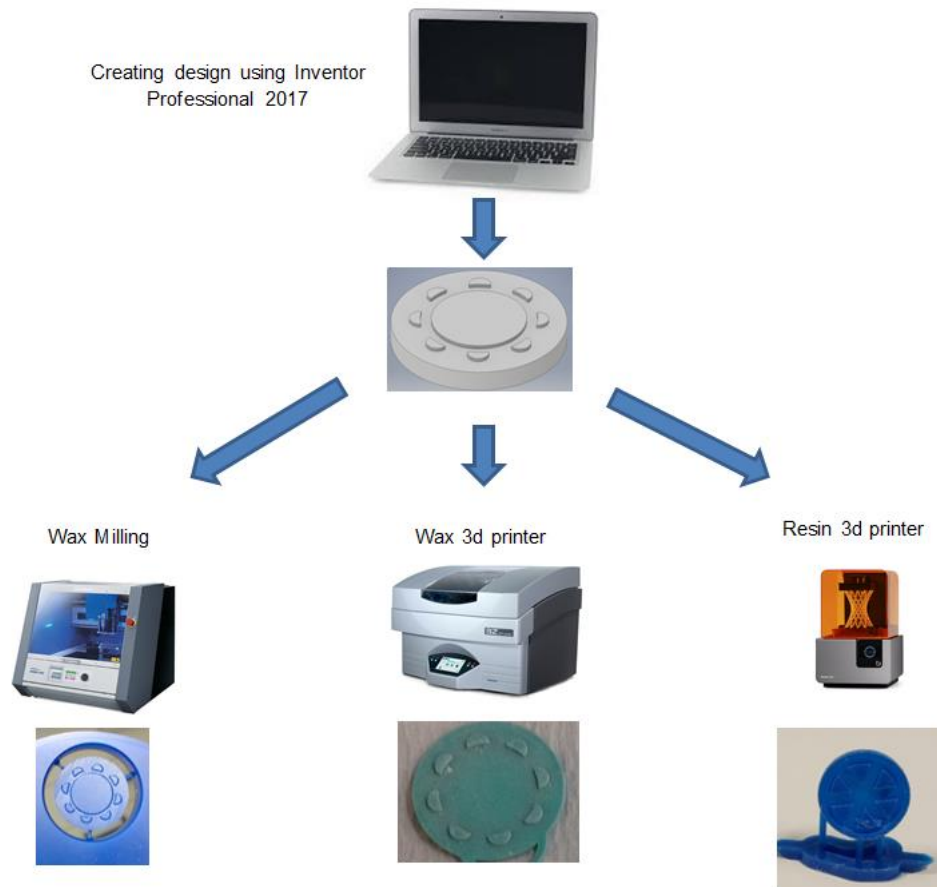


**Figure 4.2** Schematic representation of the process of creating the collector models before casting as described previously. From left to right; Wax milling, wax 3D printer, and Resin 3D printer.

### c) Collector casting:

This protocol allows the use of the wax or resin models to create metal collectors that can be used in electrospinning. The metal collectors will take the form of the wax or printer designs made by the 3D printers.

The wax or resin collectors are fixed with wax sprue to standard cylinders. Wetting agent (Sheramaster) is added to the fixed structure before adding the Sherafina solution as it works as a surface tension release agent. To make the Sherafina solution, a bag of Sherafina – rapid® (60 grams each) is added to 16 mL of sheraliquid® and intensively mixed to acquire a homogeneous solution. After adding the solution to the cylinders (filling them to the top) 30

minutes are needed for the solution to solidify. Then the cylinders with the solidified solution are heated to 900°C for 30 minutes, so the wax and resin can be completely melted off of the cylinders. For the casting, a Galloni Modular 3S Induction Casting Machine was used with Tilite alloy as the metal (the amount of tilite alloy to use depends on the size of the collectors; in the collectors of 14 mm diameter we used one unit, and in the collectors of 20 mm two units were used). Finally, the metal collectors can be extracted from the cooled cylinders. Additional processes can be performed including the cleaning of the metal collectors and the removal (cutting of) imperfections. Figure 4.3 displays this collector casting protocol.

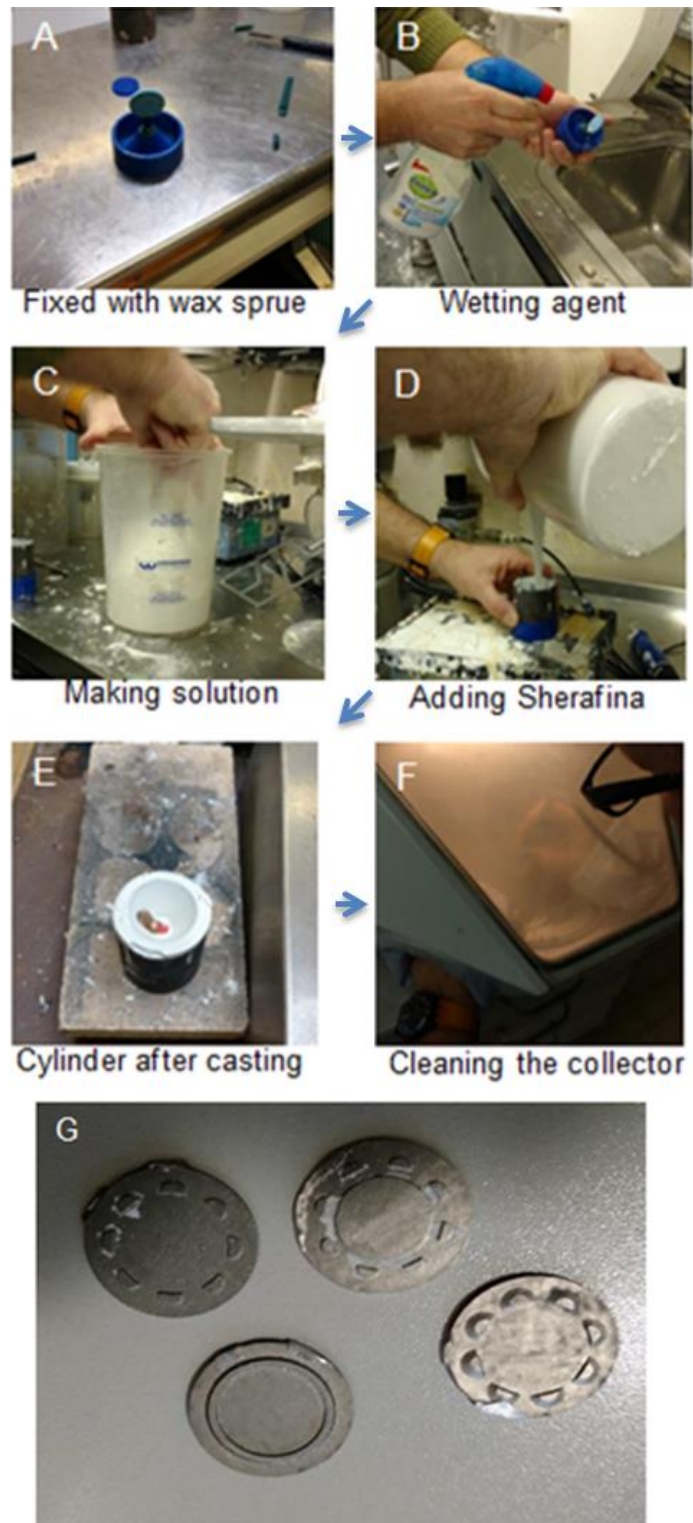


**Figure 4.3** Collector casting protocol. The figures summarise the process of casting wax collectors with Tilite alloys. The first two figures (A and B) show the process of fixing and adding the wetting agent to the collectors with wax sprue. The second two figures (C and D) show the Sherafina solution being made and added to the cylinders. (E and F) show how a cylinder looks after casting and how they are cleaned. Finally, G shows how the collectors look after being cleaned.

### 4.3.3.- Electrospinning on collectors

Collectors were fixed using carbon adhesive to baking paper (non-wax) which was used to cover the metallic plate receptor of the electrospinning set-up, as was seen in figure 2.1. Electrospinning was carried out using the protocol described in 2.3.2. The electrospinning solutions used were pure PLGA for the experiments realized in L.V. Prasad Eye Institute and 30%PCL – 70%PLGA for the fibre alignment experiments. The electrospinning conditions were as described in 2.3.2b. For a better peeling off of the electrospun membranes over the collectors, we covered the metallic plate with baking paper (non-wax) which we have experienced in the lab have the same results as using bake-o-glide in helping ease the separation of the electrospun membranes from the collectors (Deshpande, Ramachandran, Sangwan, *et al.*, 2013). In figure 4.4 can be seen how the collectors are fixed to the baking paper to be used in electrospinning.

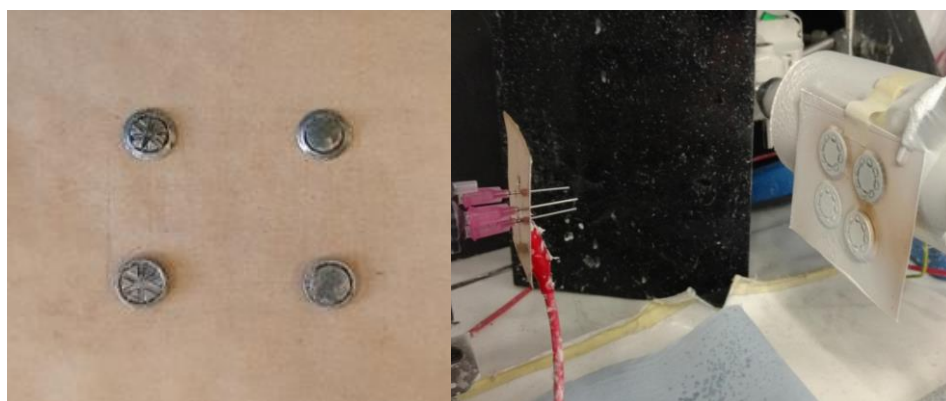


**Figure 4.4** Collectors fixed to baking paper before electrospinning (left) and electrospinning on collectors using a horizontal electrospinning setting as example.

### 4.3.4.- Human limbal cell culture

Human limbal cell culture was done in L. V. Prasad Eye Institute in Hyderabad, India. The protocol used for human corneas is similar to the protocols described in 3.3.2 and 3.3.4 with the following differences:

1.- The tissue arrived as a clean cornea from the tissue bank of L.V. Prasad Eye Institute, instead of a complete eyeball, so there was no need to clean it with a videne solution.

2.- Once the limbus was separated from the cornea, it was immediately meshed and seeded into the membranes instead of having an incubation time to check for contaminations as we do with animal limbus.

3.- For comparison with the current SLET methodology used in clinical practices, the same human explant culture was performed in an amniotic membrane.

4.- Due to the limited time of my visit in this institute, the culture only lasted 8 days.

5.- The explants were fixed to the scaffolds with two techniques, one by simply putting them on the scaffold as was done in chapter 3, and the other by fixing the explants with fibrin glue as is done in SLET surgery.

After 8 days culture, light microscopy was used to acquire images of cell outgrowth.

#### **4.3.5.- Shrinkage of electrospun PLGA membranes**

Shrinkage in electrospun membranes used in human limbal cell culture in L.V. Prasad Eye institute was measured by comparing 2 membrane designs with and without fibrin glue (as described in 2.3.5). The measurement was done as follows:

1. Each membrane had its diameter measured in X and Y axis at the start of the human limbal cell culture experiment. This way, an average diameter is achieved (figure 4.5).
2. In the case of scaffolds without fibrin glue, the measurement was done after 1.5 and 96 hours after incubation, while the scaffolds with fibrin glue was measured only after 96 hours as no visual shrinkage was recorded at the moment.
3. Areas of the scaffolds are calculated with the average diameter of the scaffolds.
4. Shrinkage is calculated by dividing the area of the scaffold with its original area (at the start of the experiment) to later be multiplied by 100 to get the shrinkage in %.

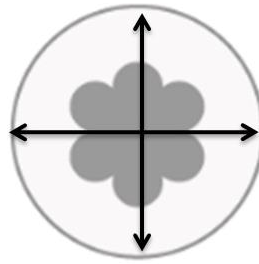


**Figure 4.5** Measurement of diameter in scaffolds in X and Y axis to get an average diameter.

#### 4.3.6.- Analysis of alignment in complex scaffolds

##### a) Imaging of samples

Scanning Electron microscopy was used to analyse the electrospun membranes as described in 2.3.8. For analysis of designs in membranes, 5 images were taken of the regions of interest that present a characteristic pattern at a magnification of  $\times 5000$ .

##### b) Fibre orientation and alignment

Using ImageJ software to treat the SEM images, the alignment and fibre orientation of the images were analysed. As no standardised method of measuring fibre alignment is found in the literature, we present a new method of measuring that was developed together with a Bioengineering MEng student Matthew Graham as part of his thesis work. The method will be described in details in the results section of this chapter, but can be outlined as follows:

1. Open the SEM images on ImageJ software.
2. Measure all the fibres from left to right using the straight line option.
3. Fibres with angles  $< -45^\circ$  must be adjusted by adding  $180^\circ$ .
4. When all the angles are measured, the mean is calculated.
5. Using the mean, the percentage of alignment of each fibre is calculated using the following equation:

$$\left| 1 - \left( \frac{|mean-angle|}{90} \right) \right| \times 100 \quad (1)$$

6. Repeat the process with all the fibres to obtain the average percentage of alignment.

This methodology will be used when analysing the section with some sort of visual alignment, whilst, when measuring sections with completely random alignment, the same protocol will be used but without using step 3 of adjustment. The information obtained through this methodology can be represented on a histogram, outlining the distribution of angles throughout the image. As well, Gaussian Kernel Density (KDE) can be used to display a smooth curve based on the histogram. Further explanation can be seen in 4.4.3 in this chapter.

#### **4.3.7.- Statistical analysis**

GraphPad Prism 7 software was used for one-way ANOVA analysis with p value  $<0.05$  in consideration for statistical significance.

## 4.4.- Results

### 4.4.1.- Design of collectors to create complex topography in electrospun membranes.

The collector is the piece that will allow us to obtain the desired scaffold design to be used in future SLET surgeries. Previous research developed at Sheffield by our group (Ortega, McKean, *et al.*, 2014) successfully developed first prototypes of PEG-DA and Metal-based electrospun ring-shaped collectors. After evaluation of the new collectors and after feedback from clinical collaborators from L.V. Prasad Eye Institute, it was agreed that new designs were needed in order to further investigate how both scaffold design and the presence of microfeatures can influence SLET surgery. In Figure 4.6 we can see the first generation of collector designs that have been developed in this project and were used to compare wax milling with 3D printing as a manufacturing technique of collectors. These models had 15 mm diameters as in SLET surgery a collector a bit bigger than the area of the cornea is needed for a better fixing with the rest of the eyeball.

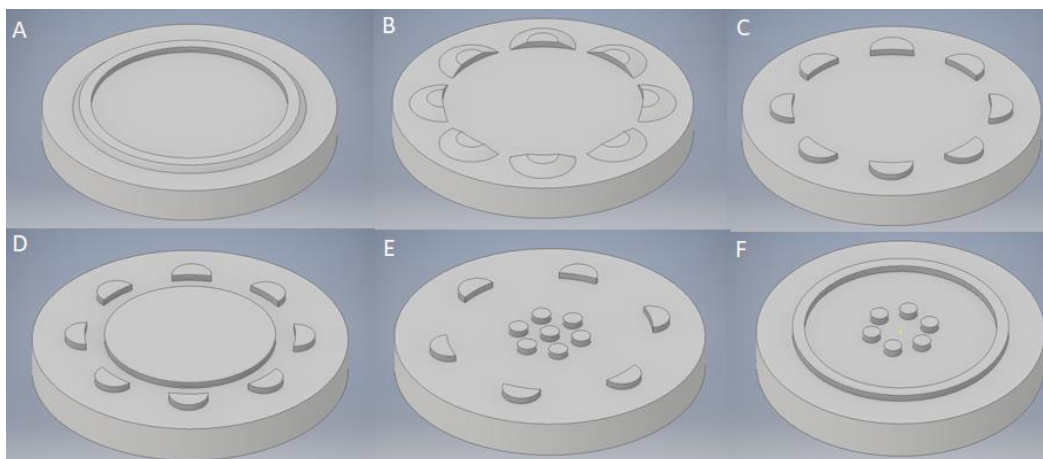


**Figure 4.6** Collector designs: images A – B – C in this figure are the collector designs considering only limbal explants of SLET in the limbal zone. Images D – E – F are the collector designs considering limbal explants in the limbal zone and the centre of the cornea.

The models presented in figure 4.6 were made with the objective of presenting different ideas to the design preferences that L. V. Prasad Eye Institute clinicians mentioned previously. In those comments they mentioned they needed bigger space to put explants in the

membranes compared to the ones developed previously in our group (Ortega, Deshpande, *et al.*, 2013). As well, we have noticed that in SLET surgery they fix the limbal explants to the membranes randomly apart to each other, rather than simulate a limbus in the cornea by placing the explants creating an outer ring in the membrane. Therefore, the models presented in figure 4.6 have outer rings of 2 mm diameter that could be continuous (A and F) or in niches (B, C, D, and E) and is located at 11 - 13 mm diameter to the centre of the collector simulating the size and position of a human limbus (Smerdon, 2000). As well, and considering the random explants fixing done in SLET surgery, the models D E and F have an additional design in the middle in case fixing explants in the centre is needed.

After testing the manufacture of the collectors, model D of figure 4.6 was used to test different thicknesses of the model and see the impact of the electrospinning on them. Figure 4.7 shoes different thickness of metal in the same collector design.



**Figure 4.7** Different thickness of metal collectors. 1 mm (down left), 1.5 mm (upper left), 2 mm (upper right), and 3 mm (down right).

In figure 4.7 we can see that the collector with 1 mm thickness produced better results over the other collectors. Also, a thicker collector implies that the peeling off process of the scaffold is more difficult as the fibres are easy to break in the perimeter ring contour. The previous statement can be demonstrated in the figure 4.4 that was shown in 4.3.3 where the scaffold with 3 mm thickness (down right) does not present as many fibres in the contour as the others. Due to equipment limitations, it was not possible to create collectors with thickness inferior to 1 mm.

In consultation with our collaborators in L.V. Prasad Eye Institute we decided to focus on the design with large retaining pockets. In figure 4.8 is presented the model that was used in LVPEI after the first feedback was given to us and the end of the first generation of collector created in this research.

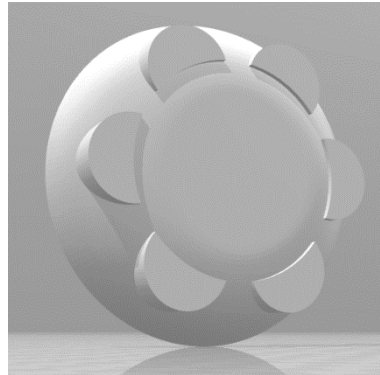


**Figure 4.8** Last model of the first generation of collectors manufactured. The outer ring is made by 6 big niches of 3 mm diameter and has a hemispherical design to add more niche space to place explants on them.

Figure 4.8 shows the collector model that was used to create the PLGA scaffolds used in my visit to L. V. Prasad Eye Institute that is detailed in 4.4.3. Design-wise, the membranes received positive feedback from the clinicians when showed to them, adding that an outer ring might be better than big niches as they prefer to have more freedom when adding the explants to the membranes.

Considering studies of Kim's and Connon's group about the impact of a hemispherical design of the corneal membrane, a second generation of collectors were designed to explore this impact in our electrospun membranes (Gouveia *et al.*, 2017, 2018; Kim, Kim and Park, 2018). These second generation models were designed considering the previous feedback from the first generation models but adding the hemispherical vs plane difference we wanted to study and are presented in figure 4.9.

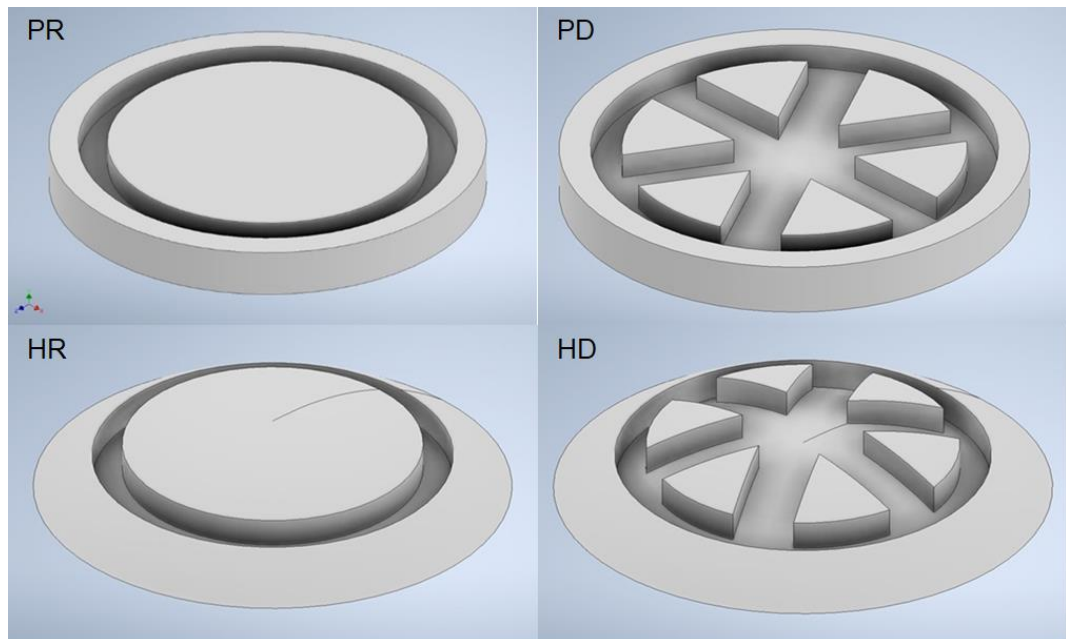


**Figure 4.9** Second generation of collector models. Images created using Autodesk Inventor Professional. 4 models are presented; PR (plain ring), PD (plain design), HR (hemispherical ring), and HD (hemispherical design).

Figure 4.9 displays the second generation of collector models. All 4 models have 15 mm diameter, plain models (PR and PD) have 2 mm collector thickness, and hemispherical models (HR and HD) have a radius of curvature of 8 mm (simulating curvature of the cornea). All 4 models present an outer ring of 2mm diameter with 1 mm depth as was preferred by the clinicians with their previous feedback. PD and HD differentiate from PR and HR by displaying “roads” connecting the outer ring with the centre of the collector. The roads design was created to compare the fibre alignment from the outer ring to the centre.

#### **4.4.2.- Exploring a reliable methodology of collector manufacturing for electrospun membranes.**

As highlighted in the methods section, the manufacturing process of collectors can be divided in two parts (i) making a wax or resin structure of a collector design, and (ii) casting it to create the metallic collector. Even though there are available in the market different casting methodologies with different materials, the casting done in the School of Clinical Dentistry showed good results at manufacturing collectors and electrospinning our polymer to them, and

so in this research we will use this technique. On the other hand, to create the model to be used in casting, we presented three different techniques in methodology. In this section we will compare them and choose one for future work.

First is making a wax or castable resin collector. For this, two techniques were compared, wax drilling and 3D printing. Wax drilling was able to manufacture the wax collector without any visual imperfection and with the sizes of niches as needed. Nevertheless, this technique is limited by the size of their drills and even though this wax design showed good results, designs like E or F from figure 4.6 will not be able to be done by this technique as the small niches of the middle are too small for being developed by this technology. As well, the amounts of copies that can be acquired of a design are limited by the milling wax as seen in figure 4.2.

The second technique used was 3D printing. Using the 3d printer 3ZLab from Solidscape®, all the collector designs showed previously in figure 4.6 were able to be printed (figure 4.10). This technique showed to be more accurate in manufacturing our collector design, and therefore, 3D printing was chosen as a working technique. Even though, for our case, this technique is more accurate than wax milling, it is also interesting to mention its limitations. For example, trying to make a wax collector thinner than 1 mm is a challenging task (figure 4.10).

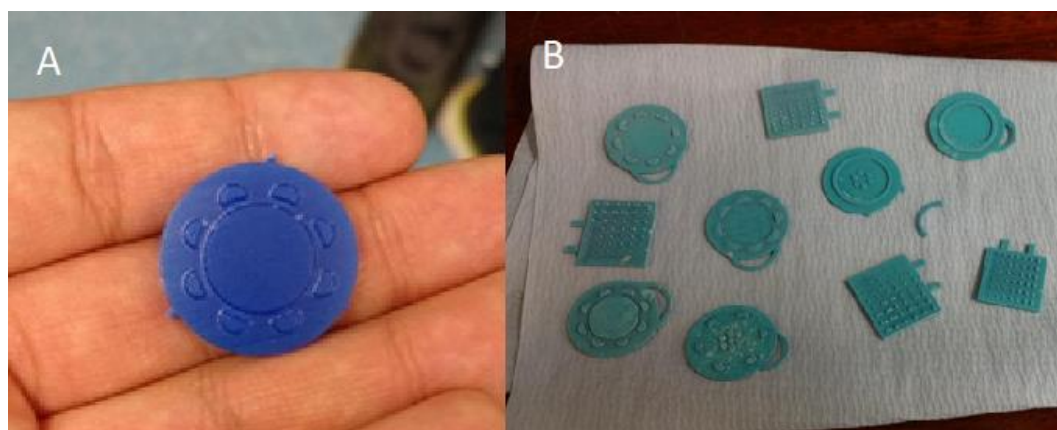


**Figure 4.10** A- Wax collector made by wax drilling technique. B- 3D printed wax collectors

Considering that 3D printing was the technique that showed better results to produce collector designs, two 3D printing manufacturing techniques were compared; the previous wax printing using the 3d printer 3ZLab, and castable resin printing using Form2 of FormLab.

3D printing with the printer 3ZLab required to be left overnight to warm the printer before using, with a calibration process previous to printing that lasted approximately two hours, printing with this methodology took more than 12 hours. On the other hand, printing with Form2 takes approximately 10 minutes of preheating, 2 hours of 3d printing, and 1 hour and a half of washing and curing. Considering that both collectors have the same casting potential and the quality of the printing in both cases was comparable, it was decided to move forward with castable resin as the process takes considerably less time.

#### **4.4.3.- Human limbal explant culture on electrospun PLGA membranes with topographical cues**

In March 2018 I was granted the MeDe Innovation PhD secondment scheme (<https://mede-innovation.ac.uk/news-article/mede-innovation-phd-secondment-scheme-2018-now-open/>). With this grant I travelled to L. V. Prasad Eye Institute (India) to do a 3-week secondment under the guidance of Dr. Vivek Singh. Similarly to the explant work presented in chapter 3, in this secondment we developed a similar set of experiments, but using human corneal tissue. For these experiments we used the final first generation design (figure 4.8) and 1 amniotic membrane was used as a control. Due to the time limitations, this experiment was only done once and it had a culture time of 8 days. Figure 4.11 shows the outgrowth of human limbal explants in amniotic membrane after 8 days. It is important to mention that in appendix C of this thesis we have added the ethics approval by L.V. Prasad Eye Institute to perform this research, which lately was validated by the University of Sheffield.

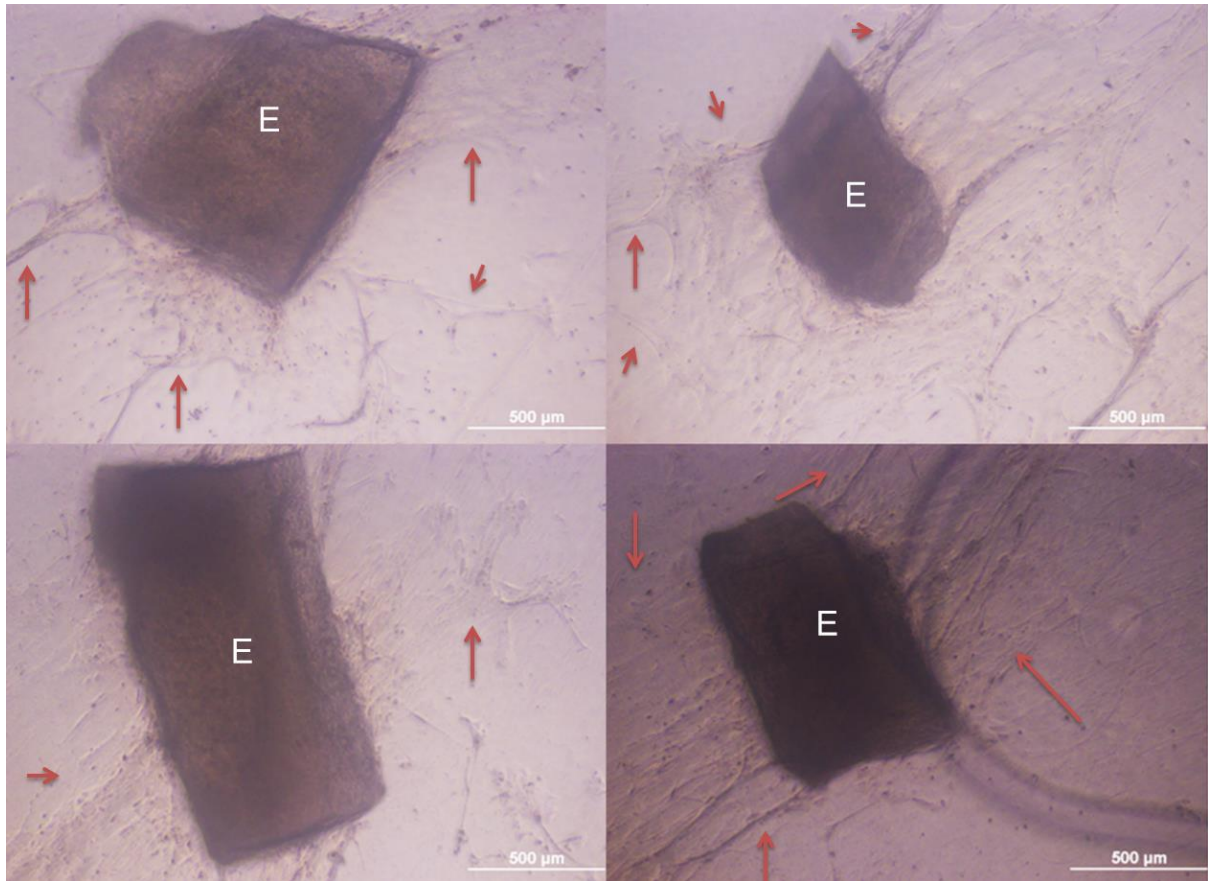


**Figure 4.11** Cell outgrowth from human limbal explants on amniotic membrane after 8 days. Image shows different outgrowth from 4 limbal explants that were seeded in an amniotic membrane as cell carrier. e is the limbal explant and the arrows indicate the cell outgrowth more clearly. Scale bar = 500 μm.

Figure 4.11 displays 4 human limbal explants that were seeded into an amniotic membrane as cell carrier. This methodology is what is currently used in SLET surgery. In the figure the outgrowth can be seen easily in light microscopy. After 8 days a healthy outgrowth can be seen from the explants.

In comparison, analysing the cell outgrowth of human limbal explants on the electrospun PLGA membranes with only light microscopy created the following figure 4.12.

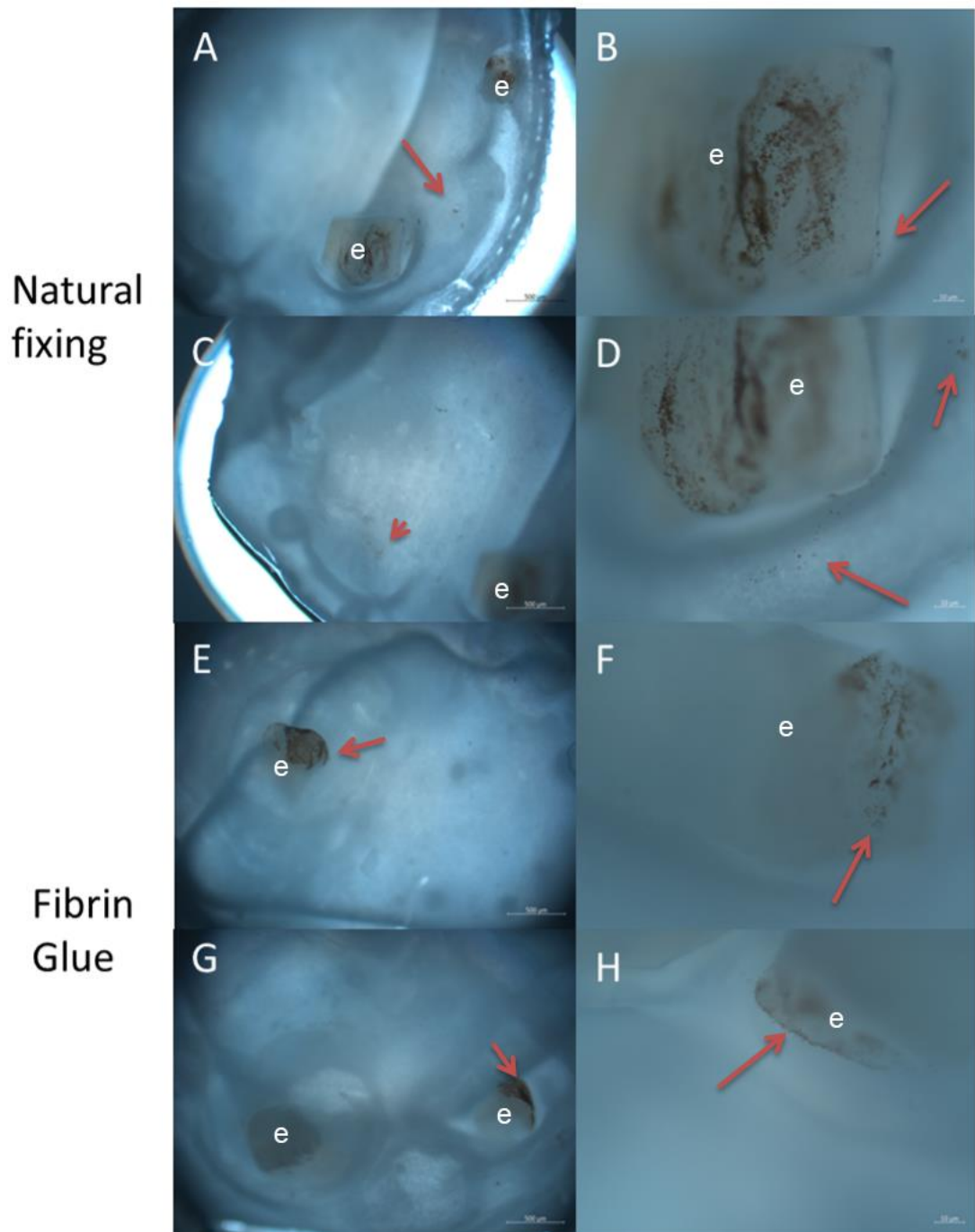


**Figure 4.12** Cell outgrowth from human limbal explants on electrospun PLGA membrane after 8 days. A B C and D are images of membranes where the explants were fixed by contact. E F G and H are images of membranes where the explants were fixed with fibrin glue. e is the limbal explant and the arrows indicate the cell outgrowth clearer. A C E and G have a scale bar of 500 μm; B D F and H have a scale bar of 10 μm.

Figure 4.12 shows human limbal explant culture on electrospun PLGA membrane. Two types of fixing of explant to the membrane were used; natural fixing or by contact, and fixing using fibrin glue. When comparing these images to the one using amniotic membrane in figure 4.11 it can be seen that the cell outgrowth is not as clear due to the lack of transparency in the

electrospun membranes. Nevertheless, figures 4.12 B D F and H show cell outgrowth fixed on the membrane after only 8 days of culture.

As a result of the limitations of the secondment, doing a comparison between the cell outgrowths of the amniotic membrane with the electrospun membranes was not achieved. Therefore, the data presented was just used to see if our membranes were able to produce human limbal cell outgrowth and how the outgrowth looks in amniotic membranes in similar conditions.

Additionally, in this secondment we presented the electrospun membranes to the clinicians in LVPEI. They considered it was an improvement to the previous ones presented by our group but they would prefer to have more freedom on where to put the explants, preferring an outer ring rather than niches.

#### 4.4.4.- Analysis of electrospun membrane shrinkage

After finishing the 8 days of culture, shrinkage of the electrospun membranes was noticed. Figure 4.13 shows the change in one of the membranes.

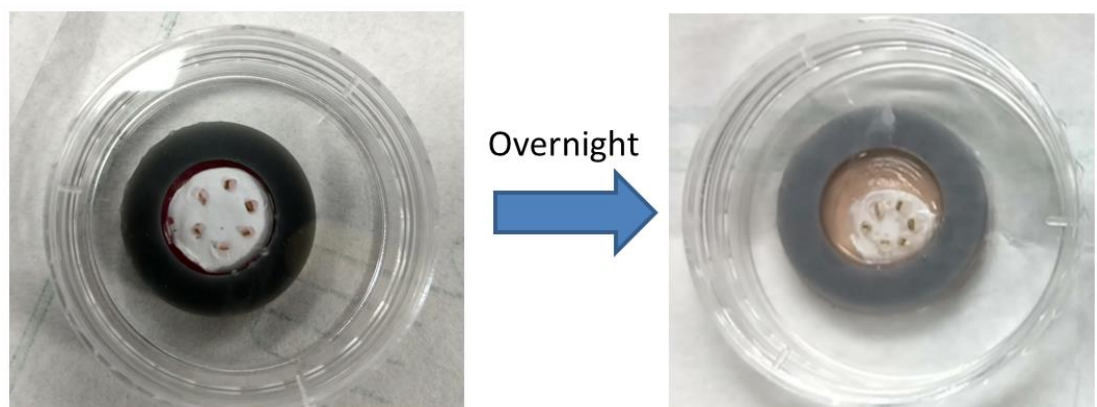


**Figure 4.13** Electrospun membrane shrinkage after overnight of culturing.

Figure 4.13 reveals an important visual shrinkage of the electrospun membrane after being in culture overnight. This shrinkage was not observed previously in our laboratory in Sheffield. Nevertheless, this membrane shrinkage was studied, and in table 4.3 can be seen

the area reduction in the membranes at 1.5 hours and 96 hours after culture. Two conditions were used considering the nature of the explant seeding, natural fixing (N) and fibrin glue fixing (FG).

**Table 4.3** Electrospun PLGA membranes shrinkage after 1.5 and 96 hours after being cultured.

<b>Sample</b>	<b>Shrinkage 1.5 h (%)</b>	<b>Shrinkage 96 h (%)</b>
<b>N1</b>	34.33	61.83
<b>N2</b>	39.08	60.50
<b>N3</b>	63.76	76.76
<b>N4</b>	72.75	78.06
<b>N5</b>	51.75	69.37
<b>N6</b>	64.59	64.49
<b>N7</b>	57.74	75.84
<b>N8</b>	63.44	62.56
<b>FG1</b>	n/d	66.70
<b>FG2</b>	n/d	43.20
<b>FG3</b>	n/d	68.34
<b>FG4</b>	n/d	55.87
<b>FG5</b>	n/d	48.96
<b>FG6</b>	n/d	60.33
<b>FG7</b>	n/d	39.10

Table 4.3 shows 8 electrospun membranes with natural fixing and 7 electrospun membranes with fibrin glue fixing. The natural fixing membranes were measured at 1.5 hours and at 96 hours after culture, while the fibrin glue ones were only measured at 96 hours. Table 4.3 shows that on average the membranes with natural fixing after 1.5 hours of culture lost 55.93 +/- 13.35 percentage of their area. After 96 hours, natural fixing membranes lost 68.68 +/- 7.31 percentage of their area, while fibrin glue fixed membranes lost 54.64 +/- 11.34 percentage of their area.

It is important to mention that in this experience in LVPEI, the membranes did not have weight to fix them to a position, as we do in the laboratory in UoS. The fact of not having weight on them, or any sort of position fixing technique, showed us a behaviour we were not expecting. In SLET surgery, the membranes are fixed to the eyes with fibrin glue. Further analysis of the degradation of the electrospun membranes in wounded cornea model would give a better understanding of the degradation versus shrinkage happening on them. Furthermore, these membranes were made of pure PLGA, which when we analysed its degradation in section 2.4.7 showed the fastest losing of its fibrous microenvironments compared to the other electrospun membrane conditions being explored in this PhD research.

#### **4.4.5.- Analysing topographical cues included in electrospun membranes made with special shaped collectors.**

As previously mentioned, studies from Kim's and Connon's group about the impact of a hemispherical pattern in the membrane of a cornea showed positive results, especially in the collagen arrangement that cells produced in this particular scenario (Cardona *et al.*, 2017; Gouveia *et al.*, 2017; Kim, Kim and Park, 2018). Therefore, second generation collectors were developed as shown in figure 4.9, where two designs (ring and road) have a plane and hemispherical version of themselves. These designs have in mind as well the feedback made by LVPEI about the first generation, and then all of these designs have an external ring simulating the limbus with enough space to seed explants.

Considering as well that the manufacturing technique to produce our membranes is through electrospinning, fibre orientation can affect or give us clues about the effect of this kind of microenvironment on the cells' behaviour on them. Following figure 4.14 shows these electrospun membranes created from the collectors of figure 4.9.

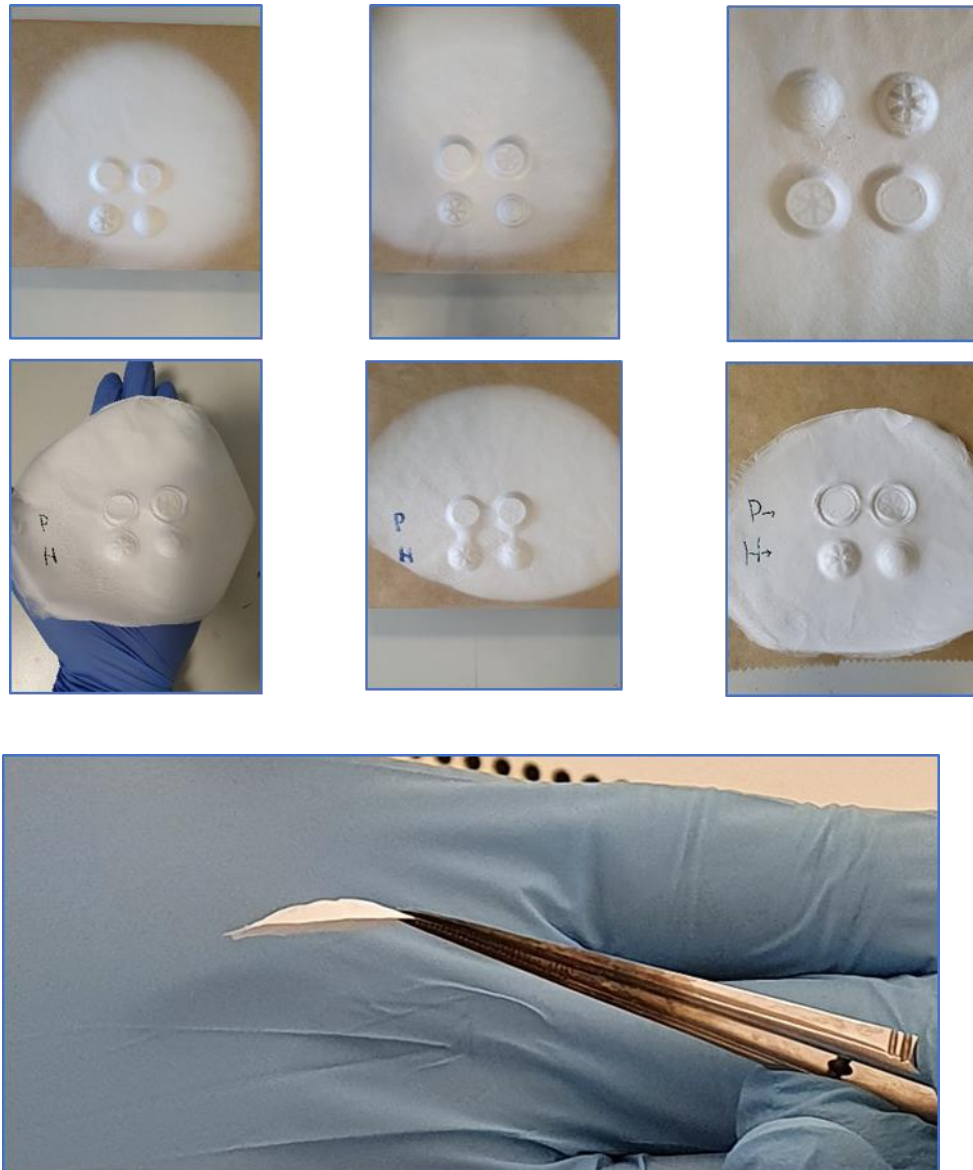


**Figure 4.14** Examples of electrospun membranes made of the 4 types of collectors. In the bottom can be seen better that the hemispherical membranes preserve the hemispherical shape of the collectors.

Figure 4.14 displays that the electrospun membranes obtained using the collectors shown in figure 4.9 remain with the topographical cues of the collectors. In the following figure

4.15 is displayed how these designed electrospun membranes are affected by their pattern, paying special attention to the fibres arrangement in the membrane.

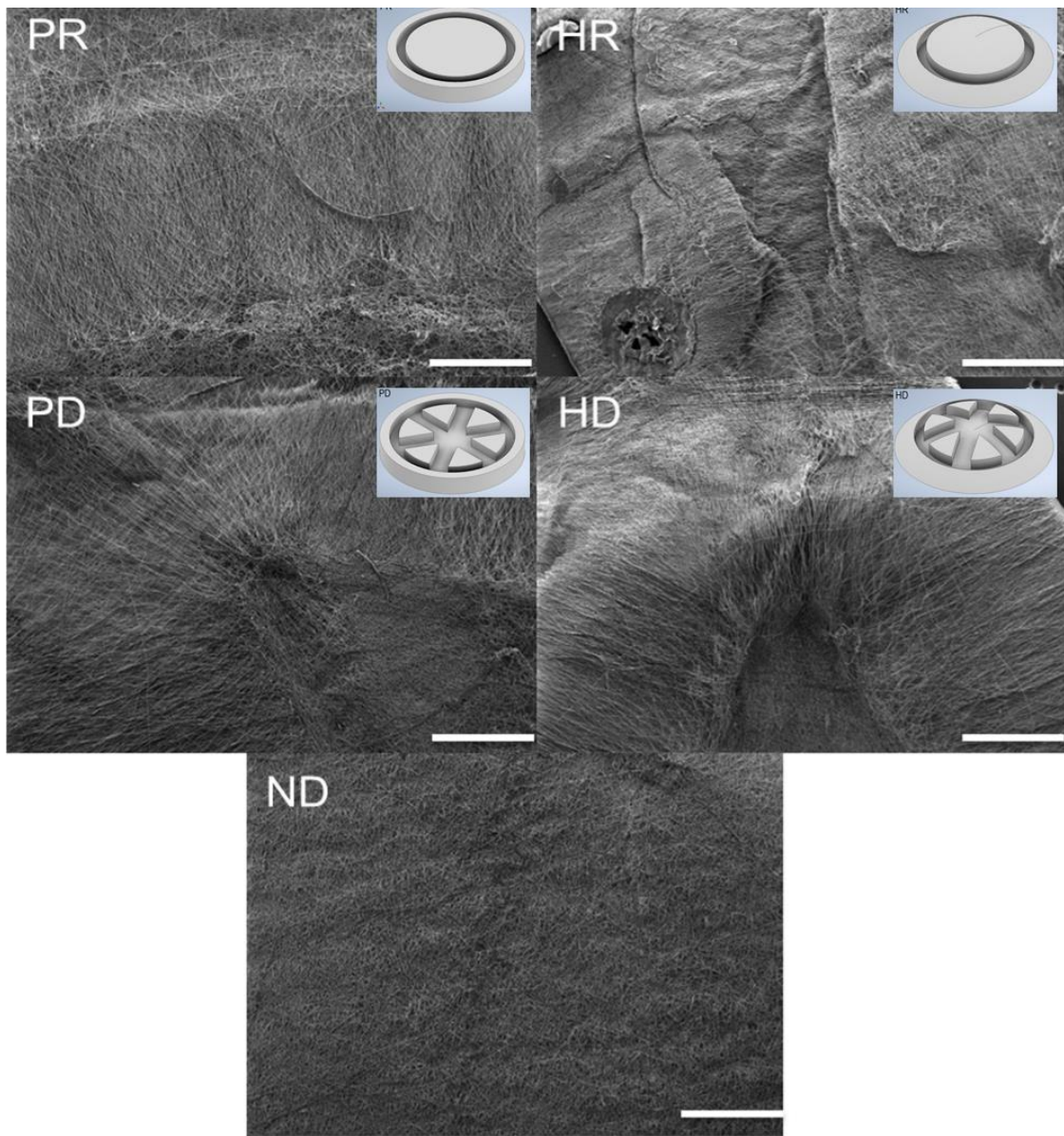


**Figure 4.15** SEM images of the electrospun membranes acquired using the second generation collectors at 100X magnification. PR = Plain Ring, HR = Hemispherical Ring, PD = Plain design, HD = Hemispherical Design, ND = No design. Scale bar = 500  $\mu\text{m}$ .

In figure 4.15 we can see the microenvironment features of our membranes made with the second generation collectors. PR and HR stand for plain ring and hemispherical ring. PD and HD stand for plain design and hemispherical design, design is the name given to the collectors that aside of having a ring, as well have “roads” across the collector. Finally, ND stands for no design which is a normal electrospun membrane made of a normal

electrospinning set-up with no special collector model as with the previous 4 PR, HR, PD, and HD. ND shows a well-known microenvironment as is the random alignment membranes we extensively saw in chapter 2. What is interesting to see is that the 4 membranes created by the second generation collectors show distinctive patterns with some levels of fibre alignment that can be explored.

#### 4.4.5.1- Fibre orientation in complex membranes made of second generation collectors.

Second generation collectors (figure 4.9) were used to create complex electrospun membranes with special patterns as seen in figure 4.15. The collectors in figure 4.9 were given the following names considering their features: PR = Plain Ring, HR = Hemispherical Ring, PD = Plain design, HD = Hemispherical Design, ND = No design. In figure 4.15, it can be seen that the membranes present different zones of fibre orientation. In the following images (figures 4.16-4.19), we separate the zones with different fibre orientation for every different membrane model at 5000x, to see these different zones more clearly.

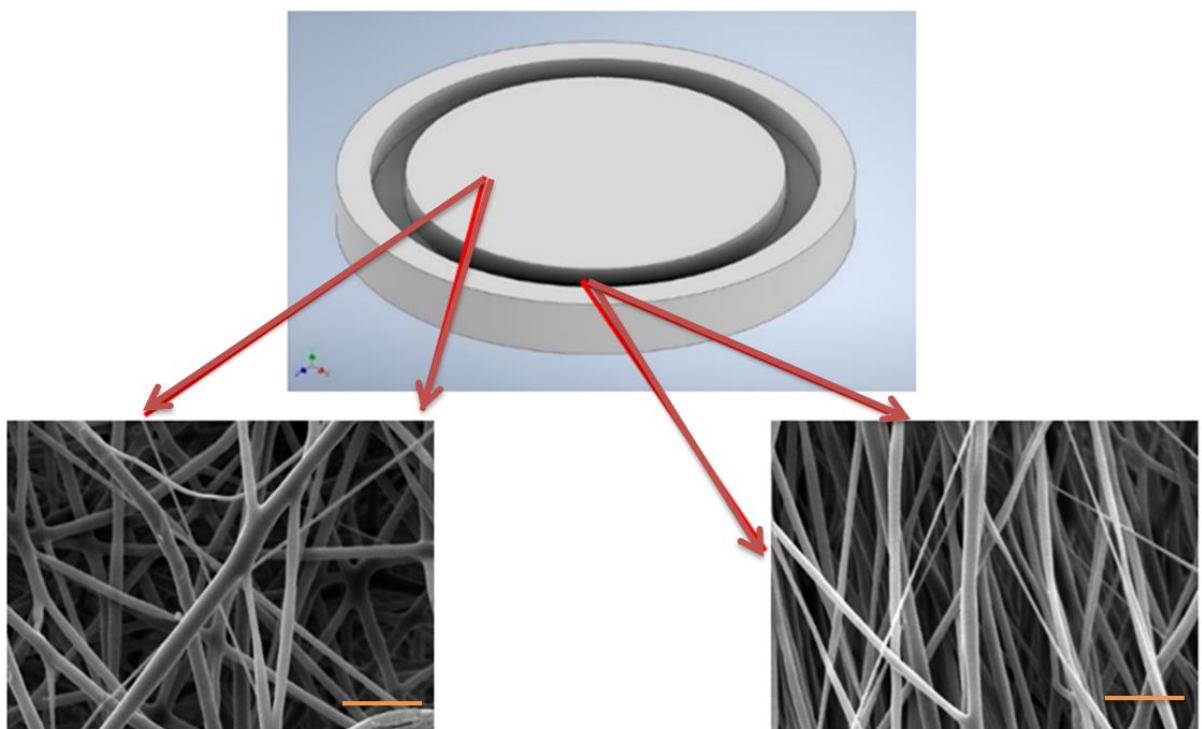


**Figure 4.16** fibre alignment zones created using the second generation collector PR. Images were taken using SEM at 5000x. Two zones can be differentiated, the fibres in the ring and the fibres in the rest of the model. Scale bar = 10  $\mu$ m

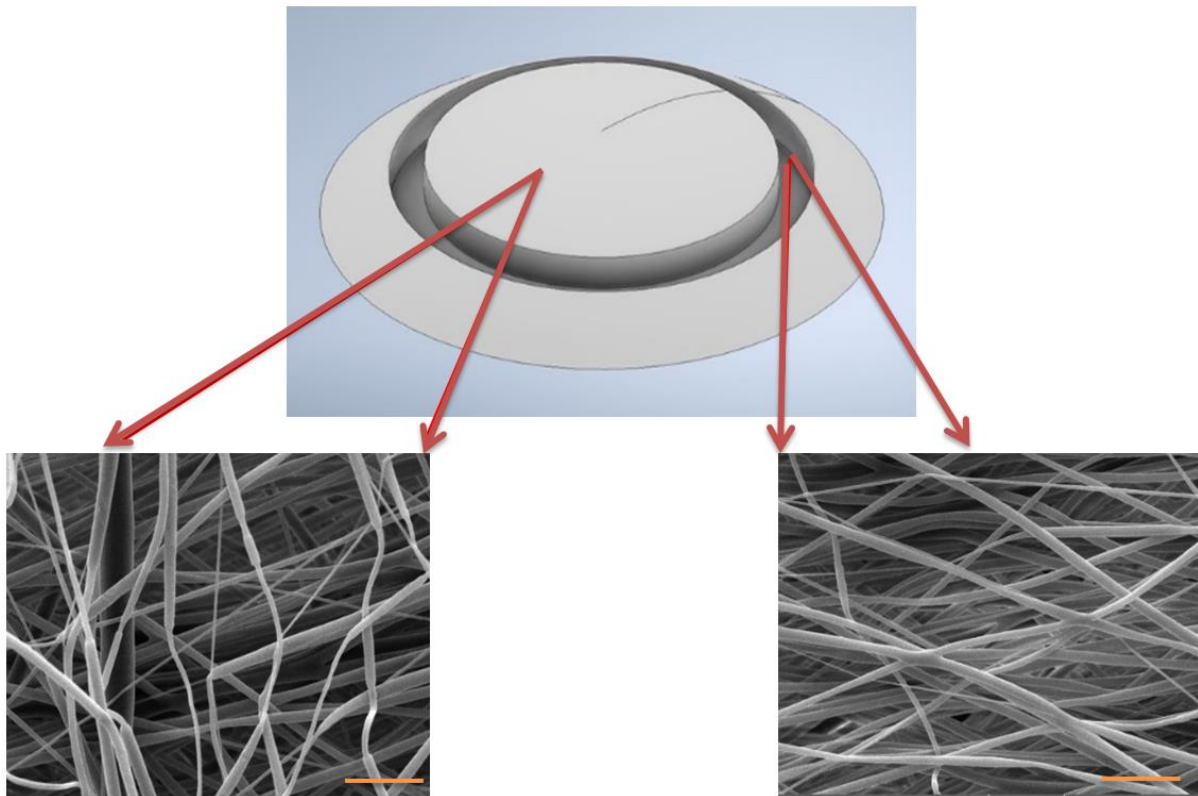


**Figure 4.17** fibre alignment zones created using the second generation collector HR. Images were taken using SEM at 5000x. Two zones can be differentiated, the fibres in the ring and the fibres in the rest of the model. Scale bar = 10  $\mu$ m

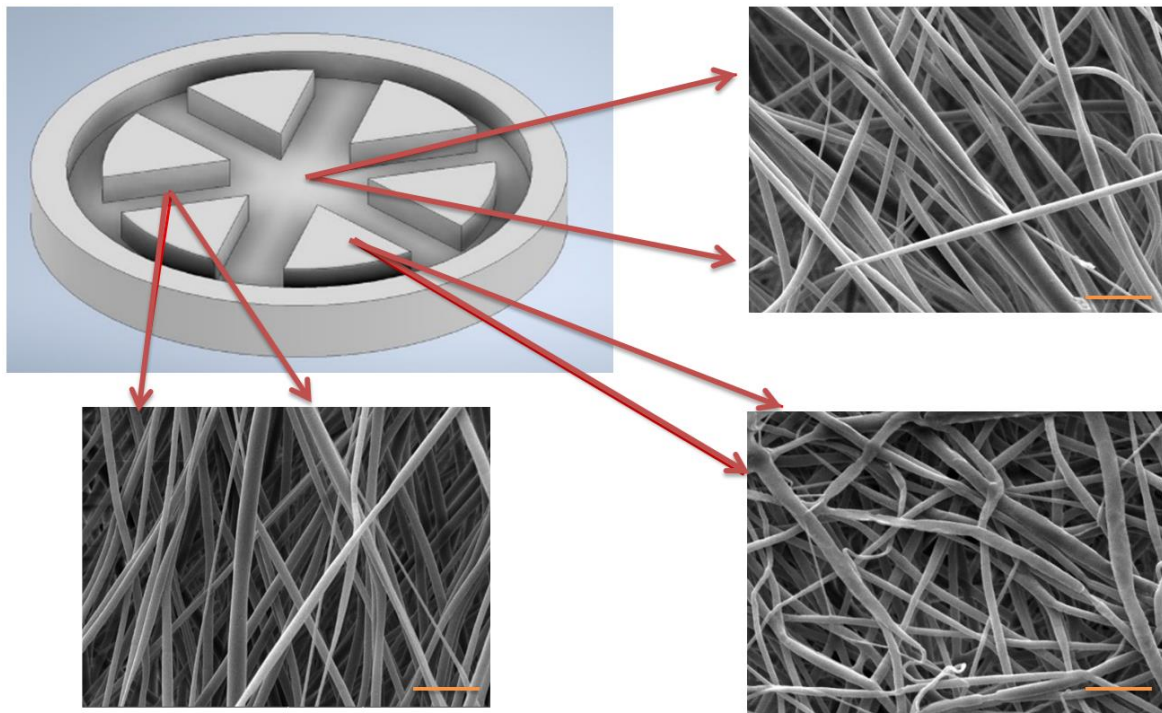


**Figure 4.18** fibre alignment zones created using the second generation collector PD. Images were taken using SEM at 5000x. Three zones can be differentiated; the fibres in the centre, the fibres in the roads (between triangles), and the fibres on the triangles. Scale bar = 10  $\mu$ m

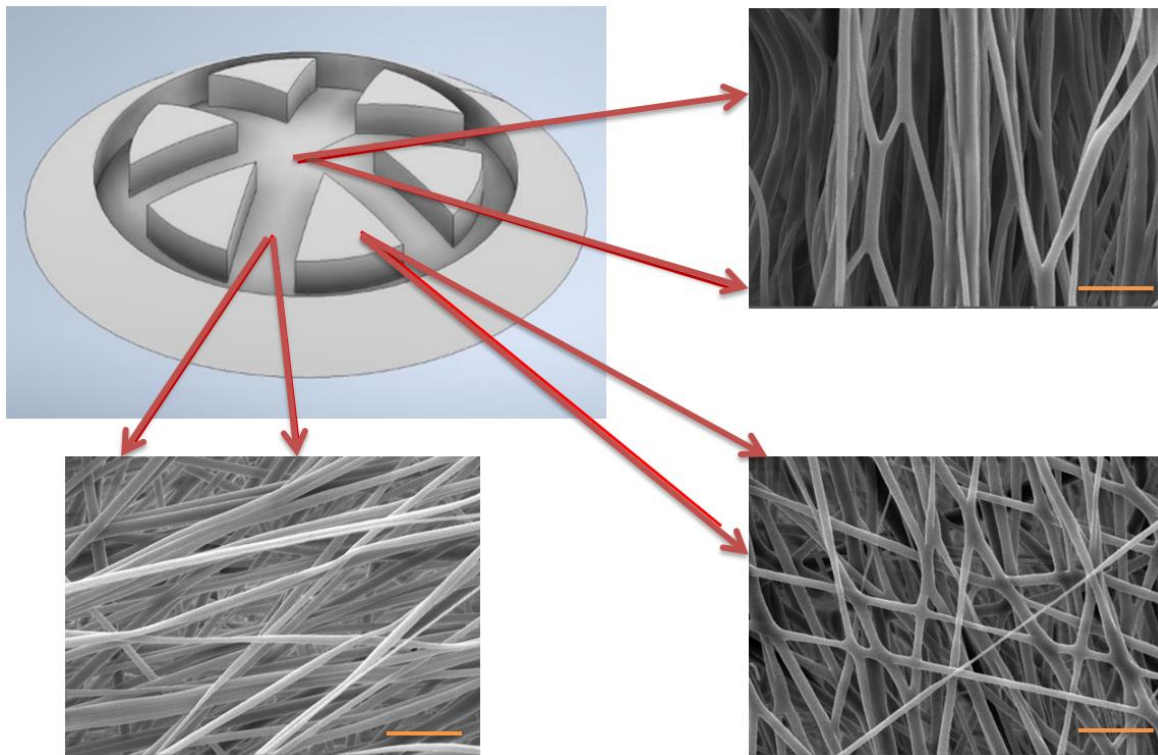


**Figure 4.19** fibre alignment zones created using the second generation collector HD. Images were taken using SEM at 5000x. Three zones can be differentiated; the fibres in the centre, the fibres in the roads (between triangles), and the fibres on the triangles. Scale bar = 10 µm

In figures 4.16-4.19 is displayed how the second generation collectors were able to introduce different zones of alignment in the electrospun membrane made using them. Figures 4.16 and 4.17 show the membranes made by PR and HR respectively. In these membranes two zones with different fibre orientation behaviour can be identified, one in the ring area and the other in the rest of the membrane. Figures 4.18 and 4.19 show the membranes created using PD and HD respectively. In these membranes, three zones with different fibre orientation patterns can be identified; the fibres in the centre of the design, the fibres in the roads (between triangles), and finally, the fibres over the triangles.

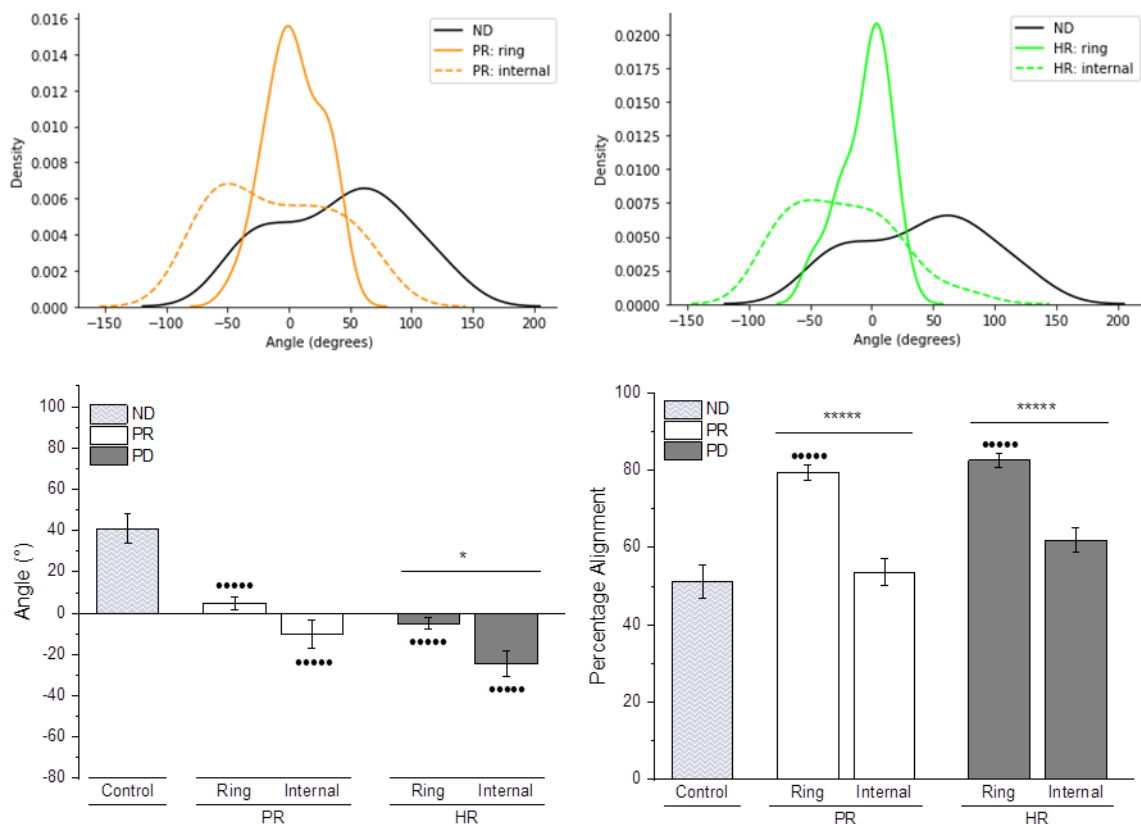
Now that we have differentiated zones with different fibre alignments in the membranes, using the protocol explained in 4.3.6 (and detailed with an example in appendix B) the fibre alignment of these zones in the membrane is calculated. In table 4.4 these results can be seen, as well as compared to an electrospun membrane made with a not modelled collector (ND).

**Table 4.4.** Average angle of orientation and percentage of alignment with standard deviation of every zone identified in 5 types of membranes; ND, PR, HR, PD, and HD. Images used were obtained using SEM at 5000x. n=5.

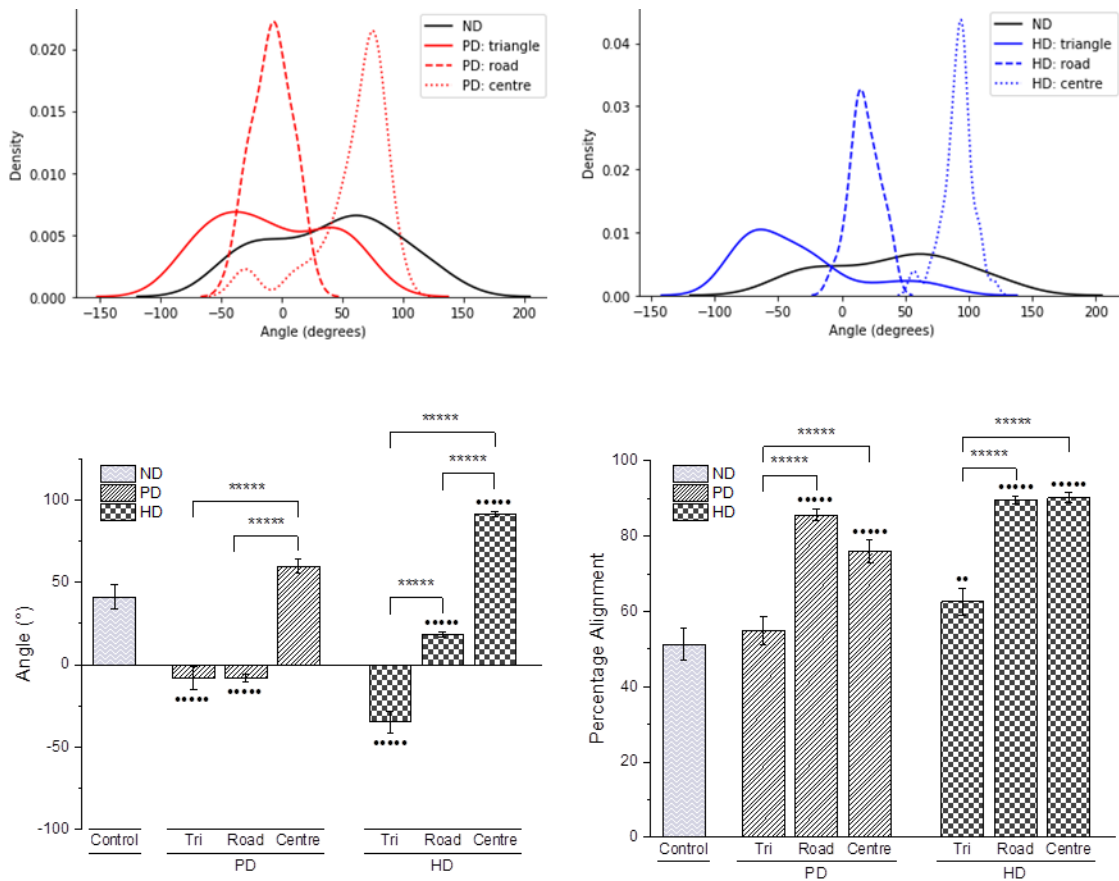
Scaffold		Percentage of Alignment (%)
Model	Zone	
ND	ND	51.27 ± 30.25
PR	Ring	79.50 ± 13.91
	Internal	53.59 ± 24.68
HR	Ring	82.51 ± 12.69
	Internal	61.94 ± 22.92
PD	Triangle	54.86 ± 25.61
	Road	85.70 ± 10.39
	Centre	75.89 ± 22.01
HD	Triangle	62.59 ± 25.36
	Road	89.57 ± 7.72
	Centre	90.19 ± 9.29

Table 4.4 shows the percentage of alignment in every zone mentioned in figures 4.16-4.19, as well as with a membrane created without a designed collector. It is important to note the different percentage of alignment that can be seen in these membranes. ND membrane has a percentage of alignment on average of 51.27%, a relatively low value of alignment, which makes sense considering we are not using in this condition any collector that could affect the fibre arrangement in the membrane. The values close to the ND membrane would be the internal zone and triangle zone of the plain ring and plain design collector respectively with 53.59% and 54.86%. On the other hand, the zones with the highest percentage of alignment were the ring zone of the hemispherical ring collector with 82.51%, and the road and centre zone of the hemispherical design collector with 89.57% and 90.19% respectively. With these results we can compare the membranes percentage of alignment between them to get a better insight of three factors: differences between a designed PD collector versus no collector; the impact of having a design connected to the centre (PD and HD) versus a design with only a

ring (PR and HR); and finally, if making a collector with a hemispherical design versus a plain one will make a difference. These assessments were developed together with Matthew Graham as his thesis work to achieve his degree of Master in bioengineering. To answer the relevance of the first factor, the percentage of alignment of PR, HR, PD and HD were compared to the percentage of alignment of ND. To compare the fibre distributions a Gaussian Kernel Density (KDE) plot was used. For these comparisons, Y axis is the percentage alignment, while X axis is the angle to which the fibres are aligned. In these plots and well-defined peaks there is a good fibre alignment, while when there is no clear peak this suggests the opposite. Additionally, bar chart plots are displayed to quantify the significance of our values. In the following figures we use this comparison methodology to contrast our membrane designs.



**Figure 4.20** Comparison of fibre alignment between a membrane made without a designed collector (ND) versus membranes made with a collector with a ring design on it (PR, HR). Top left is a KDE plot comparing ND membrane with the internal and ring zone of a PR membrane. Top right is a KDE plot comparing ND membrane with the internal and ring zone of a HR membrane. Bottom left is a Bar chart displaying the angle of orientation of all the zones in the membranes. Bottom right is a bar chart showing the percentage of alignment of all the zones in the membranes. \* shows significance between scaffold zones, while ● shows significance between the zone of the scaffold and the ND scaffold. \* =  $p < 0.05$ , \*\*\*\*\* =  $p < 0.01$ , ●●●●● =  $p < 0.01$ .

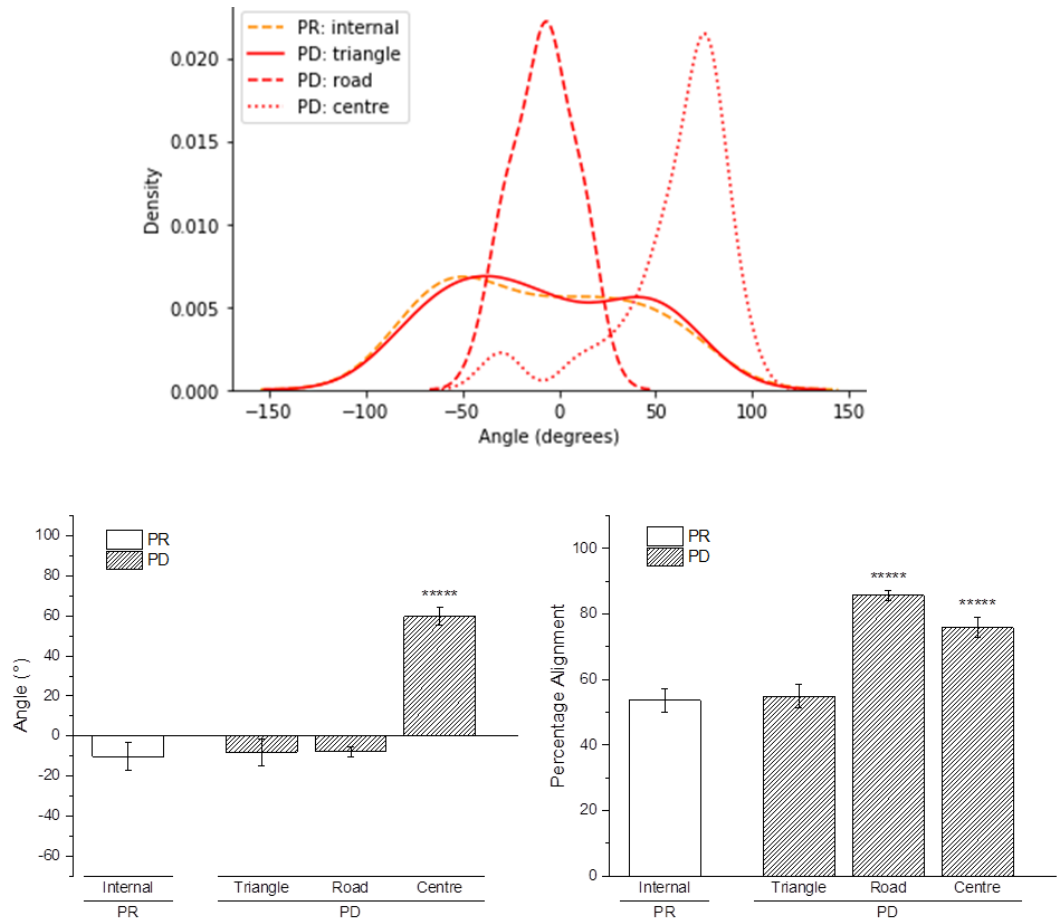


**Figure 4.21** Comparison of fibre alignment between a membrane made without a designed collector (ND) versus membranes made with a collector with road design on it (PD, HD). Top left is a KDE plot comparing ND membrane with the triangle, road and centre zone of a PD membrane. Top right is a KDE plot comparing ND membrane with the triangle, road and centre zone of a HD membrane. Bottom left is a bar chart displaying the angle of orientation of all the zones in the membranes. Bottom right is a bar chart displaying the percentage of alignment of all the zones in the membranes. \* shows significance between scaffolds zones, while ● shows significance between the zone of the scaffold and the ND scaffold. \* =  $p < 0.05$ , \*\*\*\*\* =  $p < 0.01$ , ●● =  $p < 0.04$ , ●●● =  $p < 0.01$ .

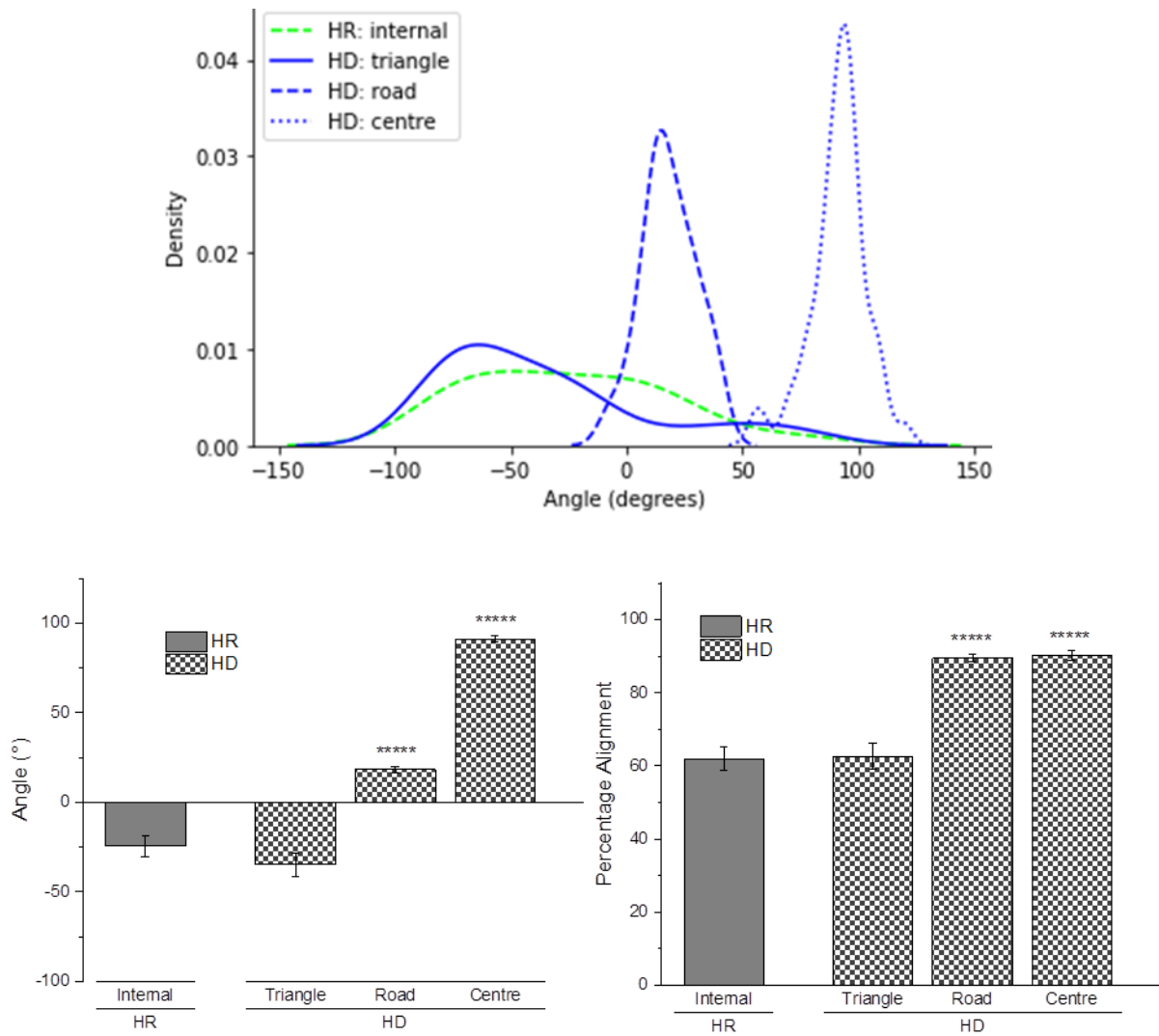
Figure 4.20 displays the contrast between electrospun membranes made with our second generation collectors with ring (PR HR) versus a normal membrane without a designed collector (ND). When analysing the KDE plots in both comparisons, we can see that the ring zone shows a clear peak in both cases, showing a high level of alignment in those zones. On the other hand, the internal zone in both PR and HR looks similar to ND in the aspect of not showing a clear peak. When analysing the significance of the differences in the levels of alignment between ND with PR and HR we see that the internal zones of PR and HR do not present a significant difference with the fibre alignment seen in ND. On the other hand, the ring zones in PR and HR show a significant difference with ND ( $p < 0.01$ ). In a similar way, the fibre alignment in the ring zones of PR and HR show significant differences with the internal zone of their membrane.

Figure 4.21 shows the differences between electrospun membranes made with PD and HD collectors versus ND. The KDE plots for PD and HD shows two clear peaks for the zones of road and centre, while the triangle zone does not show a clear peak similar to ND in both PD and HD. When analysing the significance of the differences between the levels of alignments in these membranes, it can be seen that only the triangle zone of PD does not have a significant difference with ND. On the other hand, the triangle zone of HD has a significant difference with ND ( $p < 0.04$ ). Road and centre zones in PD and HD show a significant difference to ND and to their respective triangle zone ( $p < 0.01$ ).

With figures 4.20 and 4.21, it can be seen that introducing topographical designs in the collector will affect the fibre alignment in the membrane. The features in the collectors that were sunken (ring, roads, centre) were shown to create major levels of alignment versus the other zones. These other zones (triangle, internal) showed values of fibre alignment similar to ND. Now that we have identified the differences between the designs and ND, we proceed to answer the second factor previously mentioned; the impact of having a design connected to the centre (PD and HD) versus a design with only a ring (PR and HR). in the following figure 4.22 and 4.23 we compared the impact of the design to the centre versus only a ring in plane and hemispherical membranes.



**Figure 4.22** Comparison of fibre alignment between membranes made with plain collectors (PR and PD). For this comparison, we consider the differences between their designs, as both have an external ring, the ring zone of PR is not considered. At the top can be seen the KDE plot showing the internal zone of PR and triangle, road, and centre zones of PD. At the bottom we can see from left to right bar charts displaying the angle of orientation of all these zones, and the fibre alignment of these zones respectively. \*\*\*\* =  $p < 0.01$ .



**Figure 4.23** Comparison of fibre alignment between membranes made with hemispherical collectors (HR and HD). For this comparison, we consider the differences between their designs, as both have an external ring, the ring zone of HR is not considered. At the top can be seen the KDE plot showing the internal zone of HR and triangle, road, and centre zones of HD. At the bottom we can see from left to right bar charts displaying the angle of orientation of all these zones, and the fibre alignment of these zones respectively. \*\*\*\*\* =  $p < 0.01$ .

In figures 4.22 and 4.23 is revealed the differences between the internal zone of the ring collectors membranes, versus the zones of the HR and HD respectively. Considering our previous analysis of these membranes, versus ND, there is no big surprise in these results from what we already saw previously. The road and centre zones in both PD and HD are statistically different ( $p < 0.01$ ) to the triangle zone and to the internal zone of the rings membrane. On the other hand, their internal and triangle zones share similar values for fibre alignment as no statistical difference between them can be obtained.

Now, moving onto the third factor, we want to see if there are any differences between membranes made of a plain collector versus membranes made out of hemispherical collectors. Following the same methodology of the previous figures, we obtained the following figure.

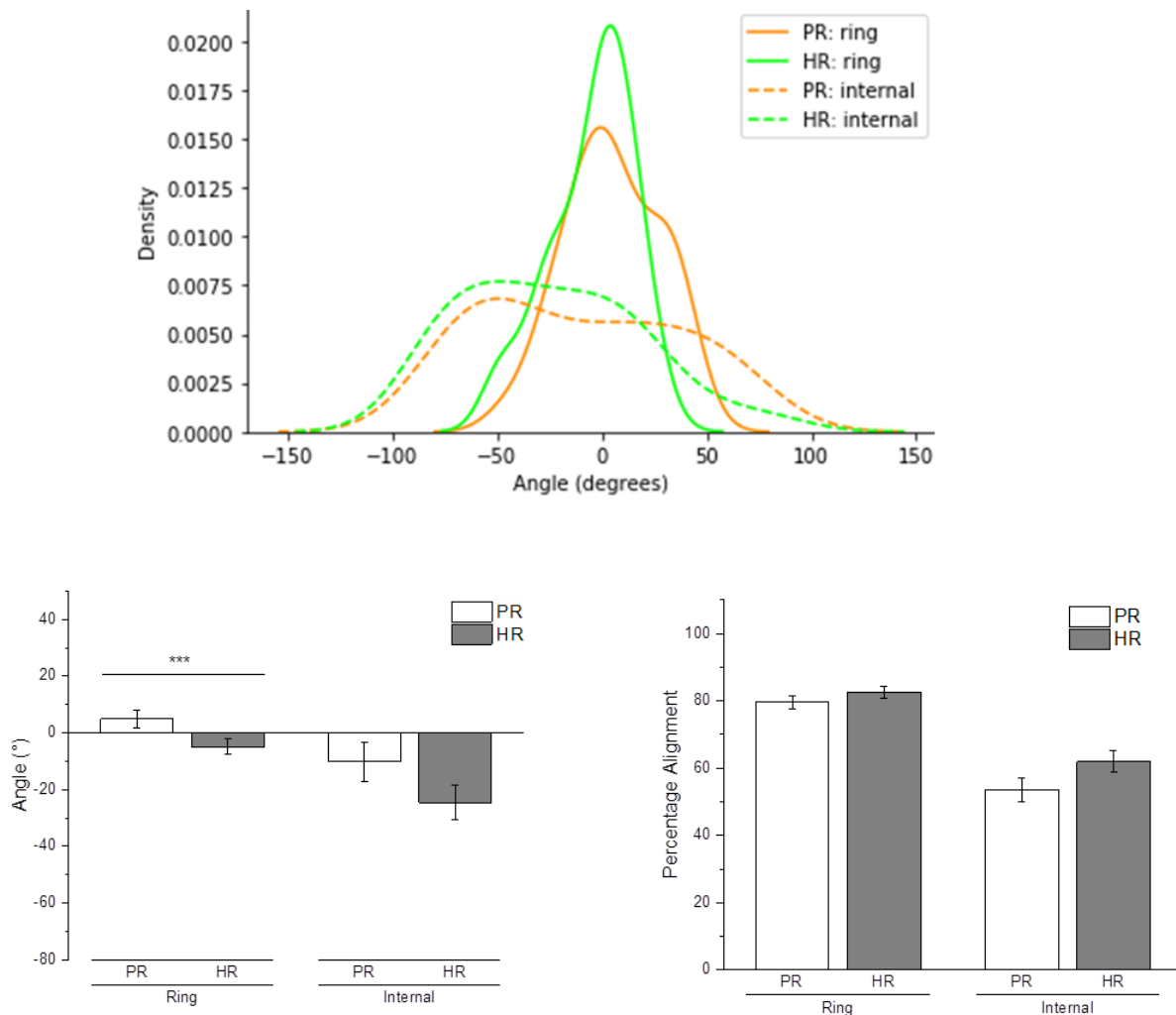


**Figure 4.24** Analysing the impact of a hemispherical collector versus a plain one using the same design (Ring). At the top can be seen the KDE plot showing the ring and internal zones of PR and HR. At the bottom we can see from left to right bar charts displaying the angle of orientation of all these zones, and the fibre alignment of these zones respectively. No statistical difference can be seen between these conditions.

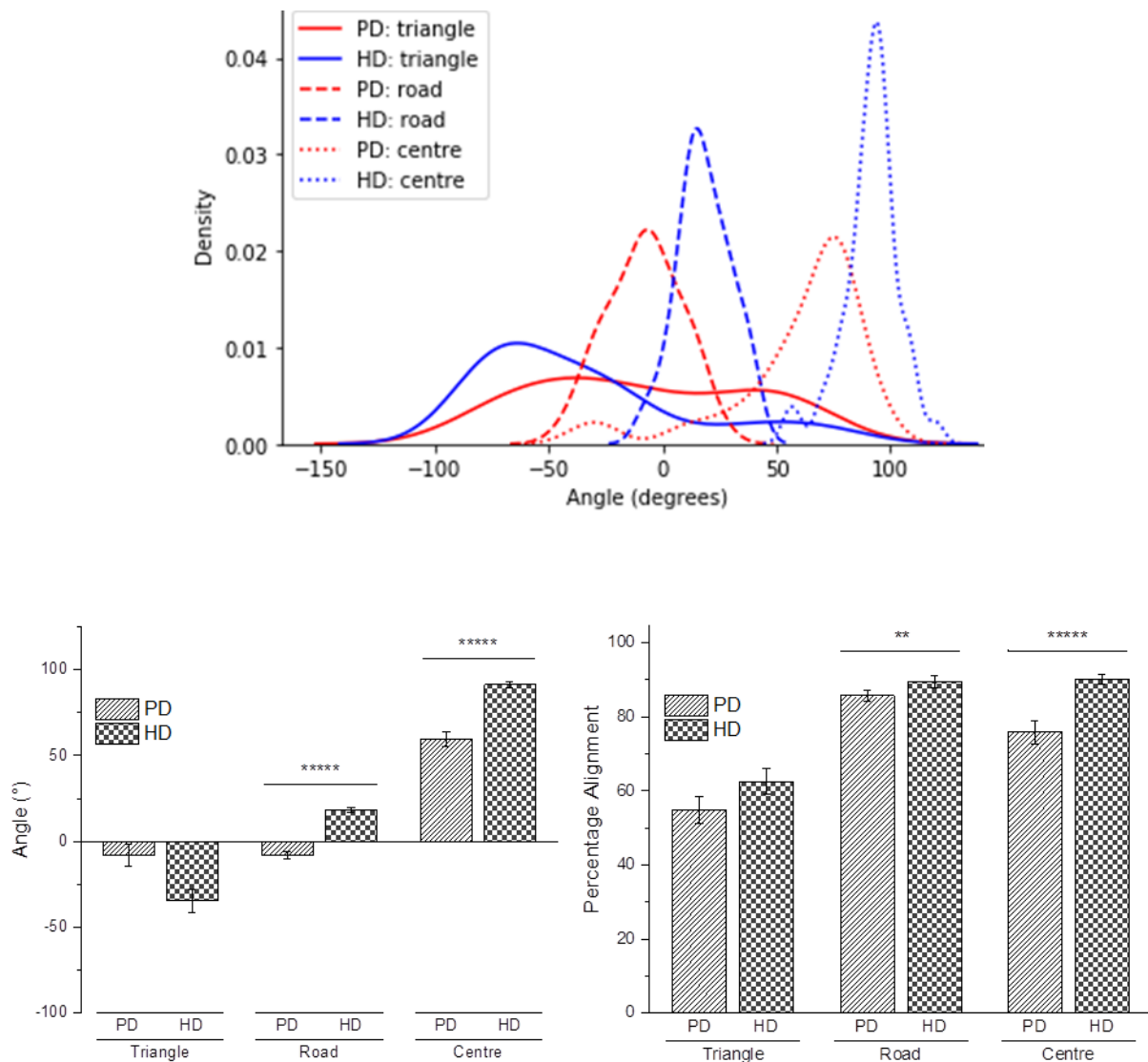


**Figure 4.25** Analysing the impact of a hemispherical collector versus a plain one using the same design (Roads). At the top can be seen the KDE plot showing the triangle, road, and centre zones of PD and HD. At the bottom we can see from left to right bar charts displaying the angle of orientation of all these zones, and the fibre alignment of these zones respectively. \*\* =  $p < 0.04$ , \*\*\*\* =  $p < 0.01$ .

In previous figures can be seen a comparison between the membranes made with the plain collectors (PR PD) versus its hemispherical ones (HR HD). In figure 4.24 we note that there is no statistical difference between the fibre alignment in PR and HR, as their ring and internal zones show no statistical difference between them. Oppositely, when comparing PD with HD the road zones are statistically different ( $p < 0.04$ ) and even more when comparing the centre zones ( $p < 0.01$ ).

#### **4.4.6.- COVID-19 Considerations**

Global pandemic COVID-19 affected us in this chapter in preventing us to incorporate the topographical cues within the mechanically-tailored membranes produced in Chapter 2 (30%PCL – 70%PLGA). It would have been interesting to combine mechanical and topographical cues within the same design and study cell outgrowth. The groups of Connon and Kim have reported the positive effect of membrane alignment using cell lines, which would have made interesting to note what kind of outgrowth we would have achieved.

## 4.5.- Discussion

Introducing complexity via the incorporation of topographical cues for corneal regeneration is a relatively new area of work which has the potential to create smart membranes for guiding cell behaviour. Previous work in our group focused on creating microniches to simulate the limbal zone in an electrospun membrane (Ortega, Deshpande, *et al.*, 2013; Ortega, McKean, *et al.*, 2014). As we have mentioned previously in this thesis, these membranes offered good results when tested *in vitro* and *ex vivo* (Ortega, Sefat, *et al.*, 2014; Ramachandran *et al.*, 2019). These microniches were made to recreate the Palisades of Vogt in the limbal area. When these electrospun membranes were used, the seeding of cell lines was mainly done within the microniches and showed that when the cell loaded membranes were used on wounded cornea models they were able to form a multilayer epithelium (Ortega, Deshpande, *et al.*, 2013). As well, some of these microniche membranes were able to show 50% more cell outgrowth when they were fibronectin coated, compared to normal electrospun rings without the microniches, suggesting the relevance in adding complexity to the membrane to improve the cell outgrowth (Ortega, Deshpande, *et al.*, 2013).

The use of membranes with topographical cues to improve cell outgrowth in tissues has been tested in different tissues with positive results (Place, Evans and Stevens, 2009; Yan *et al.*, 2011). Back in 2009, Stevens *et al.* highlighted that new biomaterials for tissue engineering must consider two key factors, which are efficiency and cost-effectiveness (Place, Evans and Stevens, 2009). The efficiency of a scaffold can be as important as having the ability to manipulate cell fate and outgrowth; guiding and targeting cell behaviour at the right place and time (Place, Evans and Stevens, 2009). New cell therapies in regenerative medicine have been able to keep improving with promising results in patients due to implemented complexity in its biomaterials, for example, to reduce aspects like immune rejection, cell loss, and death. One of these aspects has focused on adding protective structural places for stem cells to reside (synthetic niches) (Qi *et al.*, 2015; Bao, Xie and Huck, 2018).

The cornea as a tissue differs from other tissues in the body as it has 3 relevant properties: tissue transparency, mechanical strength, and refractive effect (Bao *et al.*, 2012; Wilson *et al.*, 2013). Due to these 3 properties, the cornea is a tissue that is fairly complex. In

chapter 2 and 3 we explored the relevance and correlation of limbal epithelial stem cells and the stiffness, but the relevance of another crucial characteristic of the cornea, fibre alignment, was not mentioned (Cardona *et al.*, 2017; Gouveia *et al.*, 2018). The human cornea is a tissue with a thickness of approximately 500  $\mu\text{m}$  and it consists of stroma, keratocytes, and aligned collagen fibres (Kong and MI, 2016). When collagen fibres are ordered in this alignment they show to be thicker, denser, and have better mechanical properties compared to randomly aligned collagen fibres (Gouveia *et al.*, 2018, 2019). This equilibrium between fibre alignment and mechanical properties was reported in the research carried out by Wagner and his group (Wu *et al.*, 2012). In this research they developed a matrix containing collagen fibrils similar to that of a native stroma and seeded it with human corneal stromal stem cells. They found that even though they were able to produce abundant matrix with keratocytes, the matrix was lacking orientation, and therefore they concluded that topographical considerations are needed when developing a membrane for corneal regeneration. Regarding the orientation of the collagen fibrils, we know that these fibrils circumscribe the human cornea in the back part of the tissue (one third) wrapped with mature elastic fibres that mirror the collagen alignment (Kamma-lorger *et al.*, 2010). As well, the central cornea presents an orthogonal arrangement of collagen and is restricted by the posterior stromal layers (Kamma-lorger *et al.*, 2010).

Considering the effect of fibre alignment in corneal regeneration, different approaches have been tackled in the fabrication of biomaterials via electrospinning. The Wang group used electrospun membranes made of gelatin (Type A) with PLLA and made them with random alignment and aligned. The effect of the fibre alignment on cell behaviour showed that keratocytes interact favourably with aligned scaffolds, while corneal epithelial cells interact more favourably with randomly aligned scaffolds (Yan *et al.*, 2011). Wang also mentions that fibre alignment helped the scaffolds to preserve some of their mechanical properties after wetting them (Yan *et al.*, 2011). Fernandez-Perez studied in her research the effect of adding a decellularized corneal extracellular matrix (ECM) with an electrospun PCL with differing fibre organization (random, radial, perpendiculars alignment). In her research she discovered that the human stromal cells that were seeded adopted different morphologies depending of the fiber orientation, with radial and perpendicular aligned having more cell outgrowth (Fernández-pérez *et al.*, 2020). On the other hand, aside of the fibre alignment, Kim decided to investigate

as well the effect of a hemispherical membrane versus a plane one. In his research he successfully created hemispherical PCL-Collagen membranes radially aligned and noticed that the aligned topography of the hemispherical membranes provides favourable environments for critical function in the corneal cells (Kim, Kim and Park, 2018).

In our research, we developed different collectors to create different membrane patterns. In 4.4.5 we successfully created different alignment zones in membranes with plain and hemispherical collectors. Due to the COVID-19 pandemic we were not able to assess the biological effect in the cell outgrowth of our second generation membranes. It would have been very interesting to see if the zones with different fibre alignment would have presented different levels of cell outgrowth. Theoretically, and considering the work of Kim and Fernandez-Perez we know that strong fibre alignment positively affects the cell outgrowth of corneal cells (Kim, Kim and Park, 2018; Fernández-pérez *et al.*, 2020). In our visit to L. V. Prasad Eye Institute we were able to test a first generation design membrane with human limbal explants. From this experience, and even though we had shrinkage issues, the electrospun membranes with microniches were able to support cell outgrowth, something we have seen as well with animal explants in chapter 3.

The methodology we present in this chapter to measure fibre orientation and alignment successfully let us compare different zones of alignment in a complex electrospun scaffold with different zones of fibre orientation. The limitations of the technique were mentioned, and they are the straightness of the fibres and the orientation to a point and not an axis. For both cases, we presented a methodology to measure the fibre alignment through the straightness of the fiber rather than the angle orientation. For the results we presented in this chapter, there was no need in applying the straightness factor as the zones presented orientation to an axis in the magnification used, and the fibres were relatively straight.

Shrinkage in electrospun scaffolds is something that can happen depending on the polymer and the storage conditions, and this shrinkage can have a negative impact which can lead to poor initial adhesion of the cells to the membranes (Xie *et al.*, 2011; Sundaray *et al.*, 2013; Ru *et al.*, 2015). Electrospun scaffolds made of PLGA have been reported to shrink almost by 80% of their original size when placed in cell culture media at 37°C for just 2 hours

(Liu *et al.*, 2008; Ru *et al.*, 2015). Compared to that amount of shrinkage in 2 hours, the shrinkage seen in L. V. Prasad Eye Institute was below this amount (all shrinkage values after 96 hours were below 80% of shrinkage). The use of fibrin glue helped to reduce shrinkage in the membranes; it would be interesting to see how much shrinkage can be seen in the electrospinning conditions established in chapter 2 (using 30%PCL – 70%PLGA membranes) and this is part of our future work.

## 4.6.- Conclusion

Topographical cues were introduced in electrospun scaffolds through the manufacturing of designed collectors. The optimal way of fabricating the collectors with our laboratory equipment is as follows: 1.- Design the collector using Autodesk Inventor Professional 2017 ®; 2.- 3D print the model using the 3D printer Form2 (Formlabs®) using a casting resin; 3.- Cast the resin models using tilite alloy to get metal collectors. Preliminary assessment of topography complex electrospun PLGA scaffolds about human explants compatibility was made in L.V. Prasad Eye Institute and with their feedback a second generation of collectors were manufactured. To measure the topographical cues in the collectors, a measuring technique for fibre alignment and orientation was developed. Electrospun 30%PCL – 70%PLGA scaffolds were made using the second generation collectors and successfully present topographical zones with different levels of fibre orientation and fibre alignment.

## Chapter 5: Final conclusions and future work

### 5.1 Final Conclusions

In this research, a series of electrospun scaffolds with different mechanical properties were manufactured by blending the polymers PLGA and PCL. The use of DCM and DMF as solvents produced a lower amount of remnant solvents in the scaffolds than the maximum permissible by EMA and FDA. Electrospun scaffolds with different amounts of PCL:PLGA showed similar fibrous microenvironments but preserve their individual thermal properties.. Adding PCL showed statistical differences in the stiffness of the membrane for blends with 10% or more PCL on it, an effect that is increased when the membranes are analysed in dry and wet conditions. From all the conditions analysed, 30%PCL - 70%PLGA is able to maintain its mechanical properties in wet/warm and dry conditions which we envisage is a very important point for the material to be used in theatre.

Rabbit and porcine limbal cell outgrowth was analysed in the mechanically tailored membranes. PLGA and PLGA-PCL membranes showed outgrowth from limbal explants at 2 and 3 weeks no differences were observed in the amount of cell outgrowth between them. All mechanically tailored membranes developed in this research showed good capacity as cell carriers of limbal corneal cells. 30%PCL – 70%PLGA displayed cell outgrowth in both sides of the membrane, suggesting that the cells penetrated through the membrane and populated the other side. The porosity and fibre environment of this membrane together with its mechanical properties make the 30%PCL – 70%PLGA our best candidate to take forwards as new membrane, however, further research is needed to accurately demonstrate this.<sup>3</sup>; further *ex vivo* testing using wounded cornea models would provide a better insight to assess its effectiveness as a cell carrier.

Finally, topographical cues were introduced within electrospun scaffolds by the use of designed metallic collectors. Topographical cues in the membranes were successfully characterised analysing fibre orientation and fibre alignment in different zones on them. Preliminary work for the study of cell responses within these complex membranes was developed in India through a MeDe-sponsored placement. For this we used human limbal explants. The results were positive but preliminary and more work will need to be developed to truly understand the behaviour of corneal cells on the newly designed microfabricated environments.

## **5.2 Future work**

In this research we have manufactured electrospun scaffolds with different mechanical properties. From them, 30%PCL – 70%PLGA showed the best results in its mechanical properties and its cell outgrowth when seeded with porcine limbal explants for two weeks. It would be interesting to replicate this experiment but for 3 and 4 weeks so we can analyse cell outgrowth at different culture times. As well, and considering that 30%PCL – 70%PLGA showed cell outgrowth through its membrane, we would use this membrane in wounded cornea models since we envisage the encouraged cell migration could favour corneal regeneration via the rapid formation of a multi-layered epithelium.

Regarding the effects of topographical cues, due to COVID-19 global pandemic it was not possible to explore the behaviour of limbal porcine explants on these membranes. Next steps will explore differences in the cell outgrowth in the zones with fibre alignment versus the random alignment zones. Corneal epithelial markers (such as CK3) and stem cell markers such as P63 and ABCG2 could be also used to assess cell differentiation and stem cell maintenance across the membranes.

## References

A. Ramirez-Miranda, M.N.Nakatsu, S.Zarei-Ghanavati, C.V. Nguyen, and S. X. D. (2011) 'Keratin 13 is amore specificmarker of conjunctival epithelium than keratin 19', *Molecular Vision*, 17, pp. 1652–1661.

Aboutkidshealth.ca (2019) *Eye anatomy and function*. Available at: <https://www.aboutkidshealth.ca/Article?contentid=1941&language=English> (Accessed: 20 January 2021).

Amato, A. R. D. *et al.* (2018) 'Solvent retention in electrospun fibers affects scaffold mechanical properties', pp. 15–28.

Ang, L. *et al.* (2006) 'The development of a serum-free derived bioengineered conjunctival epithelial equivalent using an ultrathin poly (caprolactone) membrane substrate', *Invest. Ophthalmol.*, 47, pp. 105–112.

Ang, L. P. K. *et al.* (2007) 'A Comparison Between Cultivated and Conventional Limbal Stem Cell Transplantation for Stevens-Johnson Syndrome', *American Journal of Ophthalmology*, 143(1), pp. 178–180. doi: 10.1016/j.ajo.2006.07.050.

Anita, P. and Sandeep, KumarAbhiyan, KumarRaseena, B. S. (2005) 'Fibrin glue in ophthalmology', p. 60093. doi: 10.4103/0301-4738.60089.

Ann, R. *et al.* (2011) 'Preparation and characterization of electrospun PCL / PLGA membranes and chitosan / gelatin hydrogels for skin bioengineering applications', pp. 2207–2218. doi: 10.1007/s10856-011-4402-8.

Arora, R. *et al.* (2017) 'Preliminary results from the comparison of simple limbal epithelial transplantation with conjunctival limbal autologous transplantation in severe unilateral chronic ocular burns', *Indian Journal of Ophthalmology*, 65(1), pp. 35–40.

Arya, S. K. *et al.* (2016) 'Simple limbal epithelial transplantation in acid injury and severe dry eye', *Journal of Clinical and Diagnostic Research*, 10(6), pp. ND06–ND07. doi: 10.7860/JCDR/2016/19306.7997.

Bao, F. *et al.* (2012) 'Assessment of the ex vivo biomechanical properties of porcine cornea with inflation test for corneal xenotransplantation Assessment of the ex vivo biomechanical properties of porcine cornea with inflation test for corneal xenotransplantation', 1902. doi: 10.3109/03091902.2011.629276.

Bao, M. *et al.* (2017) '3D microniches reveal the importance of cell size and shape', *Nature Communications*. Springer US, pp. 1–12. doi: 10.1038/s41467-017-02163-2.

Bao, M., Xie, J. and Huck, W. T. S. (2018) 'Recent Advances in Engineering the Stem Cell Niche in 3D', *Advanced science*, 1800448. doi: 10.1002/advs.201800448.

Basu, S. *et al.* (2016) 'Simple Limbal Epithelial Transplantation: Long-Term Clinical Outcomes in 125 Cases of Unilateral Chronic Ocular Surface Burns', *Ophthalmology*. American Academy of Ophthalmology, 123(5), pp. 1000–1010. doi: 10.1016/j.ophtha.2015.12.042.

Biomaterials, F. (2007) 'Tissue-Engineered Human Corneal Endothelial Cell Sheet Transplantation in a Rabbit Model Using', 84(10), pp. 10–13. doi: 10.1097/01.tp.0000287336.09848.39.

Boncu, T. E., Ozdemir, N. and Guclu, A. U. (2020) 'Electrospinning of linezolid loaded PLGA nanofibers : effect of solvents on its spinnability , drug delivery , mechanical properties , and antibacterial activities spinnability , drug delivery , mechanical properties , and antibacterial activities', *Drug Development and Industrial Pharmacy*. Taylor & Francis, 46(1), pp. 109–121. doi: 10.1080/03639045.2019.1706550.

Bozkir, G. *et al.* (1997) 'Measurements of Axial Length and Radius of Corneal Curvature in the Rabbit Eye', *Acta Med Okayama*, 51(1), pp. 9–11.

Breuls, R. G. M., Jiya, T. U. and Smit, T. H. (2008) 'Scaffold Stiffness Influences Cell Behavior : Opportunities for Skeletal Tissue Engineering', pp. 103–109.

Brinkmann, R. and Sc, M. (2000) 'Thermal and Biomechanical Parameters of', 19(3), pp. 355–363.

Brouki, P. *et al.* (2020) 'Decellularized human amniotic membrane : From animal models to clinical trials', *Methods*. Elsevier, 171(May 2019), pp. 11–19. doi: 10.1016/j.ymeth.2019.07.018.

Buch, H., Vinding, T. and Cour, M. La (2001) 'The prevalence and causes of bilateral and unilateral

blindness in an elderly urban Danish population . The Copenhagen City Eye Study', pp. 441–449.

Bunting, K. D. (2002) 'ABC transporters as phenotypic markers and functional regulators of stemcells', *Stem Cells*, 20(1), pp. 11–20.

Burton, M. J. (2009) 'Prevention, treatment and rehabilitation.', *Community eye health / International Centre for Eye Health*, 22(71), pp. 33–5.

Cardona, J. C. *et al.* (2017) 'Biomaterials Controlling the 3D architecture of Self-Lifting Auto-generated Tissue Equivalents ( SLATEs ) for optimized corneal graft composition and stability', 121, pp. 205–219. doi: 10.1016/j.biomaterials.2016.12.023.

Chawla, S. and Ghosh, S. (2018) 'Establishment of in vitro model of corneal scar pathophysiology', (May 2017), pp. 3817–3830. doi: 10.1002/jcp.26071.

Chen, B. *et al.* (2012) 'The mechanical properties of amniotic membrane influence its effect as a biomaterial for ocular surface repair', pp. 8379–8387. doi: 10.1039/c2sm26175h.

Chen, Y. *et al.* (2019) 'Determination of Electrospinning Parameters ' Strength in Poly ( D , L ) - lactide-co-glycolide Micro / Nanofiber Diameter Tailoring', 2019.

Chen, Z. *et al.* (2004) 'Characterization of putative stem cell phenotype in human limbal epithelia', *Stem Cells*, pp. 355–366.

Choi, D. J. *et al.* (2015) 'Bioactive fish collagen/polycaprolactone composite nanofibrous scaffolds fabricated by electrospinning for 3D cell culture', *Journal of Biotechnology*. Elsevier B.V., 205, pp. 47–58. doi: 10.1016/j.jbiotec.2015.01.017.

Chou, S. and Woodrow, K. A. (2017) 'Relationships between mechanical properties and drug release from electrospun fibers of PCL and PLGA blends', *Journal of the Mechanical Behavior of Biomedical Materials*. Elsevier, 65(July 2016), pp. 724–733. doi: 10.1016/j.jmbbm.2016.09.004.

Chung, S., Moghe, A. K. and Montero, G. A. (2009) 'Nanofibrous scaffolds electrospun from elastomeric biodegradable poly ( L-lactide-co-  $\epsilon$  -caprolactone )'. doi: 10.1088/1748-6041/4/1/015019.

Chye, S. *et al.* (2005) 'Effect of isothermal annealing on the hydrolytic degradation rate of poly ( lactide- co -glycolide ) ( PLGA )', 26, pp. 2827–2833. doi: 10.1016/j.biomaterials.2004.08.031.

Clinic, E. O. (no date) *Eye cornea structure*. Available at: <https://en.excimerclinic.ru/press/rogovica/> (Accessed: 20 January 2021).

Cotsarelis, G. *et al.* (1989) 'Existence of slow-cycling limbal epithelial basal cells that can be preferentially stimulated to proliferate: Implications on epithelial stem cells', *Cell*, 57(2), pp. 201–209. doi: 10.1016/0092-8674(89)90958-6.

Croisier, F. *et al.* (2012) 'Acta Biomaterialia Mechanical testing of electrospun PCL fibers', *Acta Biomaterialia*. Acta Materialia Inc., 8(1), pp. 218–224. doi: 10.1016/j.actbio.2011.08.015.

Das, S., Basu, S. and Sangwan, V. (2015) 'Molten metal ocular burn: long-term outcome using simple limbal epithelial transplantation', *BMJ Case Reports*, 1, p. bcr2014209272. doi: 10.1136/bcr-2014-209272.

Davanger M, E. A. (1971) 'Role of the pericorneal papillary structure in renewal of corneal epithelium', *Nature*, 229(560).

Dehghani, S., Rasoulianboroujeni, M. and Ghasemi, H. (2018) 'Biomaterials 3D-Printed membrane as an alternative to amniotic membrane for ocular surface / conjunctival defect reconstruction : An in vitro & in vivo study', 174. doi: 10.1016/j.biomaterials.2018.05.013.

Deshpande, P. *et al.* (2011) 'scaffolds to deliver cultured epithelial cells to the cornea R esearch A rticle', pp. 395–401.

Deshpande, P., Ramachandran, C., Sangwan, V., *et al.* (2013) 'Cultivation of Limbal Epithelial Cells on Electrospun Poly (lactide-co-glycolide) Scaffolds for Delivery to the Cornea', *Methods in molecular biology (Clifton, N.J.)*, (December). doi: 10.1007/978-1-62703-432-6.

Deshpande, P., Ramachandran, C., Sefat, F., *et al.* (2013) 'Simplifying corneal surface regeneration using a biodegradable synthetic membrane and limbal tissue explants', *Biomaterials*. Elsevier Ltd, 34(21), pp. 5088–5106. doi: 10.1016/j.biomaterials.2013.03.064.

Ding, B., Wang, X. and Yu, J. (2018) *Electrospinning: Nanofabrication and applications*.

Dobrowolski, D. *et al.* (2011) 'Cultivated oral mucosa epithelium transplantation (COMET) in bilateral limbal stem cell deficiency', *Acta Ophthalmologica*, 89.

- Donnelly, H., Salmeron-sanchez, M. and Dalby, M. J. (2018) 'Designing stem cell niches for differentiation and self-renewal'.
- Doughty, M. J. and Zaman, M. L. (2000) 'MAJOR REVIEW Human Corneal Thickness and Its Impact on Intraocular Pressure Measures : A Review and Meta-analysis Approach', 44(5).
- Dua, H. *et al.* (2005) 'Limbal epithelial crypts: a novel anatomical structure and a putative limbal stem cell niche', *Br J Ophthalmol*, pp. 529–532. doi: 10.1136/bjo.2004.049742.
- Dunnen, W. F. A. Den *et al.* (1996) 'Long-term evaluation of degradation and foreign-body reaction of subcutaneously implanted poly ( DL -lactide- ɛ -caprolactone )'.
- Elsheikh, A., Alhasso, D. and Rama, P. (2008) 'Biomechanical properties of human and porcine corneas', 86, pp. 783–790. doi: 10.1016/j.exer.2008.02.006.
- European Medicines Agency (2016) 'ICH guideline Q3C ( R6 ) on impurities : guideline for residual solvents', EMA/CHMP/I(June).
- Feng, Y. *et al.* (2014) 'Review of Alternative Carrier Materials for Ocular Surface Reconstruction', (September 2013), pp. 1–12. doi: 10.3109/02713683.2013.853803.
- Fernández-pérez, J. *et al.* (2020) 'Materials Science & Engineering C Characterization of extracellular matrix modified poly ( ɛ -caprolactone ) electrospun scaffolds with differing fiber orientations for corneal stroma regeneration', 108(November 2019), pp. 0–8. doi: 10.1016/j.msec.2019.110415.
- Flueckiger, F. *et al.* (2005) 'An Ex-Vivo, Whole-Globe Porcine Model of Corneoepithelial Wound Healing Tested Using Immunomodulatory Drugs', *Journal of ocular pharmacology and therapeutics*, 21(5).
- G. Pellegrini, O. Golisano, P. P. (1999) 'Location and clonal analysis of stem cells and their differentiated progeny in the human ocular surface', *Journal of Cell Biology*, 145(4), pp. 769–782.
- Gain, P. *et al.* (2016) 'Global Survey of Corneal Transplantation and Eye Banking', *JAMA Ophthalmology*, 134(2), pp. 167–173. doi: 10.1001/jamaophthalmol.2015.4776.
- Garner, A. *et al.* (1982) 'Corneal graft rejection', pp. 292–302.

Di Girolamo, N. (2011) 'Stem cells of the human cornea', *British Medical Bulletin*, 100(1), pp. 191–207. doi: 10.1093/bmb/ldr026.

Gouveia, R. *et al.* (2018) 'Modulation of corneal tissue mechanics influences epithelial cell phenotype', *BioRxiv*, pp. 1–44.

Gouveia, R. *et al.* (2019) 'Assessment of corneal substrate biomechanics and its effect on epithelial stem cell maintenance and differentiation', *Nature Communications*. Springer US, pp. 1–17. doi: 10.1038/s41467-019-09331-6.

Gouveia, R. M. *et al.* (2017) 'Controlling the 3D architecture of Self-Lifting Auto-generated Tissue Equivalent (SLATEs) for optimized corneal graft composition and stability', *Biomaterials*, 121, pp. 205–219. doi: 10.1016/j.biomaterials.2016.12.023.

Grieve, K. *et al.* (2015) 'Three-dimensional structure of the mammalian limbal stem cell niche', *Experimental Eye Research*. Elsevier Ltd, 140, pp. 75–84. doi: 10.1016/j.exer.2015.08.003.

Griffith, M., Alarcon, E. I. and Brunette, I. (2016) 'Regenerative approaches for the cornea', *Journal of Internal Medicine*, 280(3), pp. 276–286. doi: 10.1111/joim.12502.

Griffith, M. and Harkin, D. G. (2014) 'Recent advances in the design of artificial corneas.', *Current opinion in ophthalmology*, 25(3), pp. 240–7. doi: 10.1097/ICU.0000000000000049.

Health, N. I. of (2012) *Medical research with animals, NIH Publication Number 08-6436*. Available at: <https://grants.nih.gov/grants/policy/air/AnimalResearchFS06.pdf> (Accessed: 26 June 2020).

Hersh, P. *et al.* (2000) 'DIAGNOSTIC AND SURGICAL TECHNIQUES Limbal Stem Cells of the Corneal Epithelium', 44(5).

Hitani, K. *et al.* (2008) 'Transplantation of a sheet of human corneal endothelial cell in a rabbit model', (December 2007), pp. 1–9.

Huang, M. *et al.* (2011) 'Biomaterials Using acellular porcine limbal stroma for rabbit limbal stem cell microenvironment reconstruction', *Biomaterials*. Elsevier Ltd, 32(31), pp. 7812–7821. doi: 10.1016/j.biomaterials.2011.07.012.

J. Pe'er, G. Zajicek, H. Greifner, and M. K. (1996) 'Streaming conjunctiva', *Anatomical Record*,

245(1), pp. 36–40.

Jansen, K. *et al.* (2004) 'Long-term regeneration of the rat sciatic nerve through a biodegradable poly ( DL-lactide-  $\epsilon$  -caprolactone ) nerve guide : Tissue reactions with focus on collagen III / IV reformation'. doi: 10.1002/jbm.a.30004.

Joachim H. Wendorff, Seema Agarwal, A. G. (2012) *Electrospinning: Materials, Processing, and Applications*. WILEY-VCH.

John, P. and Madan, P. (2001) 'Corneal blindness : A global perspective'.

Joo, J. *et al.* (2014) 'Mechanical properties and degradation studies of poly ( D , L-lactide-co-glycolide ) 50 : 50 / graphene oxide nanocomposite films', (September 2013). doi: 10.1002/pat.3203.

Jue, B. *et al.* (no date) 'The mechanical properties of the rabbit and human cornea'.

Juraskova, N. *et al.* (2011) 'AlphaCor artificial cornea : clinical outcome', pp. 1138–1146. doi: 10.1038/eye.2011.122.

Kameishi, S. *et al.* (2014) 'Remodeling of epithelial cells and basement membranes in a corneal deficiency model with long-term follow-up', *Laboratory Investigation*. Nature Publishing Group, 95(2), pp. 168–179. doi: 10.1038/labinvest.2014.146.

Kamma-lorger, C. S. *et al.* (2010) 'Collagen and mature elastic fibre organisation as a function of depth in the human cornea and limbus', *Journal of Structural Biology*. Elsevier Inc., 169(3), pp. 424–430. doi: 10.1016/j.jsb.2009.11.004.

Katikireddy, K. R. and Ula, J. V (2014) 'Limbal Stem Cell Transplantation and Corneal Neovascularization', (February 2012). doi: 10.5772/26870.

Kaye, G. I. (no date) 'S T U D I E S ON THE CORNEA I . The Fine Structure of the Rabbit Cornea and the Uptake and Transport of Colloidal Particles by the Cornea in Vivo Methods for the Study of the Uptake and Transport of Colloidal Particles by the Cornea in Vivo', (13), pp. 457–479.

Keles, H. *et al.* (2015) 'Investigation of factors in fl uencing the hydrolytic degradation of single PLGA microparticles', *Polymer Degradation and Stability*. Elsevier Ltd, 119, pp. 228–241. doi:

10.1016/j.polymdegradstab.2015.04.025.

Kenyon, K. R. and Tseng, S. C. (1989) 'Limbal autograft transplantation for ocular surface disorders.', *Ophthalmology*, 96(5), pp. 709–22; discussion 722-3. doi: 10.1016/S0161-6420(89)32833-8.

Kethiri, A. R. *et al.* (2017) 'Optimizing the role of limbal explant size and source in determining the outcomes of limbal transplantation : An in vitro study', pp. 1–17.

Khanlou, H. M. *et al.* (2014) 'Prediction and optimization of electrospinning parameters for polymethyl methacrylate nanofiber fabrication using response surface methodology and artificial neural networks', pp. 767–777. doi: 10.1007/s00521-014-1554-8.

Kim, G. K. *et al.* (2013) 'Electrospinning of PCL / PVP blends for tissue engineering scaffolds', pp. 1425–1442. doi: 10.1007/s10856-013-4893-6.

Kim, H. S. *et al.* (2005) 'Morphological Characterization of Electrospun Nano-Fibrous Membranes of Biodegradable Poly(L-lactide) and Poly(lactide-co-glycolide)', *Macromol. Symp*, pp. 145–154. doi: 10.1002/masy.200550613.

Kim, J. I., Kim, J. Y. and Park, C. H. (2018) 'Fabrication of transparent hemispherical 3D nanofibrous scaffolds with radially aligned patterns via a novel electrospinning method', *Scientific Reports*. Springer US, 8(1), pp. 1–13. doi: 10.1038/s41598-018-21618-0.

Kivela, T., Messmer, E. M. and Rymgayllo-Jankowska, B. (2015) 'Cornea', in *Eye Pathology*.

Kobayashi, T. *et al.* (2013) 'Biomaterials Corneal regeneration by transplantation of corneal epithelial cell sheets fabricated with automated cell culture system in rabbit model', *Biomaterials*. Elsevier Ltd, 34(36), pp. 9010–9017. doi: 10.1016/j.biomaterials.2013.07.065.

Kong, B. and MI, S. (2016) 'Electrospun Scaffolds for Corneal Tissue Engineering: A Review', *Materials (Basel)*.

Kruse, F. E. and Schlo, U. (2005) 'Identification and characterization of limbal stem cells', 81, pp. 247–264. doi: 10.1016/j.exer.2005.02.016.

Lagali, N. S. *et al.* (2007) 'Innervation of Tissue-Engineered Corneal Implants in a Porcine Model : A 1-Year In Vivo Confocal Microscopy Study'. doi: 10.1167/iovs.06-1483.

Lawlor, M. and Kerridge, I. (2011) 'Anything but the Eyes : Culture , Identity , and the Selective Refusal of Corneal Donation', 92(11), pp. 1188–1190. doi: 10.1097/TP.0b013e318235c817.

Le, Q. and Deng, S. X. (2019) 'The Ocular Surface The application of human amniotic membrane in the surgical management of limbal stem cell deficiency ☆', *The Ocular Surface*. Elsevier, 17(2), pp. 221–229. doi: 10.1016/j.jtos.2019.01.003.

Lei, K. F. *et al.* (2013) 'Non-invasive measurement of cell viability in 3-dimensional cell culture construct.', *Conference proceedings : ... Annual International Conference of the IEEE Engineering in Medicine and Biology Society. IEEE Engineering in Medicine and Biology Society. Annual Conference*, 2013, pp. 180–3. doi: 10.1109/EMBC.2013.6609467.

Levis, H. J. *et al.* (2015) 'Tissue Engineering the Cornea : The Evolution of RAFT', pp. 50–65. doi: 10.3390/jfb6010050.

Li, Y. *et al.* (2014) 'Differences Between Niche Cells and Limbal Stromal Cells in Maintenance of Corneal Limbal Stem Cells'. doi: 10.1167/iovs-13-13698.

Li, Z. and Wang, C. (2013) 'One-Dimensional nanostructures', pp. 15–29. doi: 10.1007/978-3-642-36427-3.

Liang, H. *et al.* (2012) 'Ocular safety of cationic emulsion of cyclosporine in an in vitro corneal wound-healing model and an acute in vivo rabbit model', (February), pp. 2195–2204.

Liu, W., Thomopoulos, S. and Xia, Y. (2012) 'Electrospun nanofibers for regenerative medicine', *Advanced Healthcare Materials*, 1(1), pp. 10–25. doi: 10.1002/adhm.201100021.

Liu, X. *et al.* (2017) 'Electrospinnability of Poly Lactic-co-glycolic Acid ( PLGA ) : the Role of Solvent Type and Solvent Composition'. *Pharmaceutical Research*, (103), pp. 738–749. doi: 10.1007/s11095-017-2100-z.

Liu, Y. *et al.* (2008) 'Control of Dimensional Stability and Degradation Rate in Electrospun Composite Scaffolds Composed of Poly(D,L-Lactide-co-glycolide) and Poly(ε-Caprolactone).', *Chinese journal of polymer science*, 26(1).

Luo, H. *et al.* (2013) 'Biomaterials Construction of tissue-engineered cornea composed of amniotic

epithelial cells and acellular porcine cornea for treating corneal alkali burn', *Biomaterials*. Elsevier Ltd, 34(28), pp. 6748–6759. doi: 10.1016/j.biomaterials.2013.05.045.

Mccolgan, K. (2009) 'Corneal transplant surgery', 19(2), pp. 51–55.

Meek, K. M. and Knupp, C. (2015) 'Progress in Retinal and Eye Research Corneal structure and transparency', *Progress in Retinal and Eye Research*. Elsevier Ltd, 49, pp. 1–16. doi: 10.1016/j.preteyeres.2015.07.001.

Meek, M. F. and Jansen, K. (2008) 'Two years after in vivo implantation of poly ( DL -lactide- e - caprolactone ) nerve guides : Has the material finally resorbed ?' doi: 10.1002/jbm.a.32024.

Menduni, F. *et al.* (2018) 'Contact Lens and Anterior Eye Characterisation of the porcine eyeball as an in-vitro model for dry eye', 41(July 2017), pp. 13–17. doi: 10.1016/j.clae.2017.09.003.

Mi, S. *et al.* (2010) 'Plastic compression of a collagen gel forms a much improved scaffold for ocular surface tissue engineering over conventional collagen gels', (March), pp. 447–453. doi: 10.1002/jbm.a.32861.

Milazzo, G., De Luca, M. and Pellegrini, G. (2016) 'Holoclar: first of its kind in more ways than one', *Cell Gene Ther. Insights*, 2.

Miri, A., Al-Deiri, B. and Dua, H. S. (2010) 'Long-term Outcomes of Autolimbal and Allolimbal Transplants', *Ophthalmology*. Elsevier Inc., 117(6), pp. 1207–1213. doi: 10.1016/j.ophtha.2009.10.028.

Miri, A., Said, D. G. and Dua, H. S. (2011) 'Donor site complications in autolimbal and living-related allolimbal transplantation', *Ophthalmology*. Elsevier Inc., 118(7), pp. 1265–1271. doi: 10.1016/j.ophtha.2010.11.030.

Mittal, V. *et al.* (2016) 'Successful management of severe unilateral chemical burns in children using simple limbal epithelial transplantation (SLET)', *British Journal of Ophthalmology*, 100(8), pp. 1102–1108. doi: 10.1136/bjophthalmol-2015-307179.

Oliva, M., Gulati, M. and Schottman, T. (2012) 'Turning the tide of corneal blindness', *Indian Journal of Ophthalmology*, 60(5), p. 423. doi: 10.4103/0301-4738.100540.

Ortega, I., McKean, R., *et al.* (2014) 'Characterisation and evaluation of the impact of microfabricated pockets on the performance of limbal epithelial stem cells in biodegradable PLGA membranes for corneal regeneration', *Biomaterials Science*, 2, p. 723. doi: 10.1039/c3bm60268k.

Ortega, I., Sefat, F., *et al.* (2014) 'Combination of microstereolithography and electrospinning to produce membranes equipped with niches for corneal regeneration.', *Journal of visualized experiments : JoVE*, (91), p. 51826. doi: 10.3791/51826.

Ortega, Í., Ryan, A. J., *et al.* (2013) 'Combined microfabrication and electrospinning to produce 3-D architectures for corneal repair', *Acta Biomaterialia*, 9(3), pp. 5511–5520. doi: 10.1016/j.actbio.2012.10.039.

Ortega, Í., Deshpande, P., *et al.* (2013) 'Development of a microfabricated artificial limbus with micropockets for cell delivery to the cornea.', *Biofabrication*, 5(2), p. 025008. doi: 10.1088/1758-5082/5/2/025008.

Pang, K., Du, L. and Wu, X. (2010) 'Biomaterials A rabbit anterior cornea replacement derived from acellular porcine cornea matrix , epithelial cells and keratocytes', *Biomaterials*. Elsevier Ltd, 31(28), pp. 7257–7265. doi: 10.1016/j.biomaterials.2010.05.066.

Parenteau-bareil, R., Gauvin, R. and Berthod, F. (2010) 'Collagen-Based Biomaterials for Tissue Engineering Applications', pp. 1863–1887. doi: 10.3390/ma3031863.

Pascolini, D. and Mariotti, S. P. (2012) 'Global estimates of visual impairment : 2010', pp. 614–618. doi: 10.1136/bjophthalmol-2011-300539.

Patel, S. V (2012) 'Graft survival and endothelial outcomes in the new era of endothelial keratoplasty q', *Experimental Eye Research*. Elsevier Ltd, 95(1), pp. 40–47. doi: 10.1016/j.exer.2011.05.013.

Paterson, T. E. *et al.* (2017) 'Selective laser melting-enabled electrospinning: Introducing complexity within electrospun membranes', *Proceedings of the Institution of Mechanical Engineers, Part H: Journal of Engineering in Medicine*, 231(6), pp. 565–574. doi: 10.1177/0954411917690182.

Pellegrini, G. *et al.* (1997) 'Long-term restoration of damaged corneal surfaces with autologous cultivated corneal epithelium', *Lancet*, 349(9057), pp. 990–993. doi: 10.1016/S0140-6736(96)11188-0.

Peyton, S. R. *et al.* (2011) 'Marrow-Derived Stem Cell Motility in 3D Synthetic Scaffold Is Governed by Geometry Along With Adhesivity and Stiffness', 108(5), pp. 1181–1193. doi: 10.1002/bit.23027.

Place, E. S., Evans, N. D. and Stevens, M. M. (2009) 'Complexity in biomaterials for tissue engineering', *Nature Publishing Group*. Nature Publishing Group, 8(may). doi: 10.1038/nmat2441.

Powell, H. M. *et al.* (2009) 'Engineered Human Skin Fabricated Using Electrospun Collagen–PCL Blends: Morphogenesis and Mechanical Properties', 15(8).

Prina, E. *et al.* (2020) 'Bioinspired Precision Engineering of Three-Dimensional Epithelial Stem Cell Microniches', 2000016. doi: 10.1002/adbi.202000016.

Qi, C. *et al.* (2015) 'Biomaterials as carrier , barrier and reactor for cell-based regenerative medicine', *Protein & Cell*. Higher Education Press, 6(9), pp. 638–653. doi: 10.1007/s13238-015-0179-8.

Qi, X. *et al.* (2013) 'Characteristics of immune rejection after allogeneic cultivated limbal epithelial transplantation', *Ophthalmology*, 120(5), pp. 931–936. doi: 10.1016/j.ophtha.2012.11.001.

R. P. Revoltella, S. Papini, A. Rosellini, and M. M. (2007) 'Epithelial stem cells of the eye surface', *Cell Proliferation*, 40(4), pp. 445–461.

Rahman, I. *et al.* (2009) 'Penetrating keratoplasty : indications , outcomes , and complications'. Nature Publishing Group, (February 2008), pp. 1288–1294. doi: 10.1038/eye.2008.305.

Rama, P. *et al.* (2001) 'Autologous fibrin-cultured limbal stem cells permanently restore the corneal surface of patients with total limbal stem cell deficiency', *Transplantation*, 72(2).

Ramachandran, C. *et al.* (2019) 'Synthetic biodegradable alternatives to the use of the amniotic membrane for corneal regeneration : assessment of local and systemic toxicity in rabbits', pp. 286–292. doi: 10.1136/bjophthalmol-2018-312055.

Ramamurthi, S. *et al.* (2008) 'Penetrating Keratoplasty for the Exciting Eye in Sympathetic Ophthalmia', 27(9), pp. 1080–1081.

Ramos, T., Scott, D. and Ahmad, S. (2015) 'An Update on Ocular Surface Epithelial Stem Cells: Cornea and Conjunctiva.', *Stem cells international*, 2015, p. 601731. doi: 10.1155/2015/601731.

Ravichandran, R. *et al.* (2009) 'Effects of nanotopography on stem cell phenotypes', 1(1), pp. 55–66.

doi: 10.4252/wjsc.v1.i1.55.

Rimmer, J. *et al.* (2007) 'Epithelialization of hydrogels achieved by amine functionalization and co-culture with stromal cells. Biomaterials', *Biomaterials*, 28.

Rose, J. B. *et al.* (2019) 'In vitro evaluation of electrospun blends of gelatin and PCL for application as a partial thickness corneal graft', pp. 828–838. doi: 10.1002/jbm.a.36598.

Ru, C. *et al.* (2015) 'A Suspending , Shrinkage-free Electrospun PLGA Nanofibrous Scaffold for Skin Tissue Engineering', *ACS Publications*, pp. 3–5.

Salehi, S. *et al.* (2017) 'Acta Biomaterialia scaffold as intrinsic bio- and immunocompatible system for corneal repair', *Acta Biomaterialia*. Acta Materialia Inc., 50, pp. 370–380. doi: 10.1016/j.actbio.2017.01.013.

Sanchez, I. *et al.* (2011) 'The parameters of the porcine eyeball', pp. 475–482. doi: 10.1007/s00417-011-1617-9.

Sangwan, V. S. *et al.* (2012) 'Simple limbal epithelial transplantation (SLET): a novel surgical technique for the treatment of unilateral limbal stem cell deficiency.', *The British journal of ophthalmology*, 96(7), pp. 931–4. doi: 10.1136/bjophthalmol-2011-301164.

Sanie-jahromi, F. *et al.* (2020) 'Propagation of limbal stem cells on polycaprolactone and polycaprolactone/gelatin fibrous scaffolds and transplantation in animal model', *Tabriz University of Medical Sciences*, 10(1), pp. 45–54. doi: 10.15171/bi.2020.06.

Santocildes-romero, M. E. *et al.* (2016) 'Preparation of Composite Electrospun Membranes Containing Strontium-Substituted Bioactive Glasses for Bone Tissue Regeneration', pp. 1–10. doi: 10.1002/mame.201600018.

Schindler, C. *et al.* (2013) 'Electrospun polycaprolactone / polyglyconate blends : Miscibility , mechanical behavior , and degradation', *Polymer*. Elsevier Ltd, 54(25), pp. 6824–6833. doi: 10.1016/j.polymer.2013.10.025.

Sefat, F. *et al.* (2013) 'Production, sterilisation and storage of biodegradable electrospun PLGA membranes for delivery of limbal stem cells to the cornea', *Procedia Engineering*. Elsevier B.V., 59,

pp. 101–116. doi: 10.1016/j.proeng.2013.05.099.

Shanbhag, S. S. *et al.* (2018) 'The Ocular Surface Boston keratoprosthesis type 1 for limbal stem cell deficiency after severe chemical corneal injury: A systematic review', *The Ocular Surface*. Elsevier Ltd, 16(3), pp. 272–281. doi: 10.1016/j.jtos.2018.03.007.

Sharma, N. *et al.* (1998) 'Amniotic membrane transplantation with or without autologous cultivated limbal stem cell transplantation for the management of partial limbal stem cell deficiency', *Clinical Ophthalmology*, 12, pp. 2103–2106.

Sharma, S. *et al.* (2011) 'Cellular response of limbal epithelial cells on electrospun poly-E-caprolactone nanofibrous scaffolds for ocular surface bioengineering: a preliminary in vitro study', *Mol. Vis.*, 17, pp. 2898–2910.

Singh, R. *et al.* (2019) 'Corneal transplantation in the modern era', (July), pp. 7–22. doi: 10.4103/ijmr.IJMR.

Singh, V., Shukla, S. and Ramachandran, C. (2015) *Science and Art of Cell-Based Ocular Surface Regeneration, International Review of Cell and Molecular Biology*. Elsevier Ltd. doi: 10.1016/bs.ircmb.2015.07.001.

Sinha, M. and Gupte, T. (2018) 'Design and evaluation of artificial cornea with core – skirt design using polyhydroxyethyl methacrylate and graphite', *International Ophthalmology*. Springer Netherlands, 38(3), pp. 1225–1233. doi: 10.1007/s10792-017-0586-3.

Smerdon, D. (2000) 'FOCUS ON : THE EYE Anatomy of the eye and orbit', pp. 286–292. doi: 10.1054/cacc.2000.0296.

Southgate, J., Cameron, N. R. and Baker, S. C. (2009) 'Biomaterials The relationship between the mechanical properties and cell behaviour on PLGA and PCL scaffolds for bladder tissue engineering', 30, pp. 1321–1328. doi: 10.1016/j.biomaterials.2008.11.033.

Sridhar, M. S. (2018) 'Anatomy of cornea and ocular surface', *Indian Journal of Ophthalmology*, 66(2), pp. 190–194.

Sta, P. *et al.* (2017) 'Adhesion and metabolic activity of human corneal cells on PCL based nano fiber

matrices', 71, pp. 764–770. doi: 10.1016/j.msec.2016.10.058.

Stewart, R. M. K. *et al.* (2015) 'Human Conjunctival Stem Cells are Predominantly Located in the Medial Canthal and Inferior Forniceal Areas'. doi: 10.1167/iov.14-16266.

Subramanian, A., Maheswari, U. and Sethuraman, S. (2012) 'Fabrication , Characterization and In Vitro Evaluation of Aligned PLGA – PCL Nanofibers for Neural Regeneration', 40(10), pp. 2098–2110. doi: 10.1007/s10439-012-0592-6.

Sun, H. *et al.* (2006) 'The in vivo degradation , absorption and excretion of PCL-based implant', 27, pp. 1735–1740. doi: 10.1016/j.biomaterials.2005.09.019.

Sundaray, B. *et al.* (2013) 'Unusual process-induced curl and shrinkage of electrospun PVDF membranes', *Polymer*. Elsevier Ltd, 54(17), pp. 4588–4593. doi: 10.1016/j.polymer.2013.05.049.

Tan, D. T. H. *et al.* (2012) 'Ophthalmology 3 Corneal transplantation', *The Lancet*. Elsevier Ltd, 379(9827), pp. 1749–1761. doi: 10.1016/S0140-6736(12)60437-1.

Tarek Shaarawy, Mark B. Sherwood, J. G. C. (2009) *Glaucoma: Medical diagnosis & therapy*. Volume one. Elsevier Ltd.

Thi, N. and Lee, H. B. (2010) 'Electro-spinning of PLGA / PCL blends for tissue engineering and their biocompatibility', pp. 1969–1978. doi: 10.1007/s10856-010-4048-y.

Thoft, R. A., Friend, J. and Murphy, H. S. (1979) 'Ocular surface epithelium and corneal vascularization in rabbits. I. The role of wounding.', *Investigative Ophthalmology & Visual Science*, 18(1), pp. 85–92.

Thomasy, S. M. *et al.* (2014) 'Acta Biomaterialia Elastic modulus and collagen organization of the rabbit cornea : Epithelium to endothelium', *Acta Biomaterialia*. Acta Materialia Inc., 10(2), pp. 785–791. doi: 10.1016/j.actbio.2013.09.025.

Tong, H. and Wang, M. (2010) 'An Investigation into the Influence of Electrospinning Parameters on the Diameter and Alignment of Poly ( hydroxybutyrate- co -hydroxyvalerate ) Fibers'. doi: 10.1002/app.

Trcin, M. T. *et al.* (2020) 'Cefuroxime Antimicrobial Scaffolds for Cultivation of Human Limbal Stem

Cells', 3.

Understanding Animal Research (2015) *Understanding Animal Research - Rabbit*. Available at: <https://www.understandinganimalresearch.org.uk/animals/10-facts/rabbit/#:~:text=Studies in rabbits are key,skin conditions%2C diabetes and emphysema.&text=The rabbit has provided an,radiation produced by surgical lasers.> (Accessed: 26 June 2020).

Vajpayee, R. B., Vasudendra, N. and Titiyal, J. S. (2006) 'Automated lamellar therapeutic keratoplasty ( ALTK ) in the treatment of anterior to mid-stromal corneal pathologies', pp. 771–773. doi: 10.1111/j.1600-0420.2006.00722.x.

W. Chen, M. Ishikawa, K. Yamaki, and S. S. (2003) 'Wistar rat palpebral conjunctiva contains more slow-cycling stem cells that have larger proliferative capacity: implication for conjunctival epithelial homeostasis', *Japanese Journal of Ophthalmology*, 47(2), pp. 119–128.

Wendorff, J., Agarwal, S. and Greiner, A. (2012) *Electrospinning: Materials, Processing, and Applications*.

Wilson, S. L. *et al.* (2013) 'Functional Biomaterials Keeping an Eye on Decellularized Corneas : A Review of Methods , Characterization and Applications', pp. 114–161. doi: 10.3390/jfb4030114.

Wong, K. H. *et al.* (2016) 'Corneal blindness and current major treatment concern- graft scarcity'. doi: 10.18240/ijo.2017.07.21.

World Health Assembly, D. (no date) *Action plan for the prevention of avoidable blindness and visual impairment*.

Wu, J. *et al.* (2012) 'Biomaterials The engineering of organized human corneal tissue through the spatial guidance of corneal stromal stem cells', *Biomaterials*. Elsevier Ltd, 33(5), pp. 1343–1352. doi: 10.1016/j.biomaterials.2011.10.055.

Xie, Z. *et al.* (2011) 'Electrospun Poly ( D , L ) -Lactide Nonwoven Mats for Biomedical Application : Surface Area Shrinkage and Surface Entrapment'. doi: 10.1002/app.

Xu, K. *et al.* (2019) 'Biomaterials 3D porous chitosan-alginate scaffold old stiffness promotes differential responses in prostate cancer cell lines', 217(April). doi: 10.1016/j.biomaterials.2019.119311.

Yan, J. *et al.* (2011) 'Effect of fiber alignment in electrospun scaffolds on keratocytes and corneal epithelial cells behavior', pp. 527–535. doi: 10.1002/jbm.a.33301.

Yanoff, M. and Sassani, J. (2015) *Ocular Pathology (seventh edition)*.

Yoon, J., Ismail, S. and Sherwin, T. (2014) 'Limbal stem cells: Central concepts of corneal epithelial homeostasis.', *World journal of stem cells*, 6(4), pp. 391–403. doi: 10.4252/wjsc.v6.i4.391.

Z.-G. Wei, T.-T. Sun, and R. M. L. (1996) 'Rabbit conjunctival and corneal epithelial cells belong to two separate lineages', *Investigative Ophthalmology and Visual Science*, 37(4), pp. 523–533.

Zeng, Y. *et al.* (2001) 'A comparison of biomechanical properties between human and porcine cornea', 34, pp. 533–537.

Zhang, W. *et al.* (2011) 'Rapidly constructed scaffold-free cornea epithelial sheets for ocular surface reconstruction.', *Tissue engineering. Part C, Methods*, 17(5), pp. 569–77. doi: 10.1089/ten.TEC.2010.0529.

Zhao, W. *et al.* (2016) 'Fabrication of functional PLGA-based electrospun scaffolds and their applications in biomedical engineering', *Materials Science & Engineering C*. Elsevier B.V., 59, pp. 1181–1194. doi: 10.1016/j.msec.2015.11.026.

Zhou, Z. *et al.* (2019) 'Acta Biomaterialia Nanofiber-reinforced decellularized amniotic membrane improves limbal stem cell transplantation in a rabbit model of corneal epithelial defect', *Acta Biomaterialia*. Elsevier Ltd, 97, pp. 310–320. doi: 10.1016/j.actbio.2019.08.027.

## Appendix A – Effects of COVID-19 on this research

### Introduction

The Coronavirus pandemic (COVID-19) has affected the entire world in a way that has never been seen in our modern times. Our research has not been an exception and this project affected as many others. The coronavirus laboratory lockdown impacted our plans and we were not able to finish key experiments and consequently deliver key findings that we were scheduled to deliver. In this appendix we will see the research planning we had to finish this thesis, and how COVID-19 affected it. As well, a discussion at the end will highlight the limitations in the research due to the COVID situation.

### Research Planning affected

In the following table we can see the 2020 calendar of activities we had planned:

**Table A.1.** Calendar of activities to be done between February to April 2020. DMP stands for Different Mechanical Properties. DCD stands for Different Collector Design.

		February				March				April				
Activity		3	10	17	24	2	9	16	23	30	6	13	20	27
Mechanical	Electrospinning	█												
	Collector 3d printing	█												
	Collector casting	█												
	Mechanical testing													
	Contact angle													
Biological	Porcine limbal isolation	█												
	Porcine epithelial cell isolation	█												
	Mouse 3t3 fibroblast culture													
	Limbal explants on scaffold culture (DMP)													
	Limbal explants on scaffold culture (DCD)													
	Epithelial cells on scaffold culture (DMP)													
	Epithelial cells on scaffold culture (DCD)													
	3t3 fibroblasts on scaffold culture (DMP)													
	3t3 fibroblasts on scaffold culture (DCD)													
	Cell fixing / stain													
	Epifluorescent microscopy													
	Confocal microscopy													
	Light Sheet microscopy													
	Scanning Electron Microscopy													
	Transmission Electron Microscopy													

In Table A.1 we can see the activities we planned between February and April of this year, said activities were the last research activities to be done to finish my thesis. In that weekly Gantt chart it can be seen that on the 16<sup>th</sup> of March there is a red line, this is because the laboratories at The University of Sheffield closed that week and all the experiments were suspended.

To fully assess the impact of COVID-19, we will separate the activities done and not finished in three points; Mechanical properties, biological testing 1 (cell lines), biological testing 2 (culture on scaffolds).

- Study of Physical Properties: We successfully electrospun membranes with different mechanical properties (DMP) and with different collector design (DCD). DMP scaffolds Produced in the planning were as described in 3.3.2 table x. For DCD scaffolds, 3D printing, casting and electrospinning scaffolds was possible according to the conditions defined in

chapter 2. In all these cases, manufacturing was possible but no further mechanical testing and contact angle was possible to do. Mechanical testing was needed to perform a third analysis of the mechanical properties on the DMP scaffolds; and contact angle to be able assess the effect of PCL in changing the hydrophobicity of the scaffolds.

- Biological Testing 1 (cell lines): Epithelial cells from porcine limbal explants were successfully isolated after 7 weeks of culture only reaching passaging 2. After reaching confluency in 2 T-75 flasks, porcine epithelial cells were frozen. For the case of 3T3 cells, they were received frozen and they grew normally after defrosting them. After 4 passaging in our lab, 3T3 cells were frozen after reaching confluency in 4 T-75 flasks.

- Biological Testing 2 (culture on scaffolds): the 6 different scaffolds conditions (DMP) and 5 different scaffold conditions (DCD) were able to be seeded with porcine explants as have been described in chapter 3. The experiment had to be stopped after 2 weeks for DMP and 1 week for DCD of culture instead of 3 weeks as it was previously projected.

## Discussion

The effect of Covid-19 in our research meant that the previously described experiments were not able to be finished, and thus, some questions or objectives did not have a clear answer with my current data. The results we were expecting to have would have helped us to clarify the following questions:

- Effect of adding PCL to PLGA electrospun scaffolds in its hydrophobicity: with the 6 conditions of electrospun scaffolds described in chapter 2 we know that mechanically PCL was able to modify the mechanical properties of the scaffolds, as well as its degradability in water after time. Now, one aspect that we needed to be study as well is if the polymer blend changed its hydrophobicity. Pure PLGA scaffolds are highly hydrophobic and a less hydrophobic material could create advantages, considering the surgeon specialists have mentioned they want a scaffolds that can be easily wet.

- Effect of adding PCL to PLGA electrospun scaffolds in the cell outgrowth of porcine limbal explants: We concluded the limbal culture at 2 weeks to be able to finish this experiment on time instead of the 3 weeks initially considered.

- Simpler cell culture models in DMP scaffolds: All the data gathered in chapter 3 have achieved culturing limbal explants in our scaffolds. And even though we have achieved positive results, with cell outgrowth in the scaffolds, a more simplistic approach to assess general biocompatibility is needed using a well-known fibroblast cell line (3T3) and an epithelial cell line (porcine limbal epithelial cells). These results could deepen our knowledge in how fit our scaffolds with different concentrations of PCL – PLGA are for cell culture.

- Effect of fibre alignment complexity in scaffolds for cell outgrowth: introducing complexity in the scaffold via the design of the collector was explored in chapter 4. The biological effect that could be seen by changing the design of our scaffolds have not been studied, as the only images available are cell outgrowth from explant after 7 days, with an unrefined approach at the time. With DCD scaffolds we were aiming to see if the complexity of the fibre alignment that can be introduced through our collector designs will affect the cell outgrowth of explants. Cell alignment in corneal cell matrixes is not a novel concept (Wu *et al.*, 2012; Kim, Kim and Park, 2018; Fernández-pérez *et al.*, 2020), but in scaffolds with mixed random – aligned fibre distribution have not been analysed to be able to suggest an impact of the distribution versus cell outgrowth. We expected with this experiment to be able to analyse the cell outgrowth from the explants and see if the cell outgrowth had a tendency of proliferate toward the aligned sections of the scaffold versus the random aligned ones.

## Appendix B – Fibre Alignment methodology explained

As seen in figure 4.15, the electrospun membranes created using the second generation collectors have a distinctive pattern in their topography, which is revealed by different levels of fibre alignments on them. To measure these different fibre alignments in this complex design we proposed the following methodology:

As mentioned in 4.3.6, the fibre alignment was measured using the following protocol, which will be detailed afterwards:

1. Open the SEM images on ImageJ software.
2. Measure all the fibres from left to right using the straight line option.
3. Fibres with angles  $< -45^\circ$  must be adjusted by adding  $180^\circ$ .
4. When all the angles are measured, the mean is calculated.
5. Using the mean, the percentage of alignment of each fibre is calculated using the following equation:

$$\left| 1 - \left( \frac{|mean-angle|}{90} \right) \right| \times 100 \quad (1)$$

6. Repeat the process with all the fibres to obtain the average percentage of alignment.

### A- Open the SEM images on ImageJ software

The SEM images used for this analysis are images for the sections of the collector we want to see, mainly focused in different levels of alignment in the membranes due to the design differences of the collectors. The images selected have a zoom of  $\times 5000$ . ImageJ software was used to measure fibre diameter (as described in 2.3.8) and fibre orientation.

### B- Measure all the fibres from left to right using the straight-line option.

Using the straight-line option of ImageJ software makes it possible to measure the angles of the fibres. However, the use of this option is susceptible to the start and ending of the

line, which means that the same fibre if it is measure from left to right will show a different value than right to left. In the following figure this can be seen more clearly.

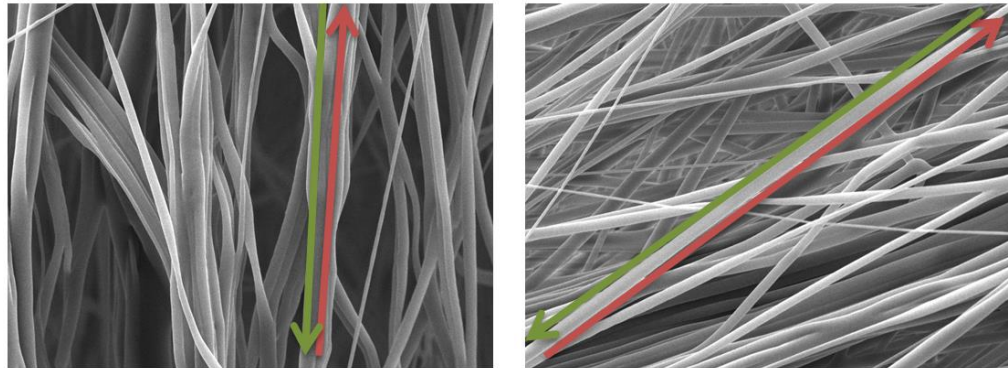
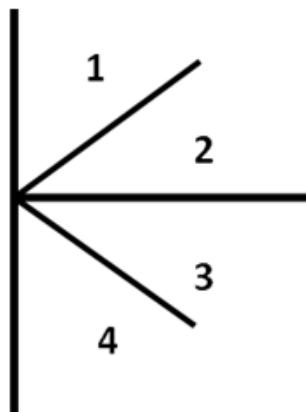


**Figure B1-** Examples of measuring orientation of the same fibre in two SEM images of electrospun membranes.

Figure B1 displays that there are two ways of measuring a fibre using ImageJ software, and both of them will have a different angle of alignment as a result. To avoid this problem, all the fibres will be measured from left to right in this study, as the red arrow in figure B1 shows.

**C-** Fibres with angles  $< -45^\circ$  must be adjusted by adding  $180^\circ$ .

When measuring the fibres in left to right as previously explained, the orientation angles will vary between  $-90^\circ$  and  $90^\circ$ . In the following figure B2 this can be seen, but as well we have decided to split it in 4 angle regions.



Region	Orientation angles
1	$45^\circ \leq x \leq 90^\circ$
2	$0^\circ \leq x < 45^\circ$
3	$-45^\circ \leq x < 0^\circ$
4	$-90^\circ \leq x < 45^\circ$

**Figure B2-** Orientation angles for the 4 possible regions when measuring left to right.

Figure B2 shows the full range of angles that we can get when measuring from left to right, divided in 4 regions of orientation. Regions 2 and 3 are orientated close to the X axis, which does not represent any problem when measuring from left to right. Regions 1 and 4 on the other hand are orientated close to the Y axis. Region 1 will still give accurate results to this methodology due to our left to right orientation of our lines, as left to right in that region is bottom to top. Region 4 however is the total opposite of region 1 and will give a different measurement to what we are looking for. To modify this, it is needed to modify in 180° the angles acquired in region 4, and thus bringing the angles orientations of those fibres to region 1. In the following example the fibre orientation angles can be seen more clearly on region 1 and 4 before and after this modification.

**Table B1** Fibre orientation in regions 1 and 4 and its orientation angles. Example of how the angles in fibres on region 4 should be modified to achieve a real mean.

Orientation angle	Fibre region 1	Fibre region 4	Mean	
Normal measurement	73.696°	-73.784°	-0.044°	
Adjusted measurement	73.696°	106.216°	89.956°	

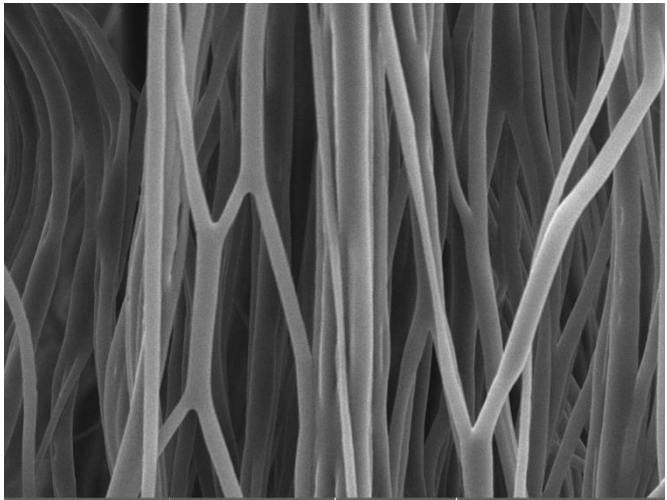
In table B1 can be seen two fibres examples, one in region 1 and other in region 4. The fibre in region 1 has an angle orientation of 73.696° when measured in imageJ software. The fibre in region 4 has an angle orientation of -73.784° when measured the same way. Calculating the mean of these two fibres shows a result of -0.044° which even though it is mathematically correct, does not show the real alignment happening between these two fibres. When bringing the region 4 to the region 1 by adding 180°, we see that the fibre orientation

angle in 106.216° and with this angle the new mean of these 2 fibres is 89.956°, which is more realistic considering the fibre alignment we can see in the example.

**D-** Calculate the mean angle orientation on a SEM image.

10 representative fibres can be selected to calculate the average fibre orientation of a SEM image. Next figure shows an example of calculating the mean of a SEM image after adjusting them as described previously

**Table B2** Average fibre orientation of a SEM image. Table shows the fibre orientation of 10 fibres with their adjusted measurement as well. At the bottom of the table is highlighted the average.

Fibre orientation	Adjusted	SEM Image
88.73	88.73	
-82.83	97.17	
-84.50	95.50	
-85.39	94.61	
-89.40	90.61	
-78.99	101.01	
70.30	70.30	
-85.89	94.12	
86.71	86.71	
-89.85	90.15	
<b>-35.11</b>	<b>90.89</b>	

To have a better visual representation of these alignments, these values can be plotted on a histogram to see the fibre distribution.

**E-** Calculating the percentage of alignment.

Now that the mean of a SEM image has been calculated, we can measure the level of alignment in this image. For doing it, the following equation is going to be used:

$$|1 - \left(\frac{|mean-angle|}{90}\right)| \times 100$$

This way, using this equation we will get the level of alignment of every fibre on the SEM image. The angle used for this calculation will be the adjustment one, same as the mean.  $90^{\circ}$  is used as that is the largest angle that can be achieved using the left to right measurement. Therefore when the mean minus the angle has a value of 90, it will represent the maximum level of misalignment, making the total value of the equation 0 (total misalignment). On the other hand, maximum alignment is achieved when the mean minus the angles is 0 or 180, as these values will give a value to the equation of 100 (total alignment). In the next table can be seen data treatment of the previous example.

**Table B3** Process of calculating the percentage of alignment for the fibres.

Adjusted angles	mean – angle	$\left(\frac{ mean - angle }{90}\right)$	$ 1 - \left(\frac{ mean - angle }{90}\right)  \times 100$
88.73	2.15	0.02	<b>98%</b>
97.17	6.28	0.07	<b>93%</b>
95.50	4.61	0.05	<b>95%</b>
94.61	3.72	0.04	<b>96%</b>
90.61	0.29	0.003	<b>99.7%</b>
101.01	10.12	0.11	<b>89%</b>
70.30	20.59	0.23	<b>77%</b>
94.12	3.22	0.04	<b>96%</b>
86.71	4.18	0.05	<b>95%</b>
90.15	0.74	0.01	<b>99%</b>

**F-** Calculating the average percentage of alignment and conclusion

Finally, with the alignment for every fibre calculated in table B3, we get an average alignment of 93.77%. With this methodology we can finally conclude that for our example SEM image **there is a 93.77% of fibre alignment to 90.89°**.

**G- Exception and limitations to this fibre alignment methodology.**

In the methodology introduced in this appendix it is mentioned that the angles in region 4 need to be modified by adding  $180^\circ$  making region 1 values. However, in cases where the average fibre orientation is between regions 3 and 4 this would need care in deciding to apply or not the adjustment technique (step c). In the following image we show an example of two fibres that align to  $-45^\circ$ , but by adjusting the angle in region 4, the average value will not represent the real mean we are seeing.

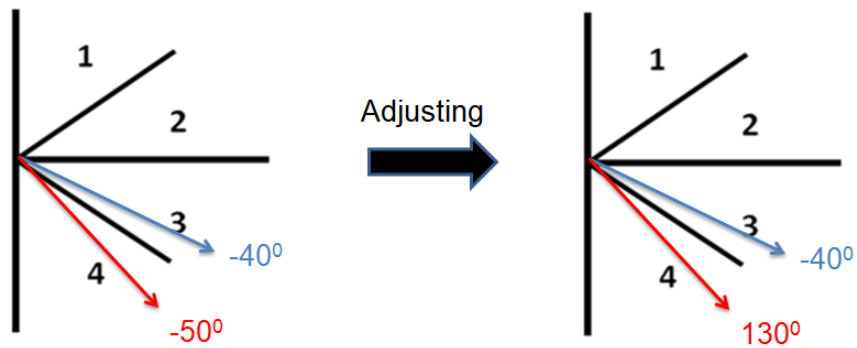


**Figure B3** Example of two fibres aligned at  $-45^\circ$ , where it is better not to adjust to get the real average alignment angle.

In figure B3 it can be seen that the fibre in region 4, when modified with the adjustment (step c) of our methodology, will dramatically change the results of the average alignment in the SEM image. Therefore, if the average alignment angle fell between regions 3 and 4, it is better to perform the analysis with and without the corrections and see which one is more representative, as can be seen in the following example.

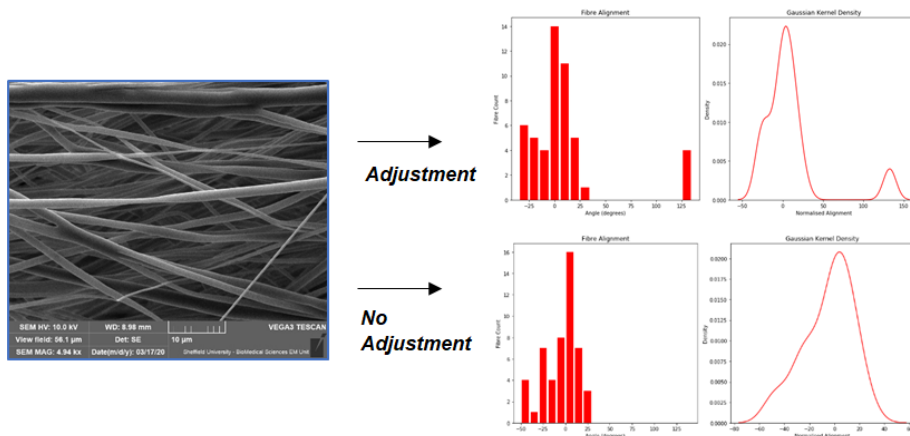


**Figure B4** Example of a SEM image with fibre orientation between regions 3 and 4. In the example, both results are represented in Gaussian Kernel Density (KDE) plots of fibre orientations with and without the adjustment. Not applying adjustment in this case shows a better fibre orientation distribution.

As well, the proposed fibre orientation methodology we are using in this research works using two assumptions: 1. All fibres are straight; 2. The alignment occurs in a single axis. In the following figure we can see an example of two images that, not considering these 2 assumptions, will significantly affect the results.

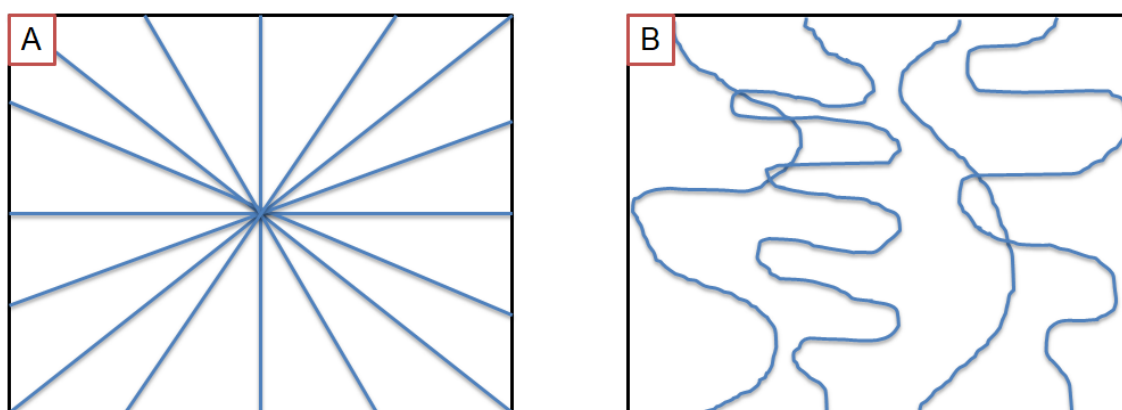


**Figure B5** Examples of two cases of fibre alignment that contradict the assumptions in the proposed fibre alignment methodology. A shows a case where the fibre alignment is to a point (centre) instead of an axis. B shows a case where the fibres are irregular.

Figure B5 displays two examples of fibre alignment that oppose the assumption in our methodology. In A can be seen an example of fibres aligning to a specific point inside the image, instead of an axis as we consider in our methodology. In this case, using our methodology will show that figure A has total random alignment, which by seeing the figure is not really the behaviour of the fibres in that image. In B the fibres are irregular, but in our

methodology we only consider the starting and finishing point as straight lines to measure. If we run our methodology in figure B, it will show a perfect vertical alignment in the figure, which can be discussed considering how irregular the fibres are. Therefore, and considering that special cases can happen when analysing results, we introduce a third concept that can be used to adjust and properly measure these cases; straightness of the fibres.

Straightness of the fibres can help as an extra tool to have a deeper knowledge of how the fibres are behaving in electrospun membranes. Taking the previous two images as examples, A will show a random alignment in our methodology, but the fibres are totally straight, giving us the information that they are not totally randomly aligned, but instead they are oriented to a point rather than to an axis. In the case of figure B, with that high level of irregularity, the concept of straightness can be used as an extra value of error associated to the measured angle of the fibre. We propose to add this percentage of error as the area between the real fibre and the straight fibre we use in our assumption for our methodology versus the total area of the image, as can be seen in the following figure.

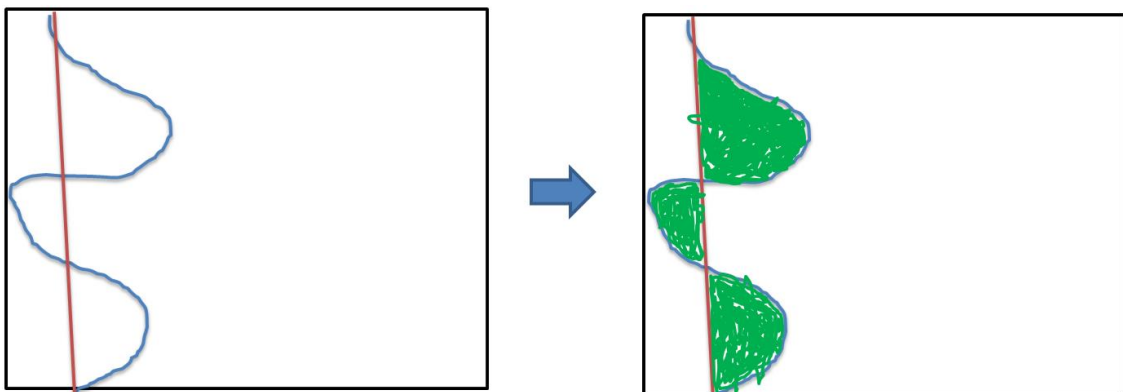


**Figure B6** selecting the area (green) between the real fibre (blue) versus the straight line used for fibre orientation calculation in our methodology (red).

Figure B6 reveals the way of selecting the area between the real fibre and the straight fibre used for the fibre orientation methodology. This area will be used to calculate the error associated in the fibre orientation angle of the fibre. We propose to use the area created between the fibres (green) versus the total area of the figure to create a percentage of error, which will be multiplied by 180, which is the total angle range when measuring by our methodology. In the next figure we can see how this can be applied to a real SEM image.

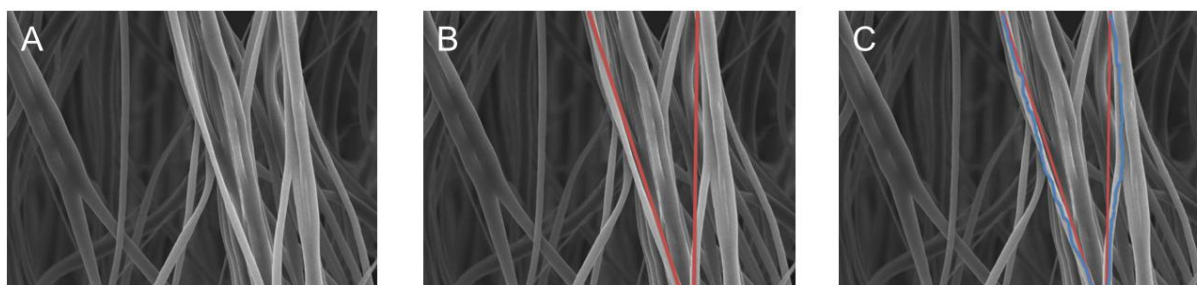


**Figure B7** Example of two fibres which are not straight. Red lines are the straight lines considered to our methodology, while blue line is the real fibre.

In figure B7 we can see an example of two fibres that are not totally straight as considered in our fibre orientation methodology. Using this image as an example, and the area between the red line (straight line) and blue line (real fibre) we get the following result:

**Table B4** Adding straightness of the fibre as error in the fibre orientation angle measurement.

Left fibre	Right fibre
Angle: 107.7°	Angle: 89.3°
Fibre area vs total area: $36.56 / 2261 = 1.61\%$	Fibre area vs total area:
Possible angle range: 180°	Possible angle range: 180°
<b>Final angle: 107.7° +/- 2.9°</b>	<b>Final angle: 89.3° +/- 4.2°</b>

Table B4 shows how the implementation of the straightness can improve our fibre orientation methodology in cases where fibres are highly irregular.

Finally, in this research and the results shown in 4.4.5.3 we used the fibre orientation methodology to measure the topographical cues in our membranes with designs on them. The first exception of the methodology (fibre angles between regions 3 and 4) was considered but the straightness was not added as the level of irregularity in our fibres was not high. Nonetheless, we identified the weaknesses in our methodology and we presented straightness as a way of improvement for SEM images with fibres like example A and B of figure 4.20.

## Appendix C – Ethical approval

### University of Sheffield Answer

---

Dear Chris

I've now arranged for UREC to consider the report you provided; UREC agrees with the conclusion that the appropriate ethics approval was in place for this research, evidenced by the letter of approval dated 17th April 2018, and checks have been undertaken to establish that this approval was provided by a suitably robust ethics process.

Ideally, the external ethics process should have been checked before the research was started, but we realise that this was not wholly clear from the Ethics Policy. We therefore agree that the student should be required to amend their thesis to include the details of the ethics approval (to be referred to in the thesis body) and the letter confirming ethics approval included in an Appendix, and it then be submitted for examination as normal.

UREC will consider further the ethical review requirements for such cases in due course.

I hope this is all clear but do let me know if you have any queries, and many thanks for your help with this.

--

Chris Deery  
Professor of Paediatric Dentistry  
Dean, School of Clinical Dentistry

School of Clinical Dentistry  
Claremont Crescent  
Sheffield  
S10 2TA

e-mail [c.deery@Sheffield.ac.uk](mailto:c.deery@Sheffield.ac.uk)  
Telephone +44(0)114 215 9305

---

### Ethics Committee Approval Letter

In the following pages is copied the full Ethics Committee Approval letter that was mentioned in the answer of the University of Sheffield.



**L V Prasad Eye Institute Ethics Committee**  
**Kallam Anji Reddy Campus, Banjara Hills, Hyderabad**  
**ECR/468/Inst./AP/2013/RR-16**

April 17, 2018

Ethics Ref. No. LEC 04-18-073

To:

**Dr Vivek Singh**  
Principal Investigator  
L V Prasad Eye Institute  
L V Prasad Marg, Banjara Hills  
Hyderabad- 500 034  
Telangana

**Subject: Ethics Committee Approval Letter**

**Protocol Entitled: "Studying the limbal explant biology in vitro: Impact on melanocytes formation and role of supporting scaffold in the stem cell properties"**

**Dear Dr Dr Vivek Singh:**

With reference to your Submission for the approval of above protocol, the Institutional Review Board, L V Prasad Eye Institute, held on April 17, 2018 has reviewed and discussed the below mentioned list of documents submitted by you and approved the same.

SI No	Documents
1.	Study Protocol
2.	Informed Consent Form

**Ethics committee**  
**L.V. Prasad Eye Institute**  
**Kallam Anji Reddy , Campus**  
**Banjara Hills, Hyderabad-500 034**  
**Reg.No. ECR/468/Inst./AP/ 2013/RR-16**

**L V Prasad Eye Institute Ethics Committee  
Kallam Anji Reddy Campus, Banjara Hills, Hyderabad  
ECR/468/Inst./AP/2013/RR-16**

It is understood that the study will be conducted under your direction at L.V. Prasad Eye Institute, Hyderabad

Please note:

- a. In the events of any protocol amendments, Ethics Committee must be informed and the amendments should be highlighted. All approval of amendments in the projects must be obtained prior to implementation of changes. The amendment is unlikely to be approved by the Ethics Committee unless all the required information is provided.
- b. Any advertisement placed in the newspapers, magazines must be submitted for approval.
- c. The results of the study should be presented in any of the academic forums of the Institute.
- d. Any SAE, which could affect any study, must be communicated to Ethics Committee within 24 hours of their occurrence and evaluate the rate of complications if any.
- e. Any protocol deviation/ waiver in the protocol must be informed to the Ethics Committee
- f. At the time of PI's retirement/intention to leave the institute, the study responsibility should be transferred to a colleague with an approval from the Ethics Committee
- g. For extension of your study you are requested to submit the status (ongoing / closed etc) and progress reports (how many recruited, how many followed up and how many left the study etc.) by mail or hard copy to the Ethic Committee one month before completion of one year of the study period as given above. The decision for extensions would be taken by the Ethics Committee Members and conveyed to PIs in hard copies. Lack of response from PI's regarding the status/inadequate progress reports or no responses beyond deadline would be deemed as closure of the study by the EC and conveyed to the PI who would now have to present the study afresh in the next EC meeting. The EC would also take a decision for PI's who fail to submit progress reports on time and refrain the PI from presenting any further study to the EC until further notice or until reports are submitted and presented in person with reason for delay/ non- response.

It is hereby confirmed that neither you nor any of the members of the study team participated in the decision making/voting procedures. After consideration, the committee has approved the study for a period of one year. (Until closing hour of April 16, 2019)

We hereby confirm that, the Institutional Review Board, L V Prasad Eye Institute is organized and operates as per GCP (Good Clinical Practice) and applicable Indian regulations.

**Ethics committee  
L.V. Prasad Eye Institute  
Kallam Anji Reddy, Campus  
Banjara Hills, Hyderabad-500 034**

LV Prasad Eye Institute, Kallam Anji Reddy Campus, LV Prasad Marg, Banjara Hills, Hyderabad 500034, India  
Tel: +91 40 30612345, Fax: +91 40 23548271, Email: info.hyd@lvpei.org, Website: www.lvpei.org  
Reg.No. ECR/468/Inst./AP/ 2013/RR-16

**L V Prasad Eye Institute Ethics Committee**  
**Kallam Anji Reddy Campus, Banjara Hills, Hyderabad**  
**ECR/468/Inst./AP/2013/RR-16**

The following members of the Ethics Committee were present at the meeting held on April 17, 2018 at 3:30pm, Godrej Hall, Level VI, L V Prasad Eye Institute, KAR Campus, Hyderabad 500 034

Name	Qualification	Designation/Title	Gender	Affiliations as to the Institution Yes/No
Justice T N C Rangarajan	M.A, B.L.	Chair person and legal expert	Male	No
Dr Sayan Basu	M.S	Member Secretary	Male	Yes
Dr. Subhabrata Chakrabarti	PhD	Basic Medical Scientist	Male	Yes
Dr Savitri Sharma	MD, FAMS	Basic Medical Scientist	Female	Yes
Dr. Nuzhat Aziz	DGO, DNB	Clinician	Female	No
Dr Sreedevi Yadavalli	M.A, M. Phil, PhD	Lay person	Female	Yes
Mr. Paul Balasundaram	B. Sc, M Div	Theology & National Coordinator	Male	No
Dr. B R Shamanna	MBBS,MD (SPM), DNB(SPM),MSC (London)	Basic Medical Scientist	No	No
Dr Usha Raman	PhD – Mass Communication	Lay person	Female	No

Thanking you

Yours Sincerely,

  
Sayan Basu, MS,

Member Secretary

L V Prasad Eye Institute Ethics Committee

L V Prasad Eye Institute, Banjara Hills

Hyderabad- 500 034

**Ethics committee**  
**L.V. Prasad Eye Institute**  
**Kallam Anji Reddy , Campus**  
**Banjara Hills, Hyderabad-500 034**  
**Reg.No. ECR/468/Inst./AP/ 2013/RR-16**

**Hyderabad Eye Research Foundation**  
L V Prasad Eye Institute Ethics Committee  
Kallam Anji Reddy Campus, Banjara Hills, Hyderabad  
ECR/468/Inst./AP/2013/RR-19  
NABH Registration No: EC-CT-2019-0126

To

Date: July 27, 2020

Dr Vivek Singh  
Principal Investigator,  
L V Prasad Eye Institute,  
KAR Campus, L V Prasad Marg,  
Banjara Hills, Hyderabad – 500 034,

**Subject: Ethics Committee Approval for Extension of the study**

**Protocol Title: “Studying the limbal explant biology in vitro: Impact on melanocytes formation and role of supporting scaffold in the stem cell properties”**

**Ethics Ref No: LEC 04-18-073**

**Dear Dr Vivek Singh:**

This is with reference to your letter dated July 22, 2020 regarding request for an extension of the above mentioned study.

The members reviewed and discussed in detail the progress report submitted by you, after consideration, the committee has approved the study for one more year.

It is hereby confirmed that neither you nor any of the members of the study team participated in the decision making/voting procedures.

We here by confirm that the Institutional Review Board, L.V Prasad Eye Institute is organised and operates as per GCP and Applicable Indian regulations

**Ethics Committee**  
**L.V. Prasad Eye Institute**  
**Kallam Anji Reddy, Campus**  
**Banjara Hills, Hyderabad-500 034**  
**Reg.No. ECR/468/Inst./AP/ 2013/RR-19**



LV Prasad Eye Institute, Kallam Anji Reddy Campus, LV Prasad Marg, Banjara Hills, Hyderabad 500034, India  
Tel: +91 40 68102020, Fax: +91 40 23548339, Email: info.hyd@lvpei.org, Website: www.lvpei.org

**Hyderabad Eye Research Foundation**  
**L V Prasad Eye Institute Ethics Committee**  
**Kallam Anji Reddy Campus, Banjara Hills, Hyderabad**  
**ECR/468/Inst./AP/2013/RR-19**  
**NABH Registration No: EC-CT-2019-0126**

The following members of the Ethics Committee were present at the meeting held on July 27, 2020 at 11 am, via zoom at L V Prasad Eye Institute, KAR Campus, Hyderabad 500 034

Name	Qualification	Designation/Title	Gender	Affiliation: as to the Institution  Yes/No
Justice T N C Rangarajan	M.A, B.L.	Chairperson and Legal Expert	Male	No
Dr. B.R.Shamanna	MBBS,MD (SPM), DNB(SPM),MSC, London	Clinician	Male	No
Dr Savitri Sharma	MBBS, MD, FAMS	Basic Medical Scientist	Female	Yes
Mr Vijay Kumar Chejerla	M A.,LLB,FIII,DPM	Social Scientist	Male	No
Dr Dilip Kumar Mishra	MBBS, MD	Basic Medical Scientist	Male	Yes
Dr Sreedevi Yadavalli	M.A, M. Phil, PbD	Lay person	Female	Yes
Dr Usha Raman	M.A. Ph D	Lay Person	Female	No
Dr. Subhabrata Chakrabarti	M SC, Ph D	Scientific Member	Male	Yes
Mrs Amita Desai	MA. M.Ed.	Social Scientist	Female	No
Mr. Paul Balasundaram	B. Sc, M Div	Theology & National Coordinator	Male	No

Yours sincerely,



**Ethics Committee**  
**L.V. Prasad Eye Institute**  
**Kallam Anji Reddy, Campus**  
**Banjara Hills, Hyderabad-500 034**  
**Reg.No. ECR/468/Inst./AP/ 2013/RR-19**

Justice T N C Rangarajan,

Chairperson

L V Prasad Eye Institute Ethics Committee

L V Prasad Eye Institute, Hyderabad 500 034

